OCS Study
MMS 2007-056

Coastal Marine Institute

Full-Water Column Currents Near the Sigsbee Escarpment (91-92º W. Longitude) and Relationships with the Loop Current and Associated Warm- and Cold-Core Eddies

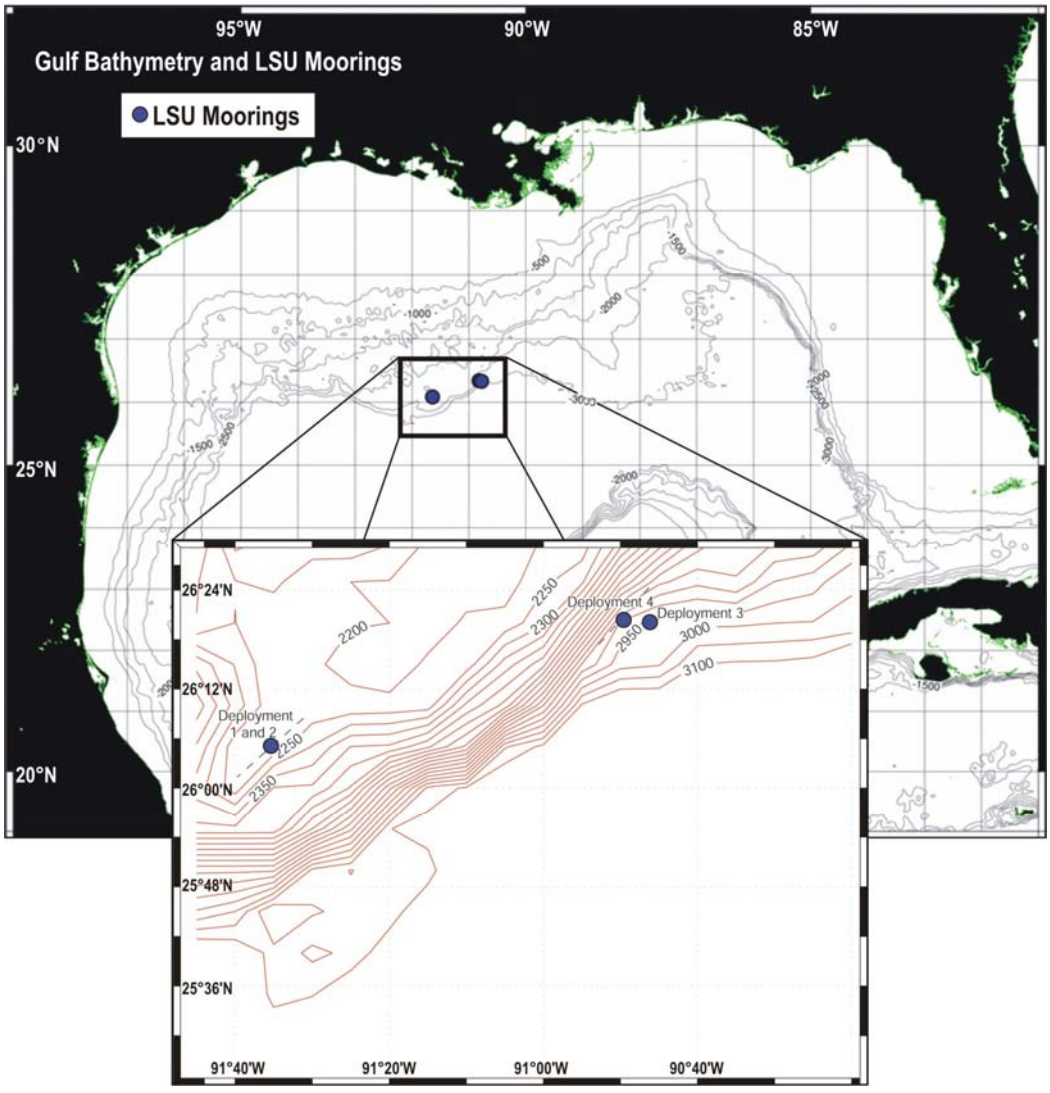

U.S. Department of the Interior
Minerals Management Service
Gulf of Mexico OCS Region

Cooperative Agreement
Coastal Marine Institute
Louisiana State University

OCS Study
MMS 2007-056

Coastal Marine Institute

Full-Water Column Currents Near the Sigsbee Escarpment (91-92° W. Longitude) and Relationships with the Loop Current and Associated Warm- and Cold-Core Eddies

Authors

Kevin P. McKone
Nan D. Walker
Eddie Weeks

December 2007

Prepared under MMS Contract
1435-01-99-CA-30951-16807
Louisiana State University
Coastal Marine Institute
Baton Rouge, Louisiana 70803

Published by

U.S. Department of the Interior
Minerals Management Service
Gulf of Mexico OCS Region

Cooperative Agreement
Coastal Marine Institute
Louisiana State University

DISCLAIMER

This report was prepared under contract between the Mineral Management Service (MMS), and the Coastal Marine Institute at Louisiana State University. This report has been technically reviewed by the MMS, and it has been approved for publication. Approval does not signify that the contents necessarily reflect the views and policies of MMS, nor does mention of trade names or commercial products constitute endorsement or recommendation for use. It is, however, exempt from review and compliance with the MMS editorial standards.

REPORT AVAILABILITY

Extra copies of this report may be obtained from the Public Information Office (Mail Stop 5034) at the following address:

U.S. Department of the Interior
Minerals Management Service
Gulf of Mexico OCS Region
Public Information Office (MS 5034)
1201 Elmwood Park Boulevard
New Orleans, Louisiana 70123-2394

Telephone: (504) 736-2519 or
1-800-200-GULF

CITATION

Suggested citation:

McKone, K., N. D. Walker, and E. Weeks. 2007. Full-water column currents near the Sigsbee Escarpment (91-92ºW. Longitude) and relationships with the Loop Current and associated warm and cold-core eddies, U.S. Dept. of the Interior, Minerals Management Service, Gulf of Mexico OCS Region, New Orleans, LA. OCS Study MMS 2007-056. 107 pp.

ACKNOWLEDGMENT

Staff of the Coastal Studies Institute Field Support Group and the Earth Scan Laboratory are recognized for their expertise and support of this project. Dr. Robert Leben, University of Colorado, is thanked for supplying sea surface height data. Steve Anderson, Patrice Coholan, and Jim Feeney are thanked for collaborations that enhanced the interpretation of mooring data.

ABOUT THE COVER

The cover shows mooring locations in the Gulf of Mexico in relationship to bathymetry.

TABLE OF CONTENTS

LIST OF FIGURES

LIST OF TABLES

Page

ABBREVIATIONS AND ACRONYMS

ADCP	Acoustic Doppler Current Profiler
AR	Auto Regressive
CTD	Conductivity Temperature Depth Profiler
GMT	Greenwich Mean Time
GOES	Geostationary Environmental Satellite
GoM	Gulf of Mexico
HLP	hourly low pass
LC	Loop Current
LCFE	Loop Current frontal eddy
LSU	Louisiana State University
MMS	Minerals Management Service
MTM	multitaper spectral estimator
NOAA	National Oceanic and Atmospheric Administration
OCM	Ocean Color Monitor
POES	Polar Orbiting Environmental Satellite
SSH	sea surface height
SST	sea surface temperature
TRW	topographic Rossby wave
WCE	warm core eddy
WOSA	Welch's overlapped segment averaging spectra

1.0 INTRODUCTION

1.1 Motivation, Objectives, and Background

As industry migrates into deeper water, the need to characterize the deep water environments of the Gulf of Mexico (GoM) has become increasingly apparent. In particular, appropriate engineering designs and enlightened stewardship of natural resources require improved understanding of the physical processes of this deeper environment in which development will occur. High speed currents along with energetic waves can affect drilling and dispersion of by-products from drilling (Offshore Engineer 2004), issues of concern to the petroleum industry and the Minerals Management Service. For several decades, researchers have studied the very energetic circulation characteristics of the Loop Current and the warm core eddies that separate from it. Surface current velocities within the Loop Current are typically 100-200 cm/s and similar speeds have been observed in hydrographic data and using drifters within the detached warm core eddies of the Loop Current (Cooper et al., 1990; Berger et al., 1996; Wiseman and Sturges, 1999). However, observational studies of the deep circulation (below 1000 m) are few in comparison with the surface circulation. Hamilton (1990) described strong bottom-trapped currents on the continental rise of the deep GoM which he attributed to topographic Rossby waves (TRW's), generated as Loop Current rings separate from the main Loop Current in the eastern GoM. The study of Hamilton and Lugo-Fernandez (2001) demonstrated the presence of high velocity flows (~100 cm/s) near the bottom (~2000 m) along the Sigsbee Escarpment near 90º W. They proposed that features such as Loop Current frontal eddies could provide trigger mechanisms for TRW's. The dynamics of the waves as well as variations in the flow field along the escarpment from east to west and at varying distances from the escarpment are issues of great concern to the Minerals Management Service and the petroleum industry. In addition, focused studies of the linkages between surface circulation and bottom current variations are lacking. The lack of knowledge concerning flow variability along the escarpment and linkages with near-surface events provided the primary motivation for this ~3 year observational study of full water column currents, first on the continental slope and later on the continental rise along the Sigsbee Escarpment between 91º and 92º W Longitude.

Initially, the study focused on characterizing current variability from surface to bottom on the plateau above the Sigsbee Escarpment in ~2200 m of water. The latter ~2 years of measurements were obtained to the east at the base of the Sigsbee Escarpment in ~3000 m of water. The locations of these deployments are shown in Figure 1 in relationship to the bathymetry of the continental slope and rise. Deployments 1 and 2, covered the time period from February 16, 2000 to May 5, 2001. Deployment 3 lasted from July 30, 2001 to June 2, 2002 and Deployment 4 lasted from April 17, 2003 to June 10, 2004 (Figure 2). The Deployment 4 mooring was about 3 km closer to the Escarpment than the Deployment 3 mooring. The placement of the moorings allowed for the comparison of current data above and below the escarpment. The last deployment coincided closely in time with the Exploratory Study reported on by Donohue et al. (2006).

One of the objectives of this project was to look for the presence of topographic Rossby waves (TRW), along with possible surface forcing for TRW's. Deployments 3 and 4, located at the base of the Sigsbee Escarpment, had the best chance of experiencing TRW's. The escarpment, with its steep slope, can act as a guide for TRW's (Oey and Lee, 2002). TRW's can theoretically be supported almost anywhere in the Gulf, so it would not be surprising if TRW signals were also detected in the Deployments 1 and 2 data, when measurements were made above the escarpment.

Another objective of this project was a statistical analysis of all mooring measurements. Basic and advanced statistical methods have been used to investigate and to characterize the flow fields from the surface to bottom. These results are considered important in helping to model the current variability in the deep GoM.

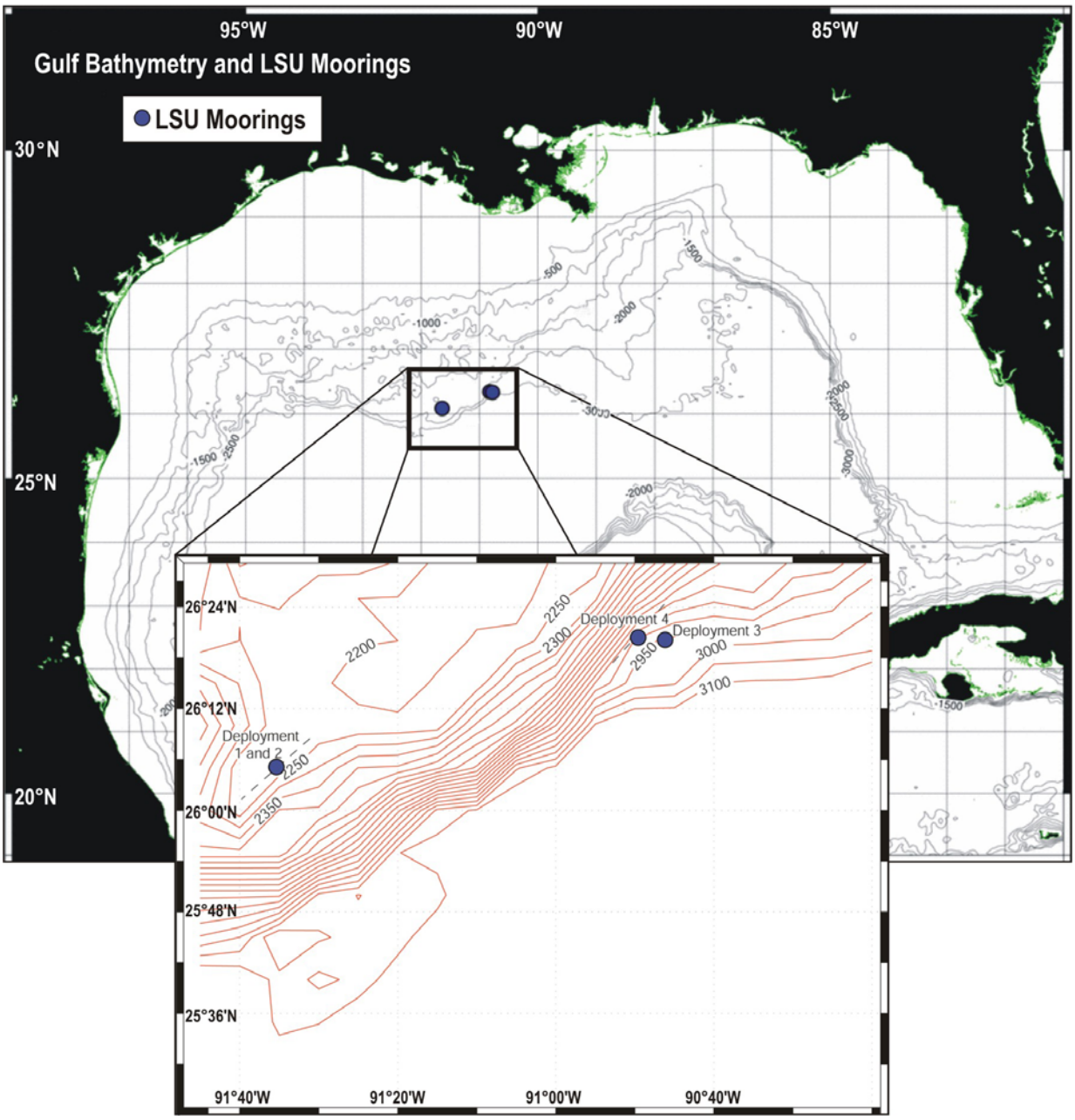

Figure 1. Locations of LSU Deployments 1-2, 3, and 4 (2001-2004) in relationship to the Gulf of Mexico bathymetry.

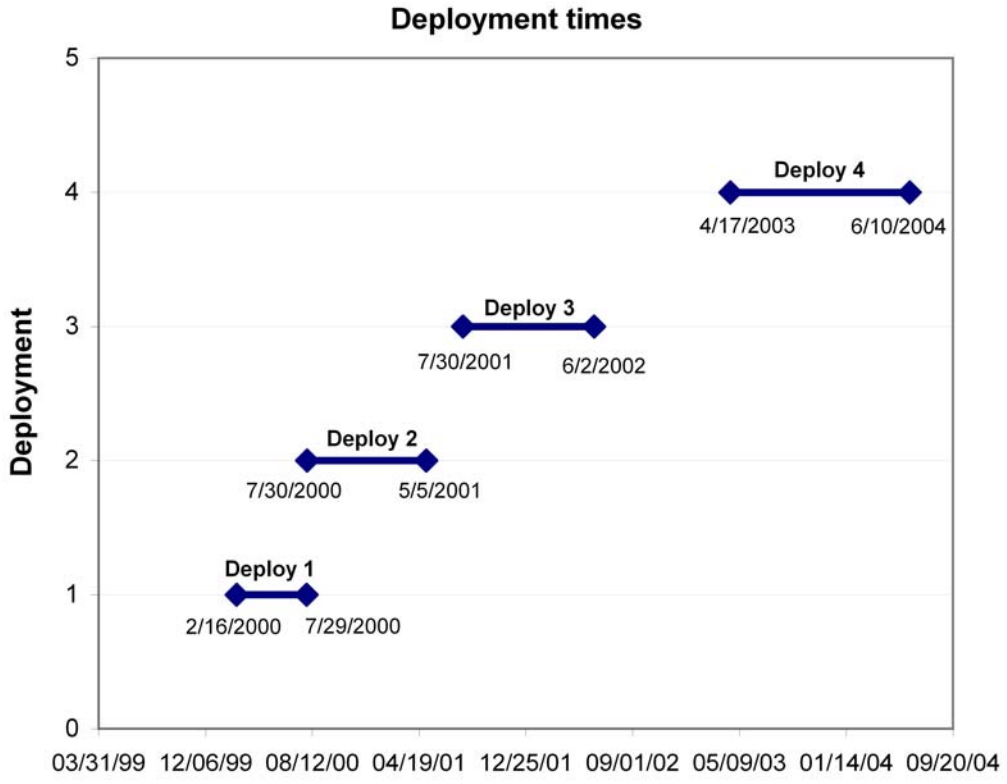

Figure 2. Time periods of Deployments 1, 2, 3, and 4.

Interpretation of current information in the GoM requires an accurate knowledge of the location and movement of the Loop Current (LC), detached warm-core anticyclonic eddies (WCE's), Loop Current frontal eddies (LCFE's), and other cold-core cyclonic eddies (CCE's). Satellite remote sensing provides an effective means of monitoring circulation processes on a daily basis in the Gulf. Much of the satellite data used in the study was received and processed at the LSU Earth Scan Laboratory, a receiving station for both polar orbiting and geostationary data from earth orbiting satellites. Additional satellite data to aid in the interpretation of mooring measurements were obtained from Robert Leben, University of Colorado.

Many WCE's separated from the Loop Current during the deployment periods, spanning February 2000 through June 2004. The first mooring was deployed in Eddy Juggernaut and the final mooring was affected towards the end of the deployment by Eddy Triton. Thus, a total of eleven WCE's separated from the LC during this ~4 year period. Nine of these WCE's had documented effects on surface and bottom currents at the LSU mooring sites. At each location, the direct effects of LCFE's along the northwest side of the LC were experienced. During Deployment 3, the LC intruded so far to the northwest that it flowed over the mooring. This intrusion is depicted in Figure 3, by combining GOES sea surface temperature data and the Leben sea surface height product for 31 January 2002. During Deployments 2 and 4, the LC extended far north in the Gulf but remained east of the mooring location. The energetic nature of the LC during our study period gave us an excellent opportunity to investigate its effects on circulation at all levels of the water column.

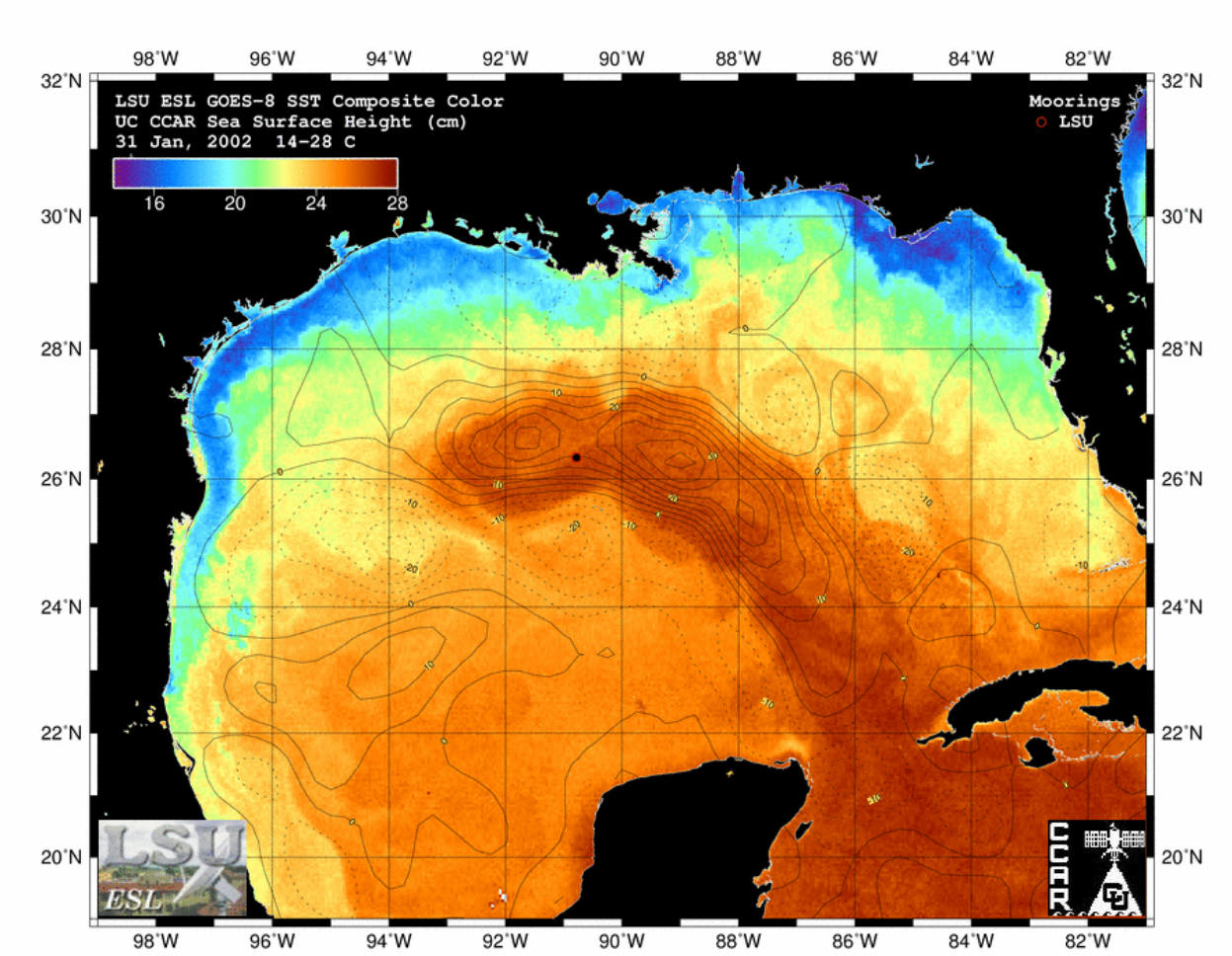

Figure 3. The extreme northwestward intrusion of the Loop Current is depicted on January 31, 2002, using a GOES night-time sea surface temperature composite superimposed with contours of sea surface height.

Key questions included the following:

(1) Do these new measurements at single, full water column moorings support the hypothesis that topographic Rossby waves influence near-bottom currents on the plateau and at the base of the Sigsbee Escarpment between 91º and 92º W Longitude?

(2) What is the nature of current variability (speed, direction, energy, coherence, energy density frequency) from surface to bottom on both the plateau and the continental rise?

(3) Can we discern any relationships between the occurrence of deep current events and major surface forcing factors (i.e. the LC, LCFE's, WCE's)?

These questions were used to guide the statistical analyses and the investigation of linkages between surface and bottom circulation processes.

1.2 Theory of Topographic Rossby Waves

Topographic Rossby Waves have been described by many scientists (see Hamilton (1990), Thompson (1977), Hogg (1981), Oey and Lee (2002)) as being a dominant source of variability in deep waters where the bottom topography can act as the restoring force for planetary type waves.

Rhines (1970) and Pedlosky (1987) both describe the theory of topographic Rossby waves. Topographic Rossby waves are transverse plane waves, (Hamilton 1990) which by definition require the particle velocity to be perpendicular to the wave vector, $\vec{K}$. The group velocity like the particle velocity is constrained to be perpendicular to $\vec{K}$ with only energy transported by topographic Rossby waves. Mizuta and Hogg (2004) recently showed that topographic Rossby waves can have a net transport of water. This gives the added possibility of TRW's contributing to the net deep circulation in the GoM.

The above ideas are important as current meters measure water particle velocity. Topographic Rossby wave signatures should show up as oscillations in the current velocity with periods between 10-100 days depending on the topographic slope and stratification.

Figure 4 shows an example of a down slope wave vector at Deployment 3 and 4 and an up slope wave vector at deployment 1 and 2. The wave vector direction is defined as perpendicular to the principal axis (Pickart 1995). The principal axis is determined from the principal angle of the variance ellipse at each level (Emery and Thomson 1997). The wave vector referenced by θ, is measured in a clockwise direction with respect ∇h, the bottom slope in the direction of increasing depth, as shown by Oey and Lee (2002). As a side, Pedlosky (1987) showed that the phase velocity will always have a component in the negative x direction, with the phase velocity being either parallel or anti-parallel to the wave vector.

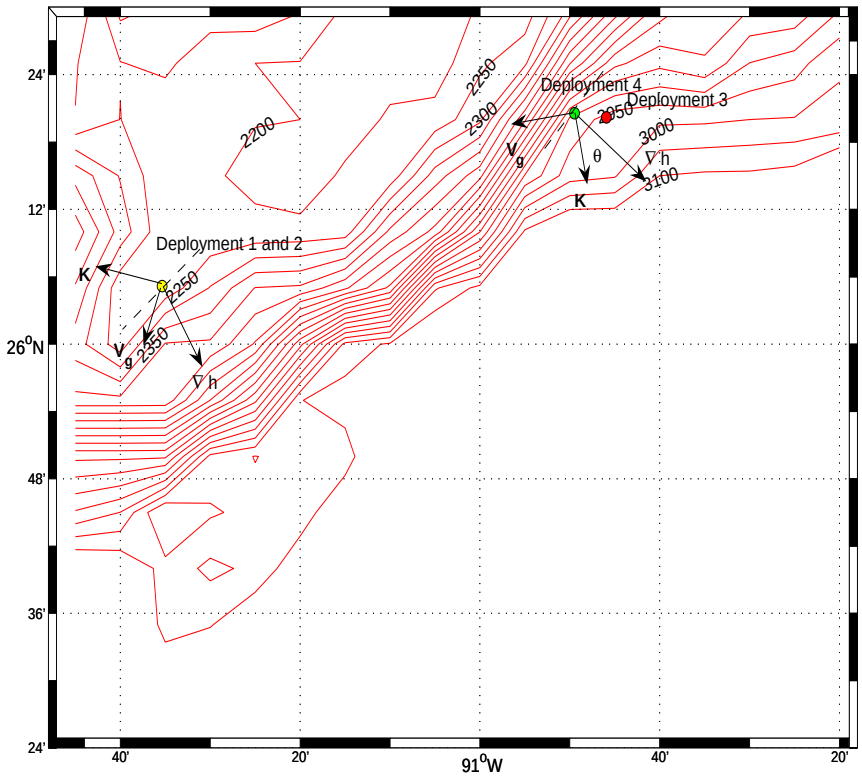

Figure 4. Bathymetry with TRW references.

Topographic Rossby waves are columnar, being nearly barotropic over the bottom 1500 m of the water column with the ambient vorticity of the bottom slope acting as the restoring force. Topographic Rossby waves are quasi-geostrophic which allows some energy transfer in the direction of ∇h , but the majority of the energy is contained along the isobaths. The amplitudes of oscillation should show a decrease with height and are referred to as bottom trapped (Rhines1970).

The following coupled equations show the dispersion relation for a TRW; see (Oey and Lee 2002).

$$\mu^2 = (K^2 + \beta k / \sigma)(N / f)^2 \quad (1)$$

$$\mu \tanh(\mu z) = \mathrm{N}^2 / (\sigma f)(\vec{\mathrm{K}} \times \nabla \mathrm{h})_z \quad (2)$$

In the above equations z is the water depth, N is the Brunt-Väisälä frequency, f is the Coriolis parameters using the β-plane assumption and $\vec{K}$ is the wave number vector in the east, north (x,y) coordinates. The wave frequency is σ (in radians/second) and 1/μ is the vertical trapping scale for TRW's. If the effects of bottom topography dominate the restoring force,

$\beta_{topo}/\beta >> 1$, then equation (1), can be simplified to

$$\sigma = |\nabla h| N \sin(\theta) \quad (3)$$

where θ is the angle between the wave number vector $\vec{K}$ and ∇h is defined in the direction of increasing depth (Oey and Lee, 2002).

In Deployment 3, $\beta \sim 2x10^{-11}$ $m^{-1}s^{-1}$, β_{topo} defined as $f|\nabla h|/h$ is equal to $5.16x10^{-10}$ m^{-1} s^{-1} giving the ratio β_{topo}/β equal to 25. Since this ratio is >>1, TRW's will be dominant at this location as compared to planetary Rossby waves and equation (3) will be valid. The value of θ varies from $0 < \theta < \pi/2$ for $\vec{K}$ down slope and $\pi/2 < \theta < 0$ for $\vec{K}$ up slope. Thompson (1977) further shows that $\sigma/k < 0$ confines the phase velocity to be left of the upslope gradient. As an example, in Deployment 3 the principal axis at z = -2578 m was found to be 46.2^o as measured counter clockwise from the east. This defines the wave vector $\vec{K}$ with a clockwise rotation of $\theta = 7^o$ from the steepest gradient of the slope. The maximum gradient of the bottom topography at Deployment 3 was estimated from Smith and Sandwell (1997) 1 km bathymetry to be $\nabla h = 0.023$. An average value for the Brunt Väisälä frequency of N = 0.0005 Hz was determined from a CTD cast taken at the beginning of Deployment 3 for the bottom 500 m of the water. The period of oscillation for a TRW using the above parameters (equation 3) should be near 52 days. Both spectral and wavelet analysis show a weak 51 day signal in the first half of the Deployment 3 at z = - 2578 m, see Figure 42 and Figure 43.

The minimum period of a TRW occurs when $\theta = \pi/2$ or $\vec{K}$ is parallel to the isobaths. In the spectral analysis below, it is will be seen that there is very little energy for periods less than 10 days. A six day minimum period was found in Deployment 3.

To determine the existence of topographic Rossby waves the following criteria are examined.

1. Spectral energy peaks between 100 days and 10 days
2. Motions of waves being coherent (columnar) in the bottom 1500 m
3. Spectral amplitudes of kinetic energy increasing with depth with the exception of the bottom current meter.
4. Variance ellipses for high frequency oscillations that are orientated perpendicular to the isobaths while low frequency oscillations being oriented parallel to the bathymetry.

To test for TRW's, spectral analysis is used to verify the first three criteria. Topographic Rossby waves as shown above should have a period between 6 and 100 days. Multiple methods of spectral analysis then determine the robustness of the spectral signal in this frequency range. Univariate along with cross-spectral analysis are used to analyze the lower layer (bottom 1500 m) barotropic aspect of TRW's by comparing the amplitudes of different current meters at a given period. Wavelet analysis is used in conjunction with spectral analysis. Wavelet analysis has the advantage of isolating a signal in time. Deployment 4 overlaps with SAIC current meters allowing the use of more than one current meter to calculate group velocity, phase direction and the wavelength. Bower and Hogg (1991), Johns and Watts (1986) and Thompson and Luyten (1976) show examples of the frequency dependence on the principal axes relative to the bathymetry

2.0 MEASUREMENTS AND METHODS

2.1 Data Processing

For all Deployments, 1-2 hours of data were removed after the mooring was deployed and 1-2 hours of data were also removed just before the time the mooring was released. All times are in GMT, the depths are in meters with all velocities in cm/s.

For all the current meters, ADCP and Aanderaa, the sample interval was set to one hour so no time averaging was done. The Seacat sample interval was 30 minutes. Since most physical processes that were analyzed were low frequency, little high frequency filtering was performed. If any data was filtered, MATLAB was used and a 6^{th} order, 40 hour Butterworth digital filter was applied. This 40 hour data was then sub sampled to 12 hours.

ADCP data was averaged in the vertical from data that was sampled at 4 meters for the 150 kHz, and 8 meters for the 75 kHz ADCP. Both ADCP's were combined then sorted by depth. Next all ADCP bins that fell between 40 m and 60 m were averaged to become the 50 m ADCP data. This 50 m ADCP data contained both 150 kHz and 75 kHz data but no Aanderaa data. All ADCP bins, for every hour, are corrected for blow over by the nearest pressure gauge. This depth was then double checked with Surface.exe by RDI. A summary of the location, dates of deployment, instrument types, depths and percent of good data returned are shown in Table 1 and Table 2.

Table 1

LSU Deep Gulf Moorings Deployments 1 and 2

Mooring Lat. Long. Date of deployment	**Instrument Depth (m)**	**Instrument Type (SN)**	**Percent good data return**	**Mooring Lat. Long. Date of deployment**	**Instrument Depth (m)**	**Instrument Type (SN)**	**Percent good data return**
Deployment 1	133	150 ADCP (150)	100	Deployment 2	162	150 ADCP (150)	100
	143	Aanderaa (10258)	100		172	Aanderaa (10258)	100
26º 05.171 N	145	Microcat (1331)	100	26º 05.5 N	174	Microcat (1331)	100
91º 38.354 W	673	75 ADCP (75)	100	91º 39.394 W	753	75 ADCP (75)	100
	675	Microcat (1332)	100		755	Aanderaa (10194)	100
02/16/00-	678	Aanderaa (10194)	100	07/30/00-	758	Microcat (1332)	100
07/29/00	893	Aanderaa (10189)	100	05/05/01	973	Aanderaa (10189)	100
	1016	Microcat (1334)	100		1073	Microcat (1334)	100
	1143	Aanderaa (10255)	100		1223	Aanderaa (10255)	100
	1381	Microcat (1337)	100		1373	Microcat (1337)	100
	1393	Aanderaa (10195)	100		1473	Aanderaa (10195)	100
	1643	Aanderaa (10256)	100		1723	Aanderaa (10256)	100
	1893	Aanderaa (10259)	99		1973	Aanderaa (10192)	100
	2133	Aanderaa (12702)	100		2213	Aanderaa (12702)	100
	water depth 2142 m				water depth 2223 m		

Table 2

LSU Deep Gulf Moorings Deployments 3 and 4

Mooring Lat. Long. Date of deployment	**Instrument Depth (m)**	**Instrument Type (SN)**	**Percent good data return**	**Mooring Lat. Long. Date of deployment**	**Instrument Depth (m)**	**Instrument Type (SN)**	**Percent good data return**
Deployment 3	136	150 ADCP	100	Deployment 4	155	150 ADCP	0
	146	Aanderaa (10258)	100		165	Aanderaa (10258)	86
26º 20.2295 N	148	Microcat (1331)	0	26º 20.56 N	167	Microcat (2447)	100
90º 45.9343 W	614	75 ADCP (75)	100	90º 49.467 W	657	75 ADCP	100
	633	Aanderaa (10194)	100		662	Aanderaa (10194)	100
07/31/01-	635	Microcat (1332)	98	04/17/03-	664	Microcat (1332)	100
06/02/02	878	Aanderaa (10189)	100	06/10/04	907	Aanderaa (10189)	46
	978	Microcat (1334)	100		1007	Microcat (1334)	100
	1128	Aanderaa (10255)	100		1157	Aanderaa (10255)	100
	1278	Microcat (1337)	100		1307	Microcat (1337)	100
	1378	Aanderaa (1378)	100		1407	Aanderaa (10195)	100
	1628	Aanderaa (10256)	100		1657	Aanderaa (10256)	100
	1630	Microcat (1691)	100		1659	Microcat (1691)	100
	1878	Aanderaa (10192)	100		1928	Aanderaa (10192)	100
	2128	Aanderaa (12702)	100		2178	Aanderaa (12702)	100
	2130	Microcat (2130)	100		2180	Microcat (1693)	100
	2578	Aanderaa (12750)	100		2628	Aanderaa (12750)	100
	2878	Aanderaa (12768)	100		2928	Aanderaa (180)	100
	water depth 2956 m				water depth 3028 m		

2.2 Spectral Methods

The major signals in all deep water deployments were determined by multiple methods of spectral analysis. As shown in Figure 5, both time domain and frequency domain analysis were used to determine if a signal was robust. A robust signal was defined as a signal that was present in all spectral methods along with being statistically significant. A signal that was weak was defined as one that was present in a majority of spectral methods, but may not be significant at the 95 % confidence interval. In the time domain an autocorrelation analysis was performed as a first order look at possible signals in the time series. The autocorreletation plots show an approximate 95 % confidence interval (Chatfield 1996). Four frequency domain spectral analysis methods were used to test for robustness of the spectral signals. All time series were averaged over 24 hours before any spectral analysis was performed. Each spectral method was tested on hourly data, 40 HLP data, along with data rotated parallel and perpendicular with the bathymetry. All methods yielded the same results. The first frequency domain method used was the periodogram in variance-preserving format. Reference to this method can be found in Emery and Thomson (1997). This is the most basic method of spectral analysis, and is used by the majority of oceanographers. The periodogram is a good reference spectral method, but is not an ideal estimator of the spectrum (Percival and Walden 1993). Since the periodogram is not an ideal estimator of the spectrum, other methods were used to improve the spectral estimation. All methods used in this analysis can be found in Percival and Walden (1993) along with McKone (2003). The other three methods consist of Welch's method or WOSA, Welch's overlapped segment averaging spectral estimator the MTM or Multitaper spectral estimator and an auto regressive or AR spectral estimator using Burg's method. Three out of four of these spectral methods are non parametric, with the AR or autoregressive method being parametric. The AR method, being parametric, is a good check of the robustness of a signal as it uses a completely different method in determining a spectral signal.

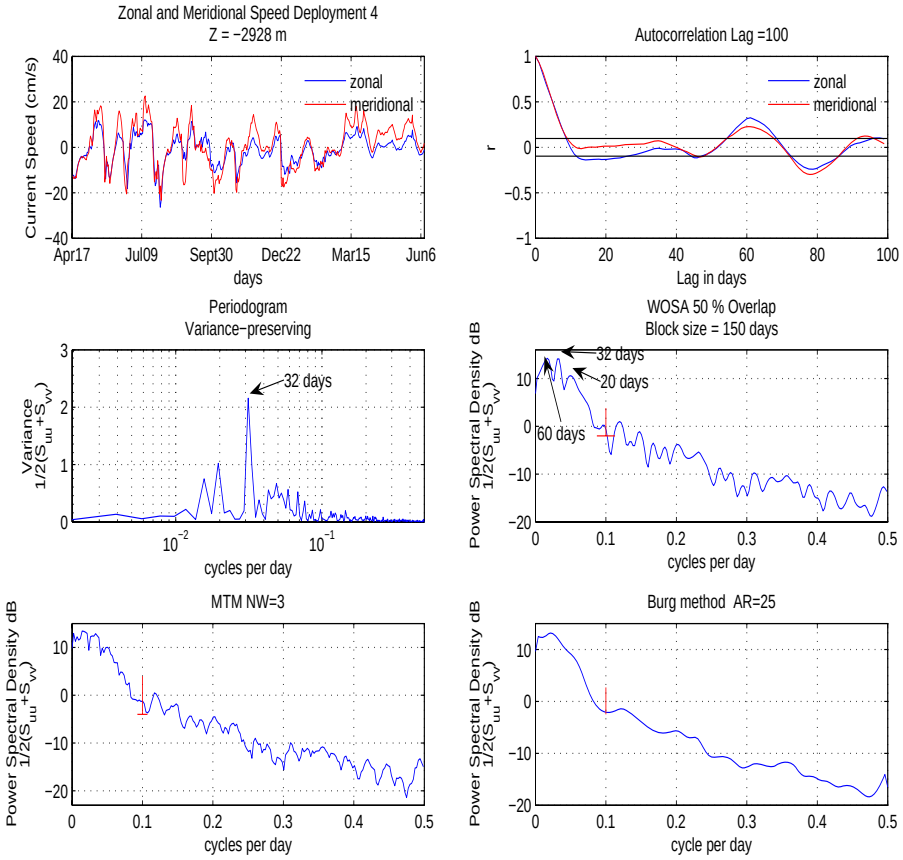

Figure 5. Multiple methods of spectral analysis z = -2928 m Deployment 4.

Confidence intervals of 95 % are shown on all spectral plots except the periodogram, which is variance preserving. Also shown on all non-parametric spectral plots is an estimate of the bandwidth. This is important as increasing the bandwidth increases the number of degrees of freedom in the spectral estimate which in turn reduces the variance of the spectral estimate. It must be kept in mind that significant bias can be introduced when the bandwidth is increased. Spectral analysis is a constant play between bandwidth and the variance of the spectral estimator. Wavelet analysis was also used as a check of the time series signals (Torrence and Campo, 1998). Wavelet analysis has the advantage of showing the temporal extent of a given signal. Some interesting patterns show up using Wavelet analysis on the LSU deep water moorings.

Along with the above univariate analysis, bivariate analysis was performed on each deployment. Welsh's overlapping segment spectral analysis method was used in the bivariate analysis (Emery and Thomson, 1997). Plots of kinetic energy, ½ $(u^2 + v^2)$ at multiple depths were shown along with the cross-spectral estimates of the zonal (east, west), meridonal (north, south), and kinetic energy $1/2(S_{uu}+S_{vv})$ spectrum. S_{uu} is defined as the cross-spectrum of the zonal velocity at two different depths and S_{vv} is the cross-spectrum of the meridonal velocity at two different depths. The Gulf of Mexico can be thought of as a three layer system (Hamilton, personal

communication; Sturges, 2005). The cross-spectral analysis took this idea into account by comparing the spectrums at a near surface, mid layer and a near bottom current meter.

Rotary spectral analysis was also performed on different frequency bands (Emery and Thomson, 1997). Part of the analysis entailed looking for TRW signatures in the current meter time series. Topographic Rossby waves are transverse and should show little or no rotation. Rotary wavelet analysis was also performed to see if any patterns of rotation occurred throughout the time series (Liu and Miller, 1996).

2.3 Satellite Remote Sensing

Both passive and active satellite sensors were used to characterize the presence and movement of water masses at the mooring site and surrounding region, especially to the east. The circulation features of most concern included the Loop Current (LC), warm-core anticyclonic eddies (WCE's), cold-core cyclonic eddies (CCE's) and Loop Current frontal eddy (LCFE) cyclones. Interpretation of the surface currents in particular required frequent updates on the position of these dynamic and rapidly varying flow features.

Satellite data from passive radiometers were received in real-time at the LSU Earth Scan Laboratory (ESL), a receiving station for both polar orbiter data (NOAA AVHRR, SeaWiFS, MODIS, Oceansat-1 OCM) and geostationary data (GOES-8 and GOES-12). Image processing (data calibration, navigation, registration, calculation of geophysical products) was performed using SeaSpace Terascan™ software. In addition, sea surface height measurements were obtained from Dr. Robert Leben, University of Colorado. The authors have made extensive use of satellite products developed with funding from a separate CMI project which focuses on developing new remote sensing products to improve the interpretation of Gulf circulation. A key component of that study has been the integration of GOES sea surface temperatures (SSTs) with multi-sensor sea surface height (SSH) data, which is posted to an LSU ESL web page daily (http://www.esl.lsu.edu/research/CMI-GOES). In this report, we have used this integrated product extensively.

Satellite imagery of sea surface temperature has provided a means of detecting the LC and WCE's for several decades (see for example, Vukovich et al., 1979; Huh et al., 1981; Paluszkiewicz et al., 1983; Maul et al., 1984; Vukovich and Maul, 1985; Huh and Schaudt, 1990; May et al., 1993; Walker et al., 1996; Walker et al., 2003; Walker et al., 2005, Walker et al., 1993) During the non-summer months, the LC, the WCE's, and LCFE's can be detected in the absence of major cloud cover using the mid-IR and thermal IR channels. During the warmer months of the year however, surface thermal contrast is weak across the Gulf and water vapor loads are high, making it extremely difficult to detect ocean features by temperature signals. Nevertheless, significant advances have been made in developing new techniques to resolve ocean features under these conditions. In the past decade, several ocean color sensors (SeaWiFS, MODIS, Oceansat-1 OCM) have been launched, providing the capability of detecting chlorophyll *a* and other pigments in the surface ocean. Muller-Karger et al. (1991) demonstrated the usefulness of ocean color data in the detection of Gulf eddies. The WCE's exhibit low chlorophyll *a* except along the margins where upwelling can occur. In contrast, the CCE's

exhibit high chlorophyll *a* due to the presence of the upwelling of nutrients within their centers, which stimulates phytoplankton blooms. For this study, imagery from the Oceansat-1 OCM sensor proved most useful due to its superior spatial resolution (360 m compared with 1 km for MODIS and SeaWiFS). Chlorophyll *a* values were estimated using the 490 nm (blue) and 555 nm (green) channels and applying an OC2 type algorithm (O'Reilly et al., 1998).

The second technique that has significantly improved the detection of Gulf features of interest is the use of GOES-8 and GOES-12 GVAR data, available every 30 minutes with a 4x4 km pixel (Menzel and Purdom, 1994; Legeckis et al., 2002). Walker et al. (2003) developed a new methodology using the mid-IR channel and a night-time de-clouding scheme which has led to significant improvements in the detection and tracking of Gulf features even during summer. The 3.7 μm channel is less affected by atmospheric water vapor (Huh et al., 1981; May et al., 1993; Walker et al., 1993) so that its use has substantially improved success in feature detection in the high humidity conditions often prevalent over the Gulf from May through September. The image frequency provides the ability to composite data over a relatively short time period, to provide nightly updates on feature location. A night-time compositing scheme which retains the warmest pixels over a 10-hour period at night effectively eliminates most of the cloud contamination present in the original images (Walker et al., 2003). The creation of image animations has enabled the visualization of feature motion, which has been a major breakthrough in resolving the movement of LCFE's along the outer margin of the LC and WCE's (Walker et al, 2003).

Significant advances in satellite altimetry have also been made as the number and accuracy of altimeters has increased in recent years (Leben et al., 2002; Leben, 2005). This study utilizes gridded and interpolated SSH data from Leben, which has been reformatted for display over the GOES SST image composites. Altimeters included in the Leben gridded dataset include TOPEX-Poseidon, ERS-2 Geosat Follow-On, Jason-1 and Envisat. A detailed description of the techniques used in the altimeter data processing can be found in Leben et al. (2002) and Donohue et al. (2006). These SSH data, obtained by active microwave radars, provide all-weather day and night data which provides the position of oceanic highs (LC, WCE's) and lows (CCE's, LCFE's). However, infrequent repetition at times limits this technique's ability to track rapidly moving features, such as the LCFE's.

3.0 MOORING LOCATION 1, DEPLOYMENTS 1-2

3.1 Initial Conditions, Major Ocean Events, and CTD Data

In this section, water column currents and temperature are discussed in relationship to the large-scale movement of Gulf water masses as revealed in satellite data. To aid the discussion, color-enhanced time series of currents and temperature in the upper 1200 m are depicted in Figure 6. Time-series of current speeds and current vectors are shown in Figure 7 and Figure 8. Satellite SST/SSH data are shown in Figures 9-16.

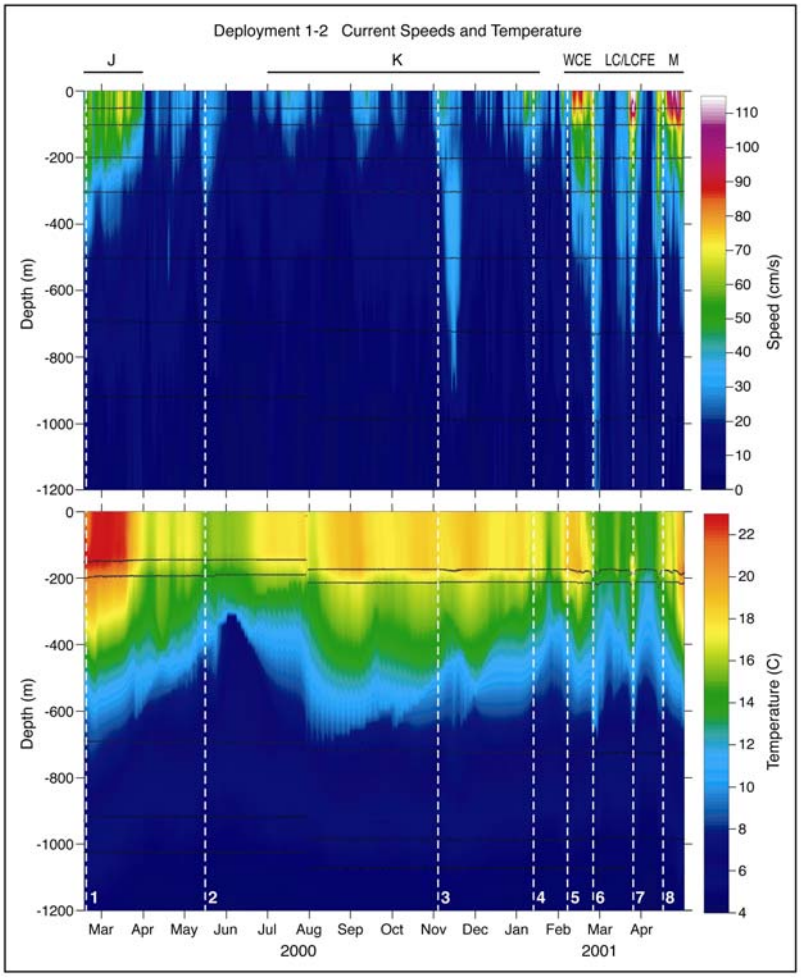

Figure 6. Color-enhanced LP current speed (cm/s) from 0-1200 m and temperature from 0-1200 m for Deployments 1-2. Vertical white lines depict times of events 1 to 8.

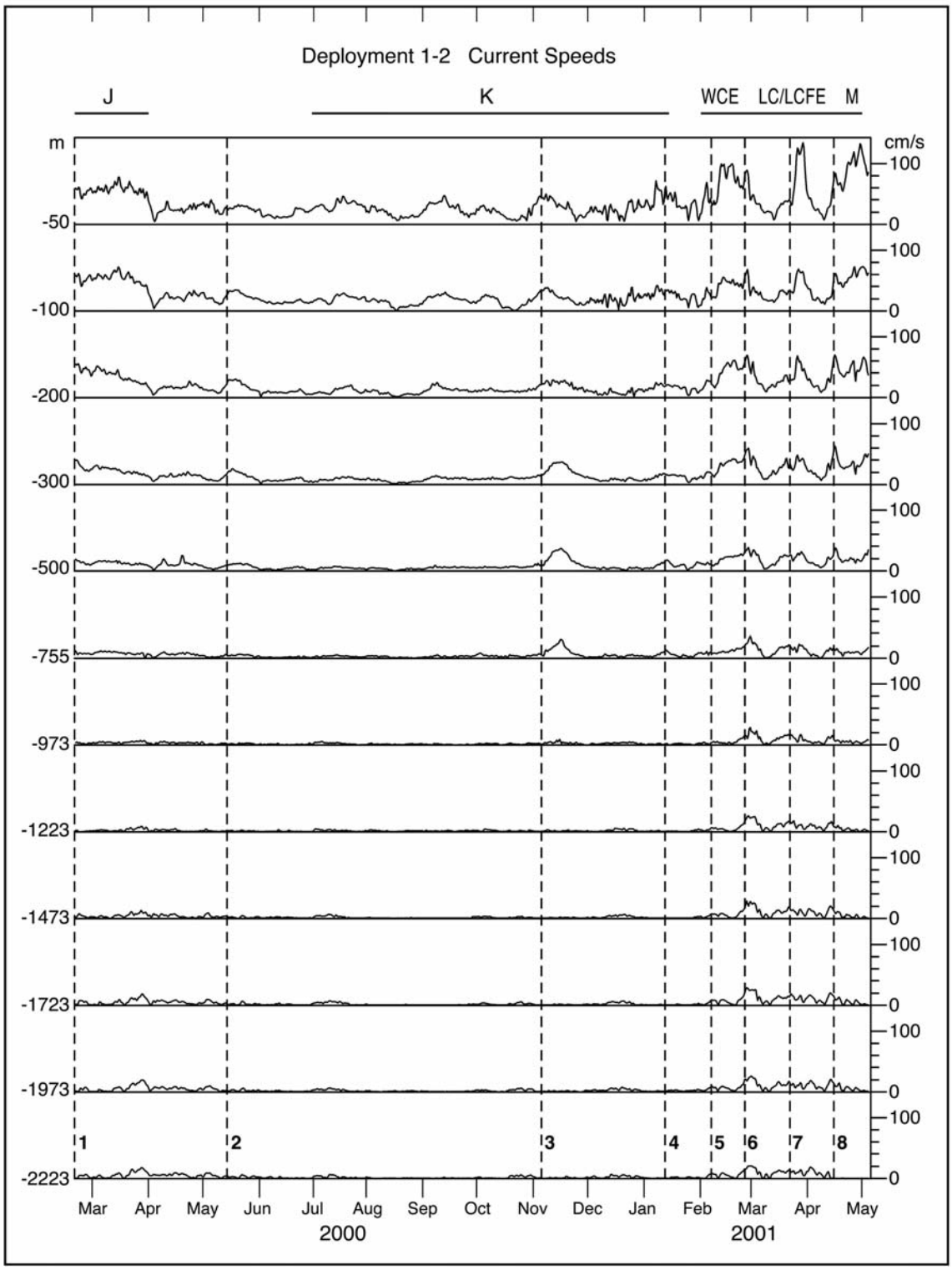

Figure 7. LP current speeds (cm/s) at 12 depths from near surface to near bottom for Deployments 1-2.

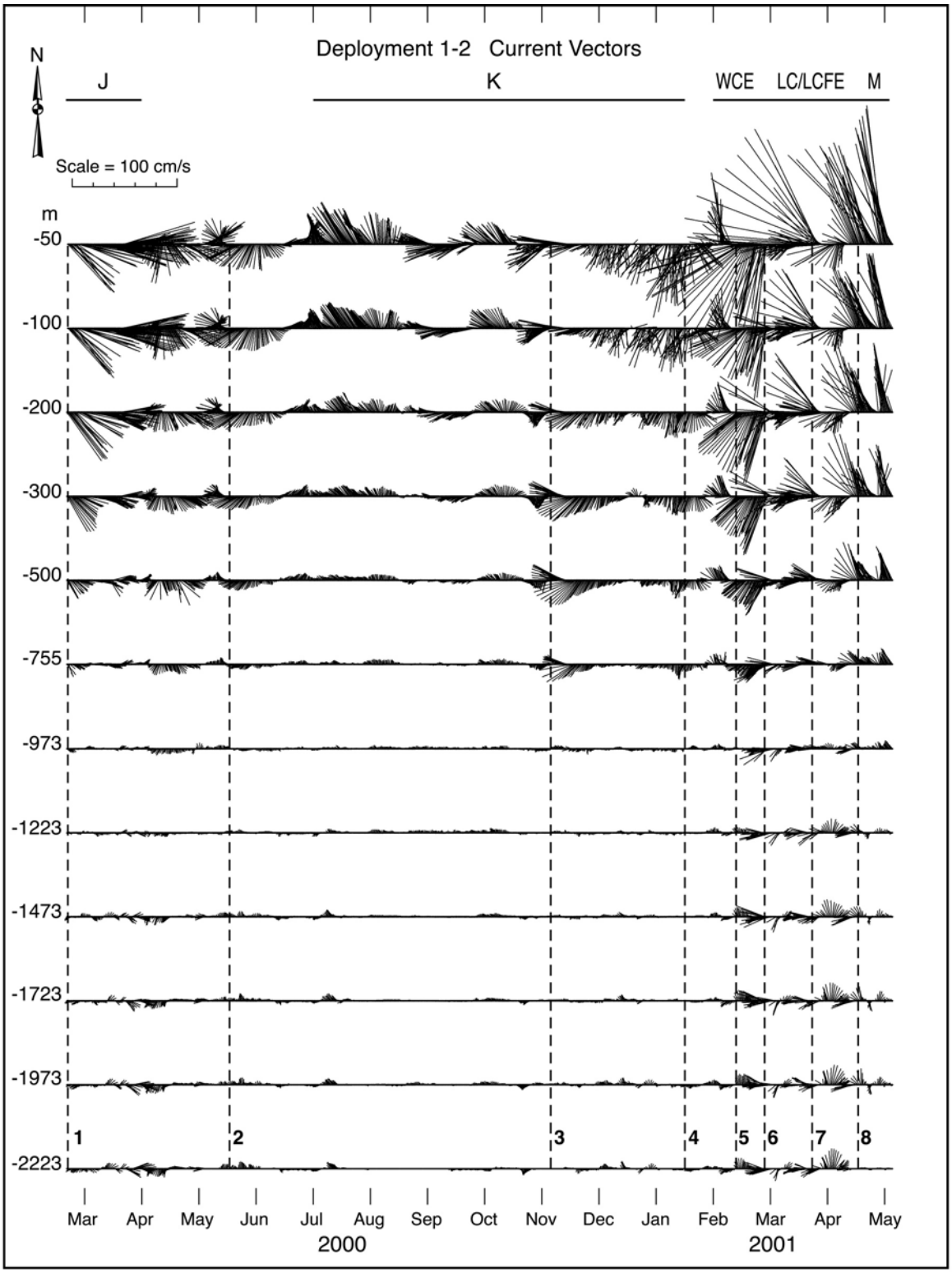

Figure 8. LP current vectors (cm/s) at 12 depths from near surface to near bottom for Deployment 1-2.

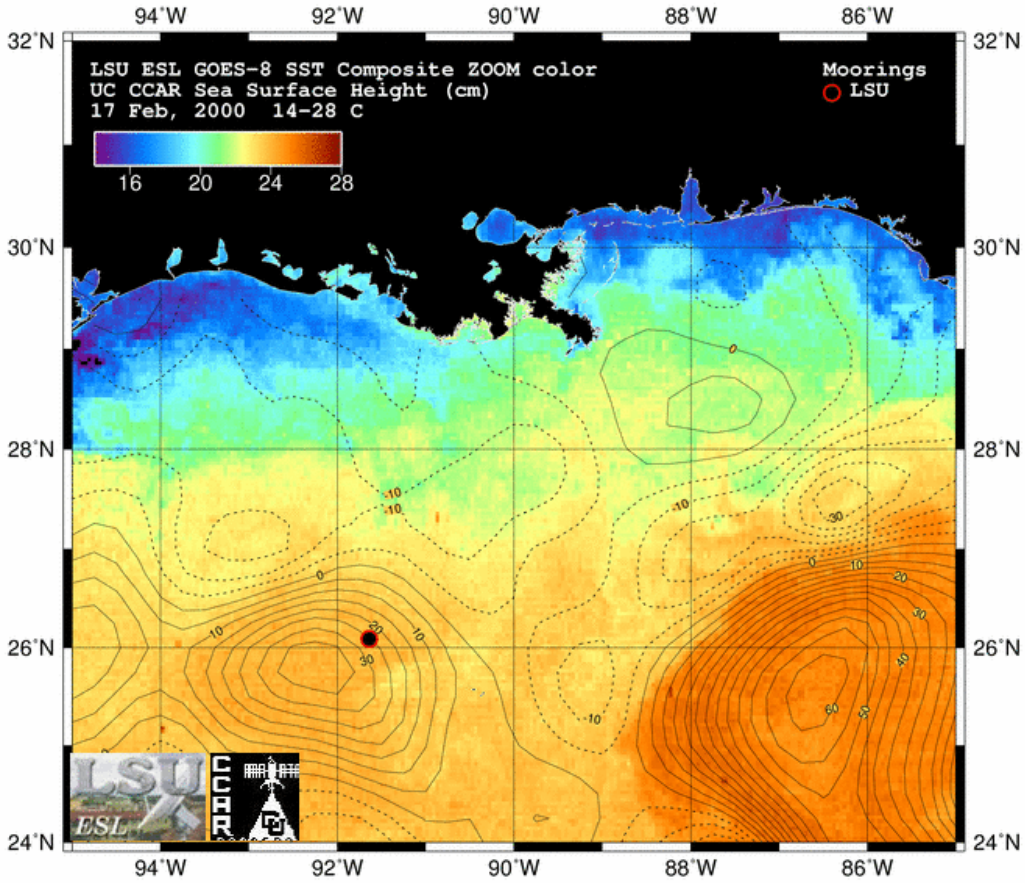

Figure 9. GOES night-time SST composites and SSH contours for Event 1 (17 February 2000).

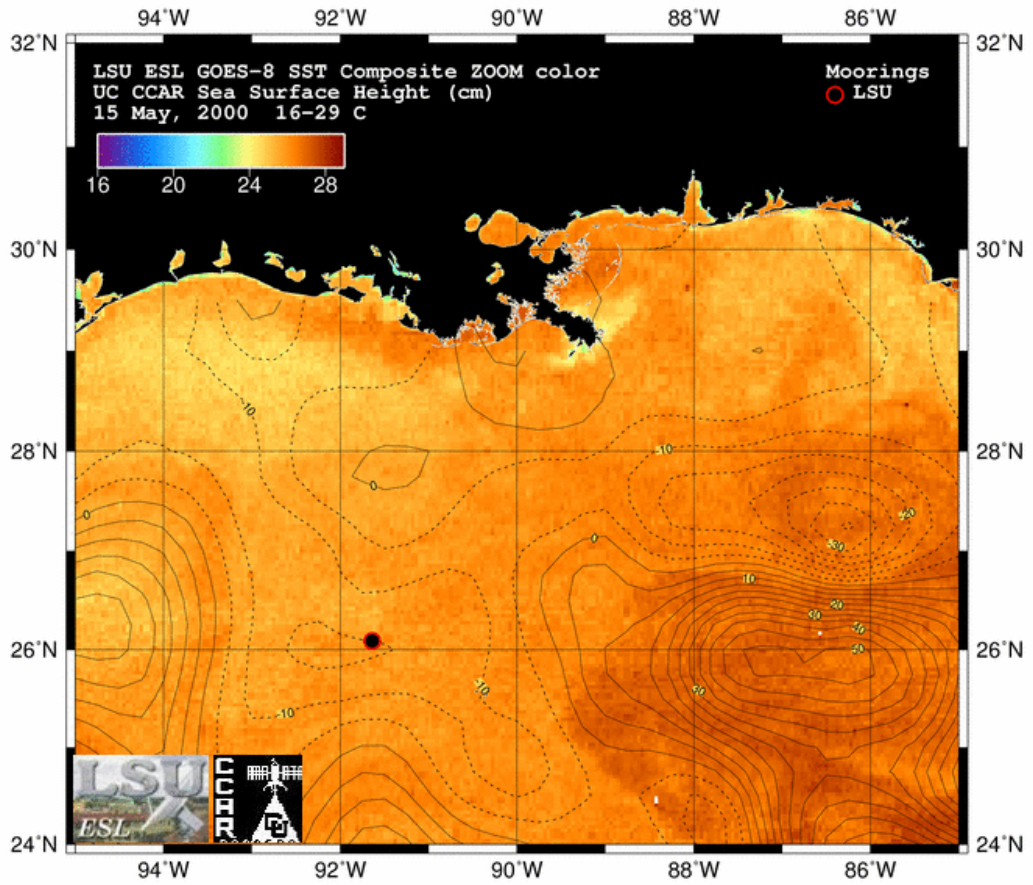

Figure 10. GOES night-time SST composites and SSH contours for Event 2 (15 May 2000).

The strongest current events occurred at the beginning and during the last three months of the 15-month deployment period, which ran from February 16, 2000 through May 5, 2001 (Figure 6-Figure 8). Remote sensing measurements of SST and SSH revealed that these events were mainly attributable to the influence of WCE's, which had separated from the LC, and associated cyclones including LCFE cyclones. Integrated SST/SSH imagery are used to identify the presence and movement of these features on selected dates of most relevance to the discussion. Image animations can also be accessed at the Earth Scan Laboratory web page (http://www.esl.lsu.edu/research/CMI-GOES/). The circulation events to be discussed are most easily visualized in this way.

The mooring was initially deployed north of the center of Eddy Juggernaut (J) at 26º 05.171' and 91º 38.354'on February 16, 2000 1143 LT, in 2226 m of water. The GOES SST/SSH composite depicts Eddy J and that the LC was about 200 km east of the eastern margin of Eddy J at this time (Figure 9, Event 1). The mooring location was chosen to be in a region with little bottom topography on the plateau landward of the Sigsbee Escarpment. Strong eastward currents (50-80 cm/s) and high water temperatures (22-23ºC) in the upper layer were experienced at the time of deployment (Figure 6-Figure 8). These conditions lasted through most of March, until Eddy J's effects diminished as it moved southwestward away from the mooring.

From mid-April through June 2000, cyclonic circulation was experienced at the mooring, a circulation regime that was bordered to the west and south by WCE's and to the east by the LC. Upper layer currents were generally southward and lower layer currents were relatively weak (Figure 6-Figure 8). The SST/SSH image of May 15, 2000 depicts this ~3 month circulation pattern near the mooring (Figure 10, Event 2). WCE K detached from the northwest margin of the LC in mid-June 2000. It began its approach towards the mooring in early July and it caused several weak surface current accelerations during its long life in this region, from July through December. The strongest and deepest high velocity event occurred during the first two weeks of November. Flow was westward as the eddy was positioned north of the mooring. During this event, near-surface currents reached 50 cm/s while at 755 m maximum current speeds reached 30 cm/s. Eddy K's position relative to the mooring site and the LC is shown on the image of 3 November 2000 at the approximate time of onset of relatively strong currents in the upper layer (Figure 11, Event 3). At the time of strongest flow, the mooring was situated between Eddy K and a well-developed cyclone south of the mooring. Eddy K finally moved west of the mooring in January 2001 (Figure 12, Event 4). Its final effect on the mooring occurred during the 2nd week of January when current speeds increased to 60 cm/s near the surface associated with increased LC and LCFE activity near the mooring. Note that temperatures from the surface to a depth of 600 m remained relatively high throughout WCE K's period of influence (Figure 6).

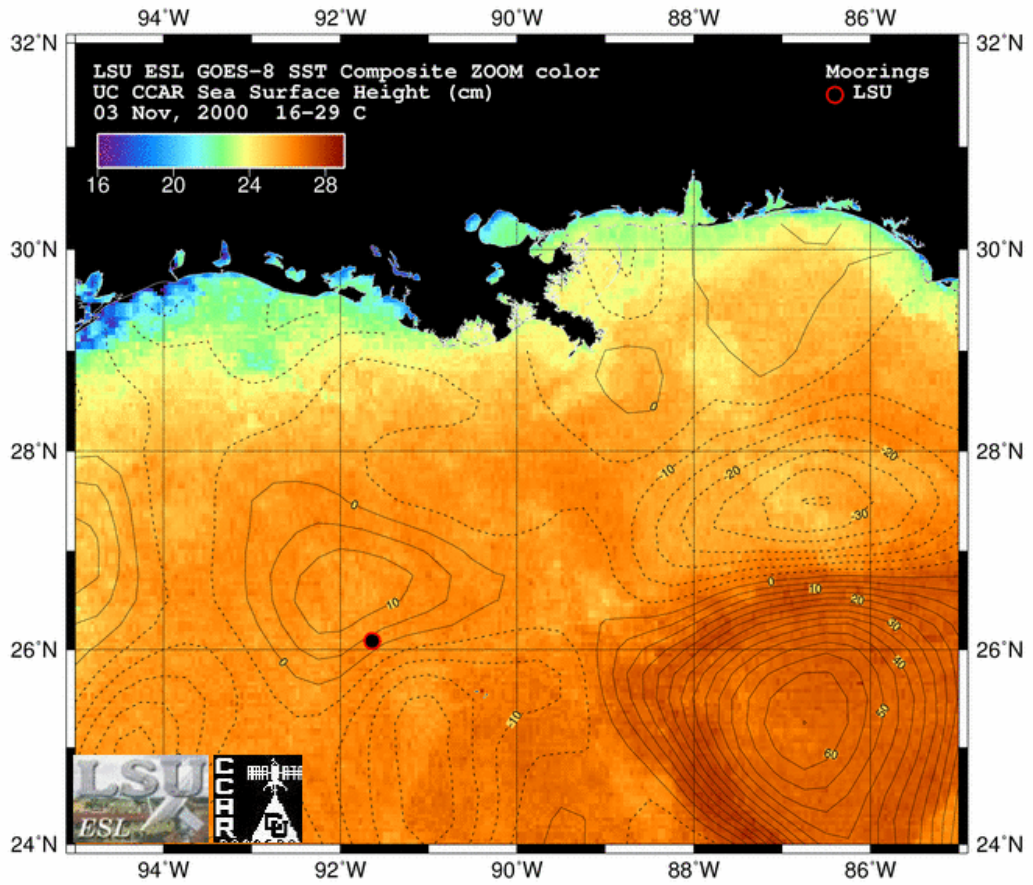

Figure 11. GOES night-time SST composites and SSH contours for Event 3 (3 November 2000).

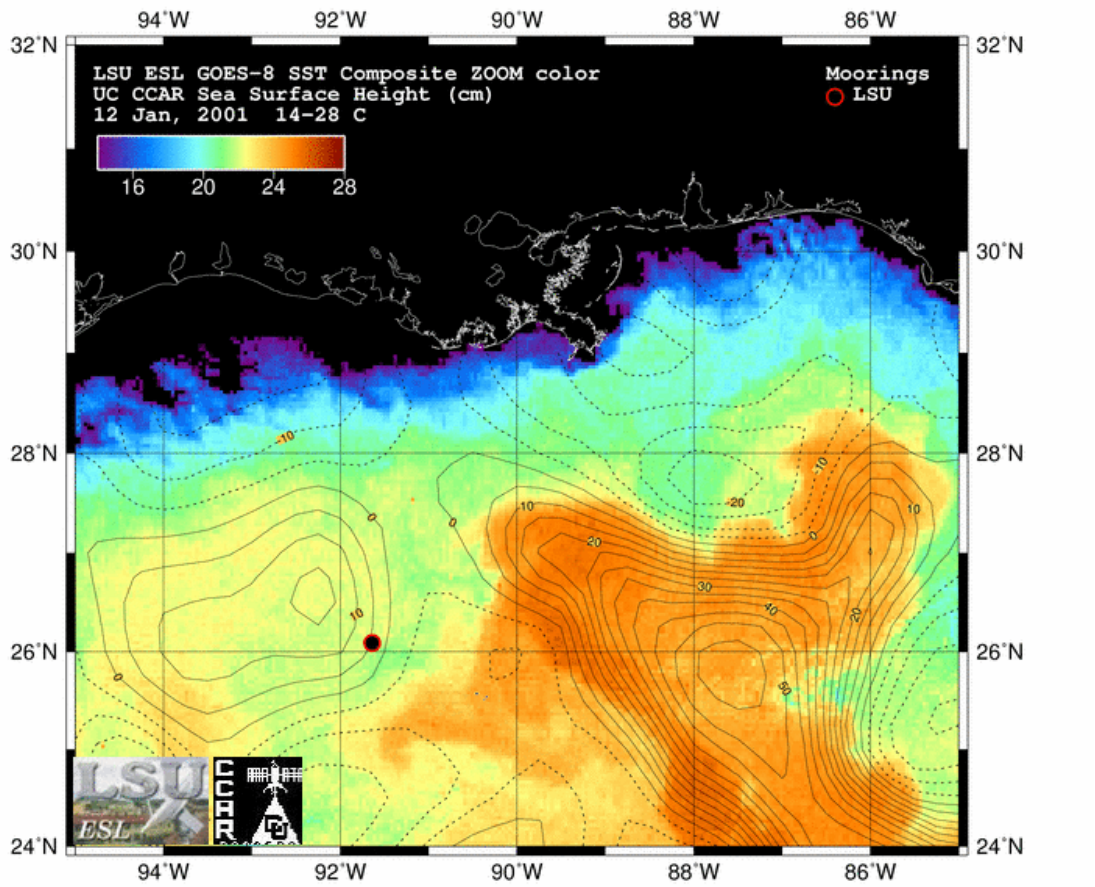

Figure 12. GOES night-time SST composites and SSH contours for Event 4 (12 January 2001).

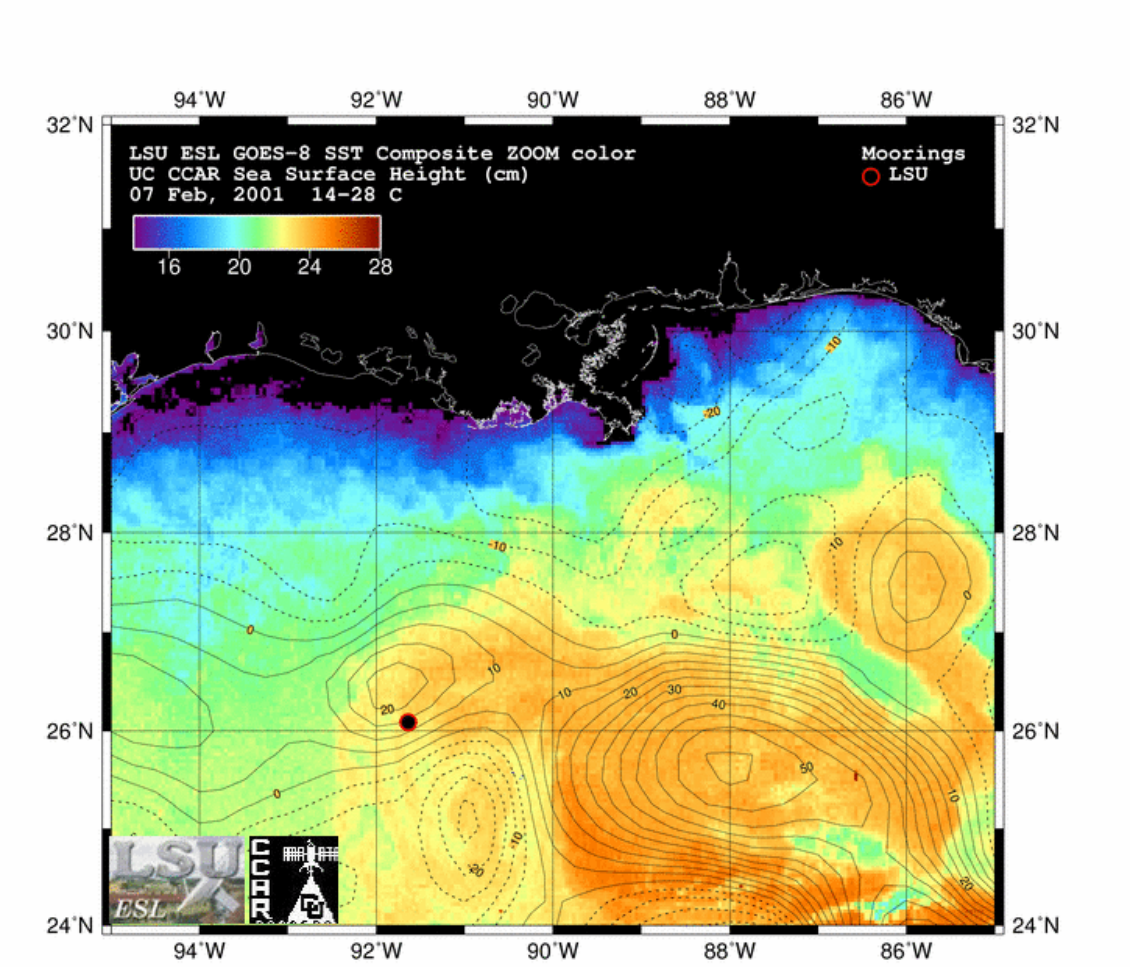

Figure 13. GOES night-time SST composites and SSH contours for Event 5 (7 February 2001).

The three most energetic upper layer current events occurred during February, March, and April 2001. Four satellite SST/SSH images (Figure 13-Figure 16, Events 5-8) were chosen to depict the time history of LC and eddy circulations near the times of the strongest currents as shown in Figure 6-Figure 8. Events leading up to the northward intrusion of the LC are first reviewed briefly. During late December 2000, the leading margin of the LC was positioned north of 27º N. During January 2001, LC meanders and LCFE's destabilized the LC as shown in the image of January 12 (Figure 12, Event 4). At the end of the month a small WCE (which was never named) was shed from the west margin of the LC. Although the larger Millenium Eddy came close to being shed at the end of January (Figure 12, Event 4), the separation was short-lived as the LC surged northwards to recapture it.

The first of the three strong current events within this active period occurred from February 11 to 28, when strong surface currents (> 50 cm/s) occurred as the small un-named WCE affected the mooring (Figure 13, Event 5). Flow in the upper water column was southwestward as the mooring was situated between the warm eddy and a cyclone to the south. Meanwhile east of the mooring, the LC surged rapidly northwestward again and on February 27 the imagery revealed a large LCFE approaching the region of cyclonic circulation (negative SSH) southeast of the mooring site (Figure 14, Event 6).

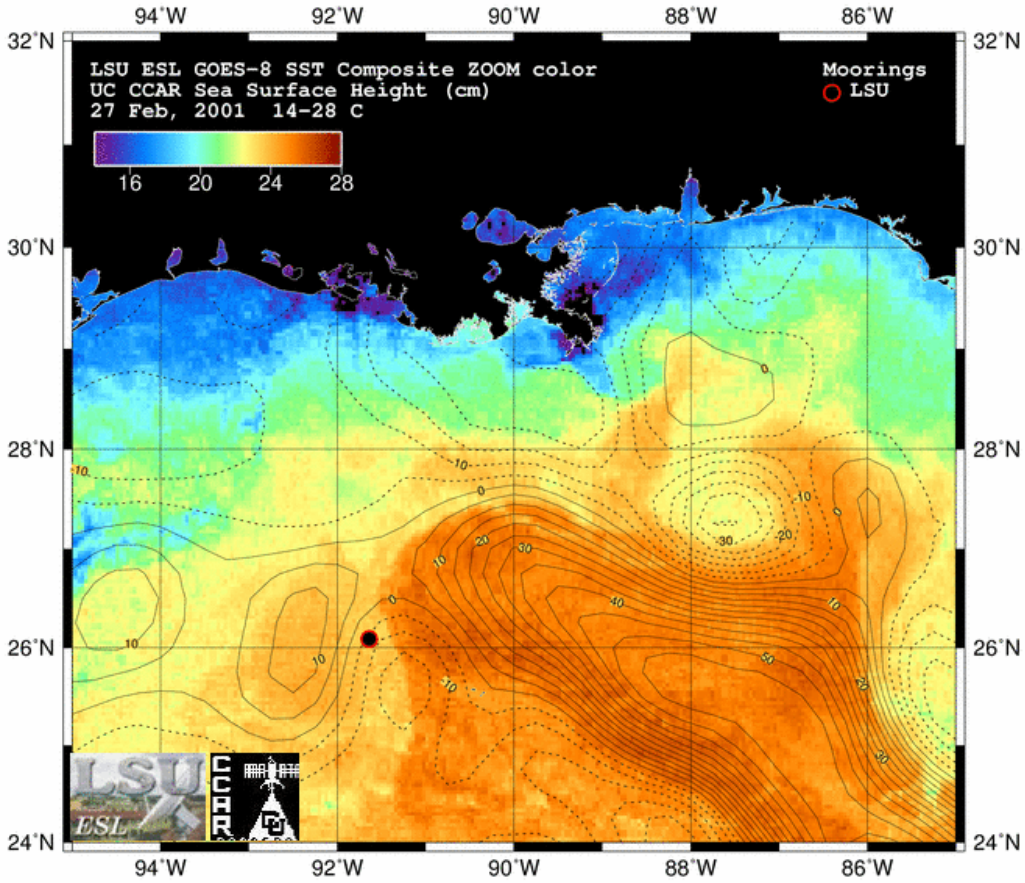

Figure 14. GOES night-time SST composites and SSH contours for Event 6 (27 February 2001).

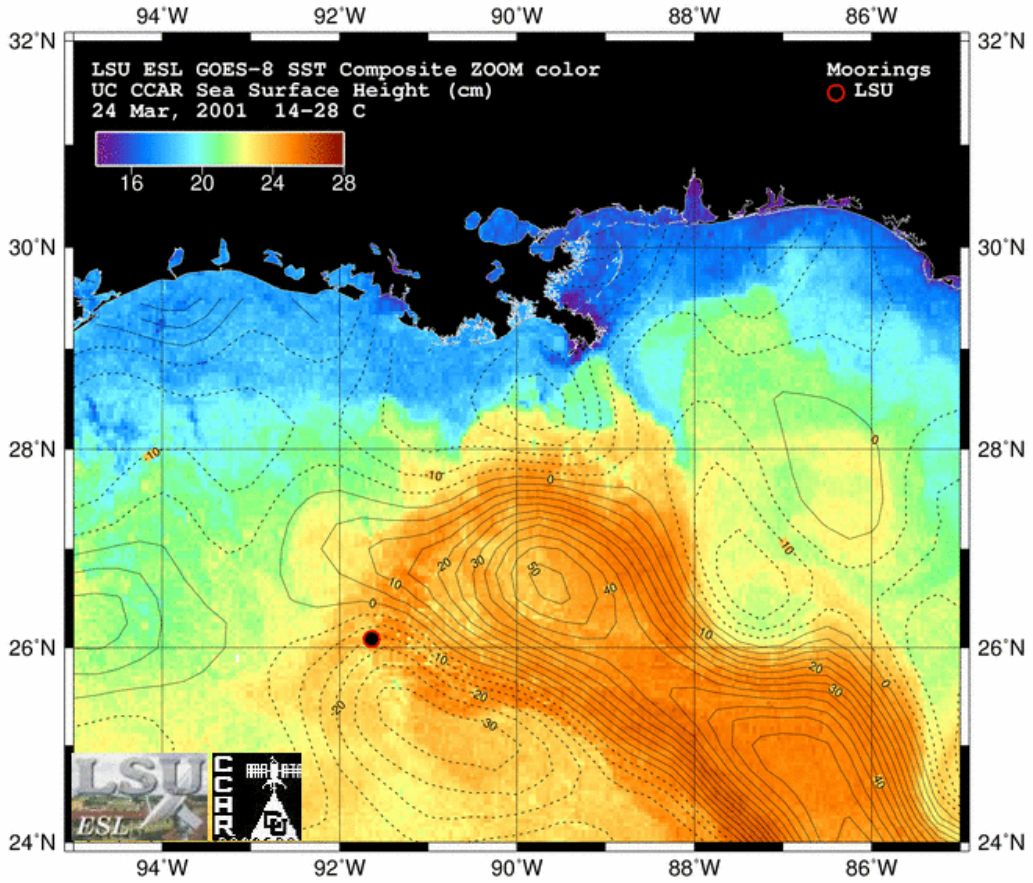

Figure 15. GOES night-time SST composites and SSH contours for Event 7 (24 March 2001).

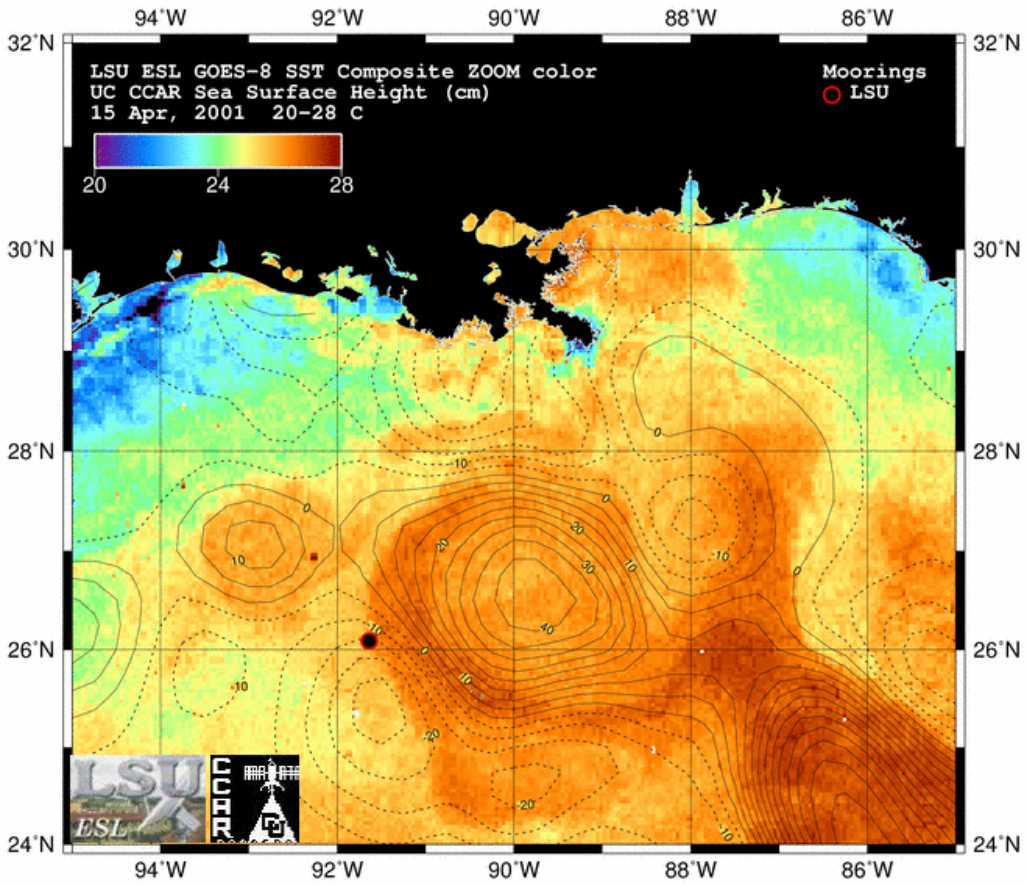

Figure 16. GOES night-time SST composites and SSH contours for Event 8 (15 April 2001).

Current speeds between 755 m and 2223 m increased to the deployment maxima at the end of February and early March (Figure 6-Figure 8), lagging the surface current accelerations. All current records below 50 m demonstrated velocity maxima in association with this energetic intrusion of the LC and associated LCFE cyclone. Surface flow was towards the southwest, as expected since the mooring was situated between the un-named warm eddy to its west and the intensifying cyclone. Flow at the bottom was also to the west and southwest. Time sequence GOES SST/SSH imagery revealed that, in this time frame, a LCFE moved northwestward over a deep cyclone that was clearly revealed in SSH data on February 27. Both the SST and SSH data indicate that the cyclonic feature, rather than the LC proper, was closest to the mooring site. However, the temperature data indicate a warming at depth coincident with the acceleration in flow throughout the water column in late February, suggesting that perhaps it was the LC or a filament of it that the mooring experienced. A rather unusual configuration of flow features characterized this event as the small warm eddy, the cyclone and the LC interacted within a small space of 100 km (Figure 14, Event 6). The temperature record (Figure 6) revealed that the short-lived increase in temperature was followed by a rapid decrease in water temperature within the water column from 200 to 700 m water depth, as the cold core cyclone moved over the

mooring soon after the current acceleration event. A maximum temperature change of 6ºC (from 20 to 14º C) was recorded over a few days at 174 m.

The LC continued to surge northward and by March 22 had reached 28º N, 90ºW. This second surface current event (> 50 cm/s) began March 24 and lasted about one week. During this time period, the mooring experienced northwestward currents exceeding 100 cm/s at the surface and decreasing to 50 cm/s at 300 m. The current acceleration was confined mainly within the upper 700 m in contrast to the preceding event. The mooring was situated between the LC and a developing LCFE cyclone at the time of strongest currents (Figure 15, Event 7). A modest acceleration in bottom flow was noted near the end of the surface event on April 1 (Figure 7, Figure 8). The temperature record again gave evidence for the intrusion of a cold core cyclone in late March over the mooring after the peak flow event (Figure 6).

The third event in mid-April (Figure 16, Event 8) began with weak acceleration through the water column as a large LCFE moved towards the mooring. Although this event was not as strong as that of late February it is distinctive in the record (Figure 7, Figure 8). It was followed by a sustained period of strong surface currents (~3 weeks) above 500 m water depth as Eddy M finally detached from the LC and moved westward towards the mooring. The mooring was recovered before the near surface currents subsided below 50 cm/s (Figure 6-Figure 8). Eddy M caused temperatures to rise within the upper 600 m of the water column at the end of the record (Figure 6). The temperature record (Figure 6) revealed the presence of three cold core cyclones that preceded each of the high velocity flow events which were experienced at the mooring. It would have been useful to have more detailed temperature records between 200 m and 600 m to better resolve the cyclones. It is also of interest that flow in the lower water column (1000-2200 m) experienced highest current speeds in association with the surface events, although not always at the same time. The strongest bottom current event in late February coincided in time with acceleration in surface flow associated with a developing LCFE cyclone.

3.2 Simple Statistics and Time Series Analysis

The 40 HLP vector plots showed coherence over the top 800 m of the water column (Figure 8). The currents in the lower 1000 m were very weak with the current meters reading at their lower limits. The bottom showed good coherence over the bottom 1000 m but little coherence with the surface. In the hour averaged vector plots there were continuous inertial currents seen at the 500 and 700 m level (not shown). A typical salinity, temperature profile, for Deployments 1 and 2 is shown in Figure 17.

The Brunt Väisälä frequency calculated from these profiles averaged over the bottom 500 m was 0.0003 Hz. As discussed by Hoffmann and Worley (1986), the salinity maximum near 220 m is characteristic of Subtropical Underwater, and the salinity minimum at 900 m is representative of Antarctic Intermediate water. The bottom 1000 m of isohaline water is upper North Atlantic Deep Water distinguish by the 34.97 PSU signature. Hoffmann and Worley (1986) described the GoM in terms of three layers, each characterized by a different water mass.

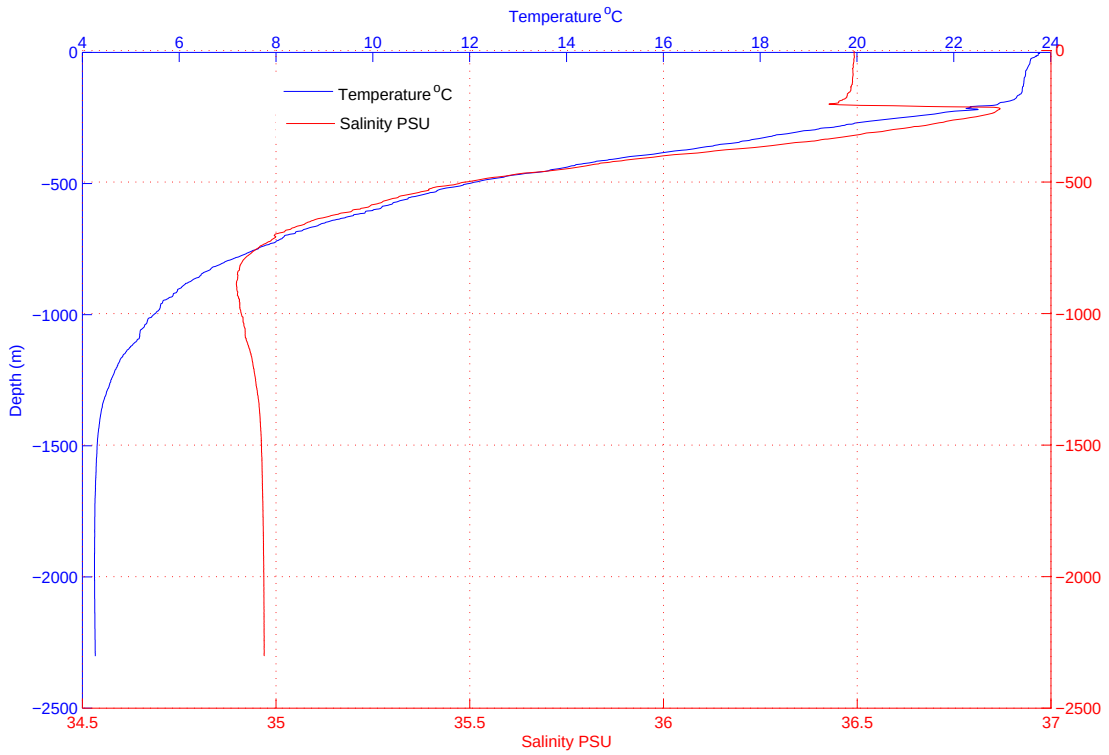

Figure 17. Temperature salinity profiles for Deployments 1 and 2.

Table 3

Mean, Maximum, and Minimum Velocities Deployments 1 and 2

Depth (m)	Mean (cm/s)			Max (cm/s)			Min (cm/s)			Standard Deviation (cm/s)		
	U	V	Speed	U	V	Speed	U	V	n	U	V	Speed
-50	-7.29	-0.02	36.39	80.99	141.39	142.63	-136.89	-109.28	10598	29.63	30.97	23.79
-100	-4.90	-1.80	28.70	75.81	90.09	91.50	-75.39	-75.49	10599	24.63	22.03	17.18
-200	-4.26	-2.56	21.83	58.40	75.54	76.94	-71.72	-75.03	10589	18.56	18.37	15.18
-300	-4.31	-2.21	17.25	41.34	63.90	67.83	-50.72	-62.40	10589	14.39	14.26	11.68
-500	-3.65	-1.63	11.99	25.34	45.50	48.37	-42.76	-35.48	10588	10.41	9.38	8.29
-755	-2.81	-0.82	8.07	18.47	22.34	43.82	-43.49	-24.33	10600	7.88	5.74	6.21
-973	-1.74	-0.05	4.90	14.96	15.31	32.48	-31.23	-21.73	10600	5.25	3.39	4.25
-1216	-1.59	0.15	3.76	13.58	16.76	33.36	-33.14	-16.46	10602	4.73	2.82	4.32
-1461	-1.82	0.28	4.17	16.02	18.21	36.26	-34.94	-15.78	10600	4.99	3.17	4.58
-1728	-1.93	0.23	4.42	21.54	20.37	33.65	-33.58	-14.64	10600	5.33	3.43	4.93
-2010	-1.66	0.44	4.73	21.99	23.40	27.25	-27.24	-15.80	10518	5.38	3.52	4.68
-2206	-1.24	0.01	4.22	20.22	21.43	23.77	-22.97	-13.39	10600	4.85	3.24	4.21

The basic current statistics for Deployments 1 and 2 are shown in Table 3. The mean currents at all levels have a net westward component with the net northward velocity in the lower 1000 m being statistically close to zero. A net velocity of zero at the surface in the north and south direction was also seen. Figure 18 shows the lower layer mean currents are westward, and parallel to the isobaths. The surface currents were affected by LCE eddies through much of the deployment. This can be seen in the large northerly maximum speed as well as the large magnitude in the minimum zonal velocities.

The lower 1000 m of the water column showed little variation in the principal axes of the variance ellipses. The major axes varied from 12.9° to 3.8°, with the major axes averaging 8.8° at all levels below 1000 m. All angles are measured from the east in a counter clockwise direction. Deployments 1 and 2 moorings were set on top of the Sigsbee escarpment, on what looks to be a small plateau. The isobaths to the south of the mooring run in east /west direction. The orientation of the variance ellipses closely follow these contours. This suggests that the particle motion in this area was being influenced by the escarpment. The mean current vectors are also in a westerly direction, again suggesting that the flow was affected by the escarpment. The area of the variance ellipses are related to the energy of the currents. Deployments 1 and 2 showed an increase in energy in the water column from 1000 m towards the bottom. This is expected for an area dominated by TRW's. The bottom current meter, z = -2213 m, showed a decrease in energy which is typical of currents in a boundary layer. The top 1000 m variance ellipses (not shown) showed little coherence. The variance ellipses in the top 800 m showed a counterclockwise rotation from -54° at z = -50 m to 3.7° at z = -755 m with the energy decreasing from the surface. Again all angles were measured counter clockwise from the x-axis which is orientated east.

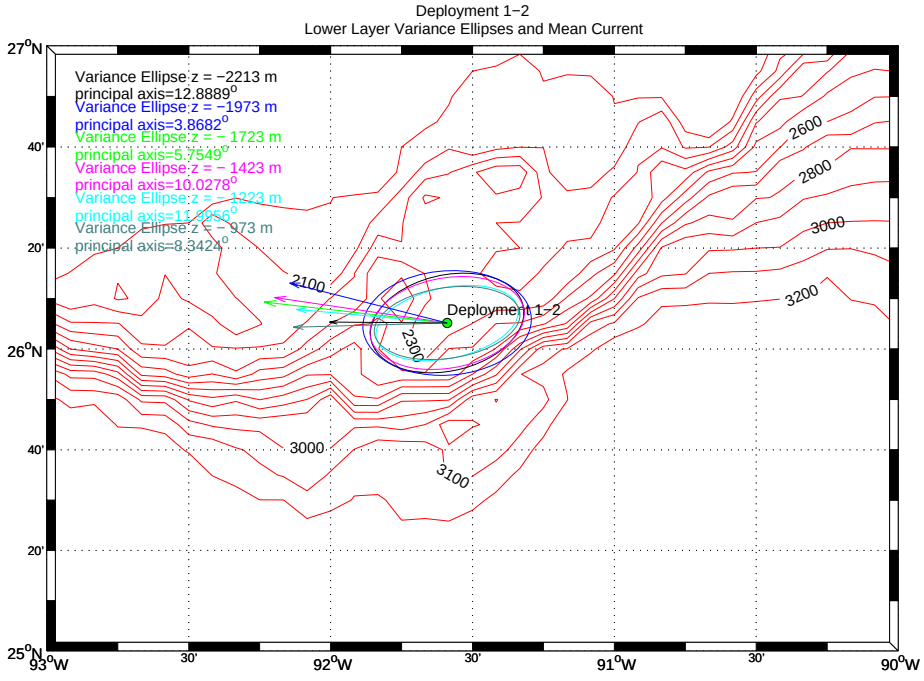

Figure 18. Lower layer variance ellipses and mean currents for Deployments 1 and 2.

Spectral analysis along with wavelet analysis showed weak signals at 40 and 50 days at the surface of Deployments 1and 2 (Figure 19, Figure 24). These signals do not show up in all methods of spectral analysis and are greatly affect by the smoothing of the time series. Wavelet analysis showed the 50 day signal at the beginning of Deployments 1 and 2 whereas WOSA spectral analysis showed the broadband signal near 44 days (Figure 21).

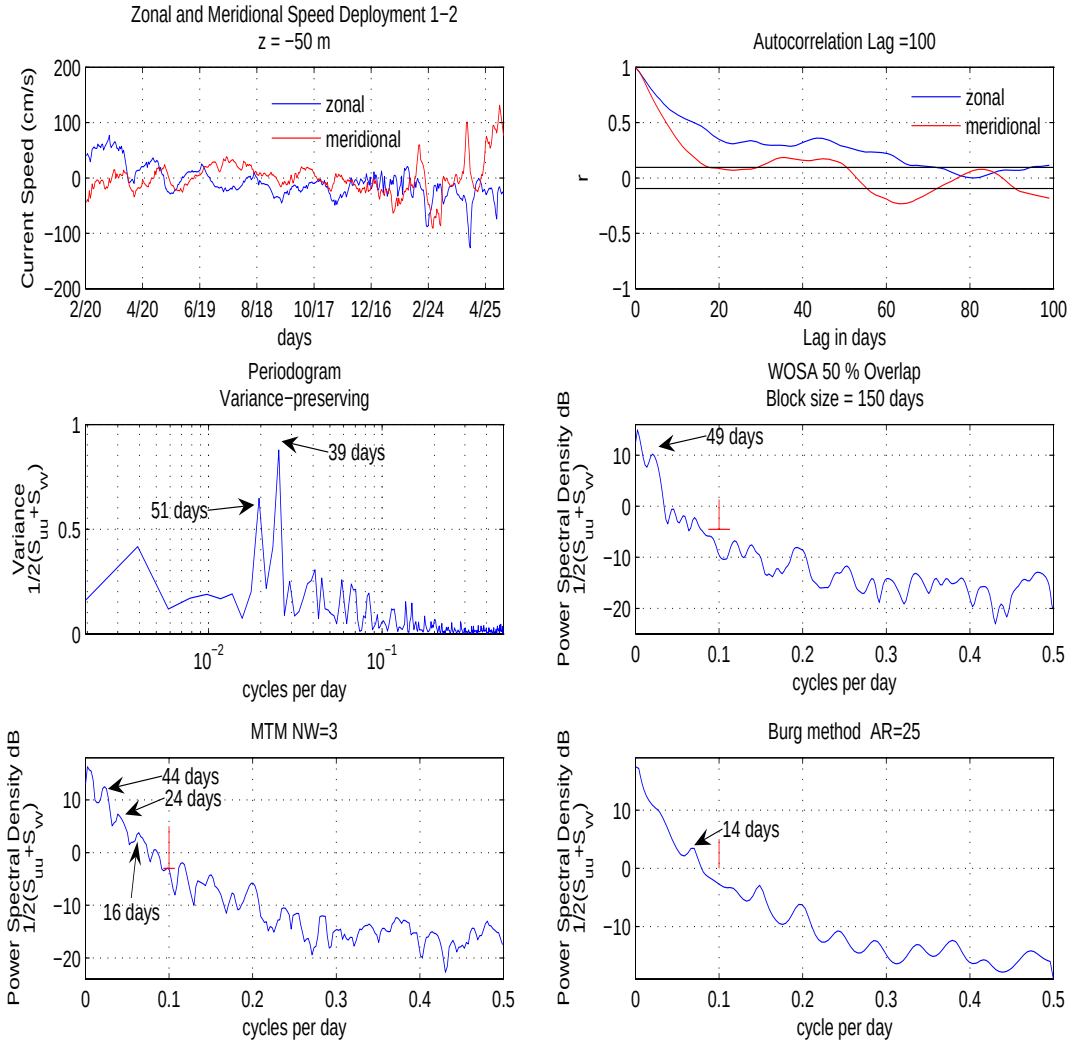

Figure 19. Multiple methods of spectral analysis z = -50 m for Deployments 1 and 2.

Spectral analysis of the hourly currents at 500 m and 755 m showed a strong 25.9 hour signal (not shown). The calculated inertial period at 26^{o} is 27.3 hours. This 25.9 hour signal corresponds to an inertial period latitude at close to 27^{o}. Surface winds tend to be the forcing of inertial currents. As this signal was continuous, as can be seen in the wavelet analysis and vector

plots, this signal was most likely tidal. The principal lunar diurnal (O_1) tidal period was 25.8 hours which corresponds closely to the 25.9 hour signal seen. Kantha (2005) discusses the near resonance signal of the O_1 signal in the Gulf of Mexico. The magnitudes of the currents seen are generally less than 5 cm/s. Deep barotropic tidal currents can be of the order of 1-2 cm/s (Kantha 2005) but are general masked by the surrounding noise. This is why inertial tidal currents are not generally seen below 1000 m.

The spectral signals seen in the lower 1000 m showed a lot of coherence. There was a strong 22-24 day signal along with a weak 13-16 day signal at z = -1973 (Figure 20). Wavelet analysis showed a 22-24 day signal in the last 3 months of the time series. The MTM and periodogram methods resolve the 13 and 16 day signal into separate signals. A spectral plot showing the first and second half of the time series verifies the 22-24 day signal in the second half of the time series (Figure 22). Wavelet analysis at the beginning and end of both time series show significant signals. There was a shift in frequency between the surface and depth at the beginning of the time series, shifting to a lower frequency, ~70 days at depth. The last three months of the time series, a cyclonic eddy at the surface affected the whole deployment. Wavelet rotary analysis (not shown) showed a weak 20-25 day counter clockwise signal (CCW) at the surface. A 20-25 day signal with weak CCW rotation was seen at depth, also using wavelet rotary analysis. A wavelet Hovmöller diagram shown in Figure 25, showed a continuous 20-25 day signal from the surface to depth. This continuous signal is seen in all LSU deployments when the mooring is between the LC and a cyclonic frontal eddy (Figure 26).

Figure 23 shows cross-spectral analysis between the surface, an intermediate layer and the bottom kinetic energy using WOSA. Also shown are plots of kinetic energy between the three levels. A 47 day signal was seen in the cross-spectrum between z = -100 m and z = -973 m. There are no significant signals in the cross-spectral analysis between the surface and depth but there is a large amount of kinetic energy towards the end of the in both areas with little correlation. Further analysis (not shown) using wavelet cross-spectral and coherence (Torrence and Webster 1999; Grinsted et al. 2004) showed broadband signals centered around 24 days for the last 3 months of the time series. This correlated well with the wavelet Hovmöller in Figure 25. The mid layer east-west velocity, z = -973 m showed a relatively strong 57 day signal correlation with depth and good correlation in kinetic energy with the bottom.

Wavelet analysis showed a decrease in frequency with depth over the first few months, with the bottom driving the middle layer (kinetic energy decreasing towards surface) even with the strong surface signal seen in both the vector plots and kinetic energy plots. Rotary analysis showed a 44 day signal at 100 m predominately CCW with the 22-24 day and 70 day signal at depth tending CW.

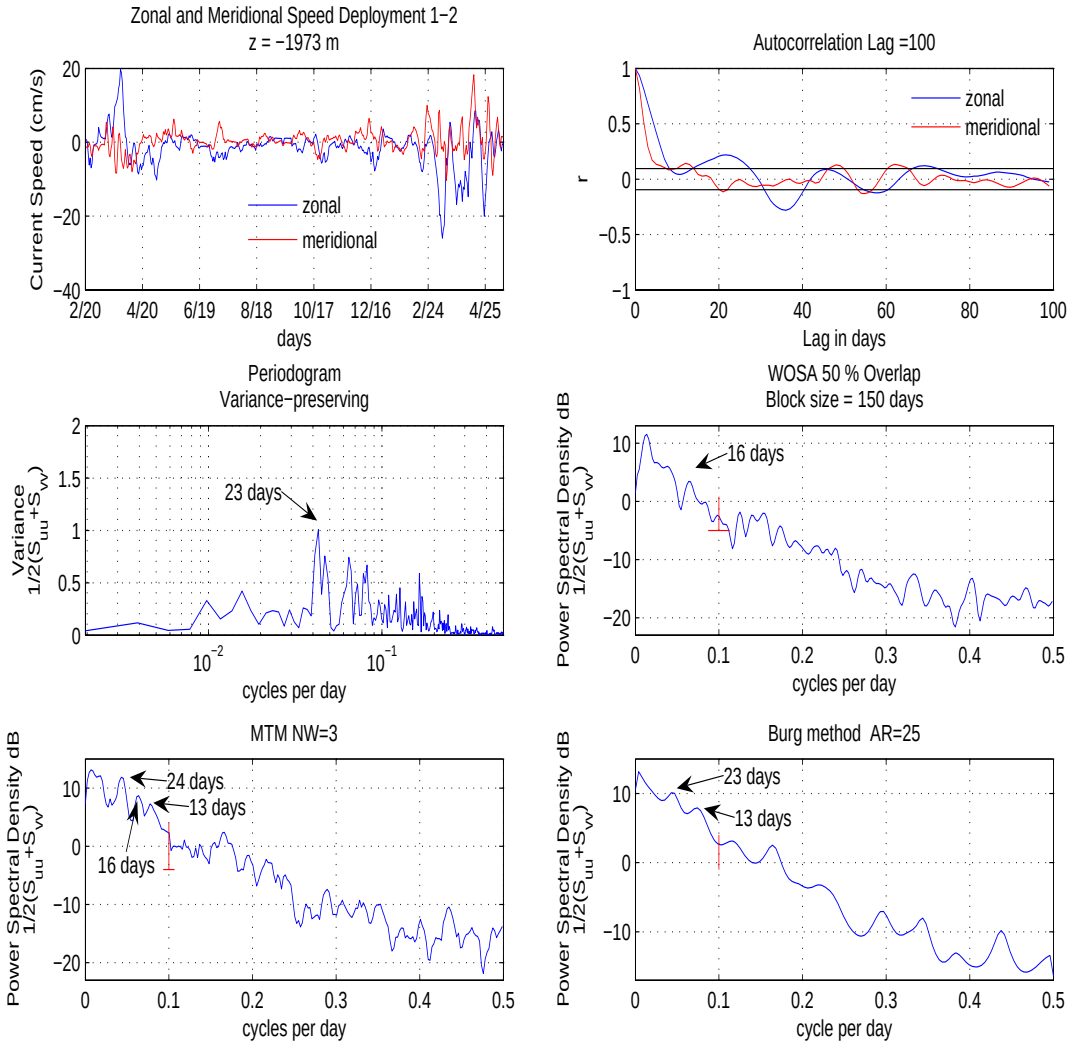

Figure 20. Multiple methods of spectral analysis z = -1973 m for Deployments 1 and 2.

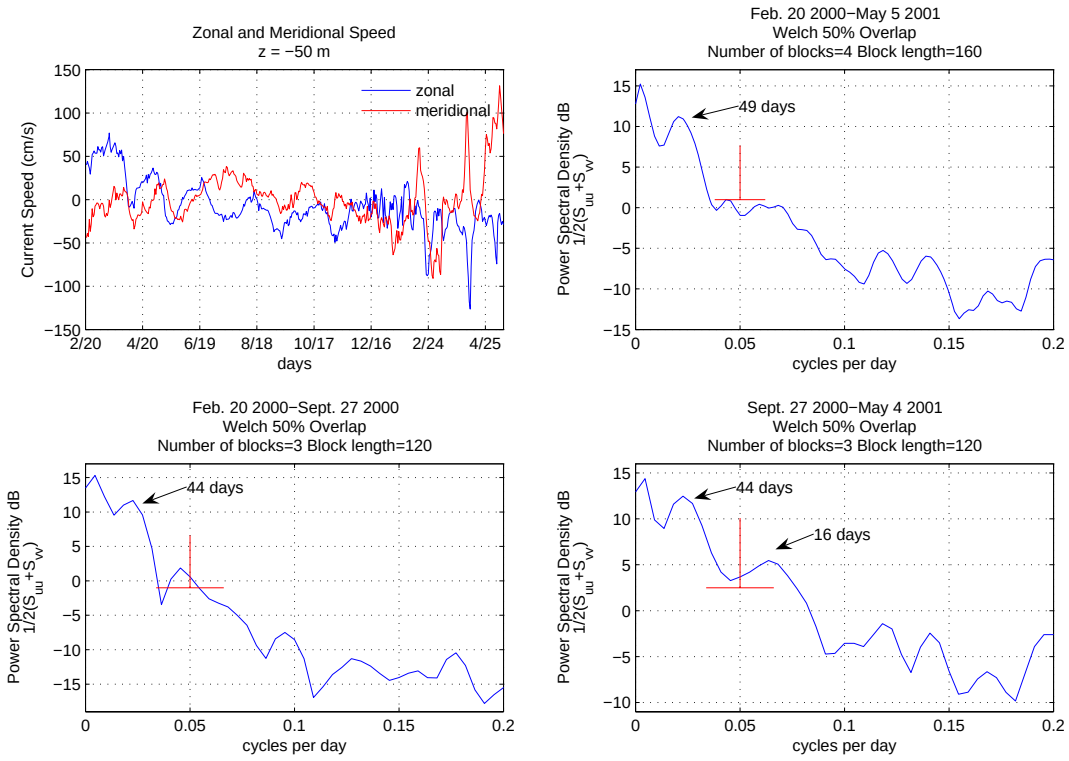

Figure 21. WOSA first and second half of time series z = -50 m for Deployments 1 and 2.

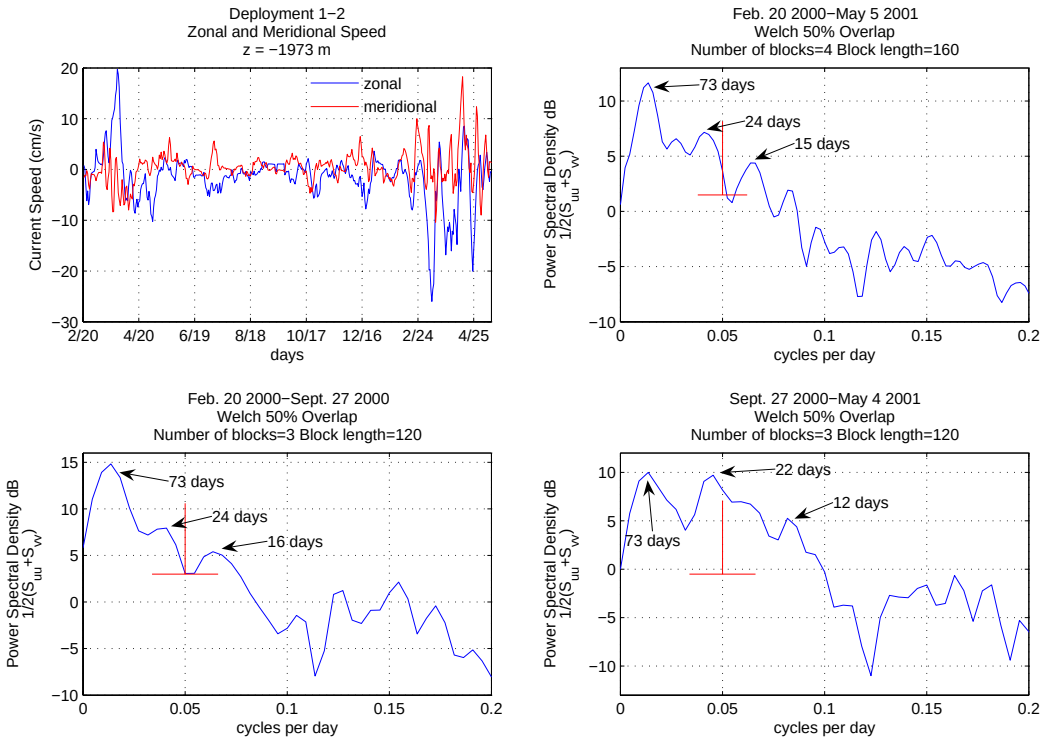

Figure 22. WOSA first and second half of time series z = -1973 m for Deployments 1 and 2.

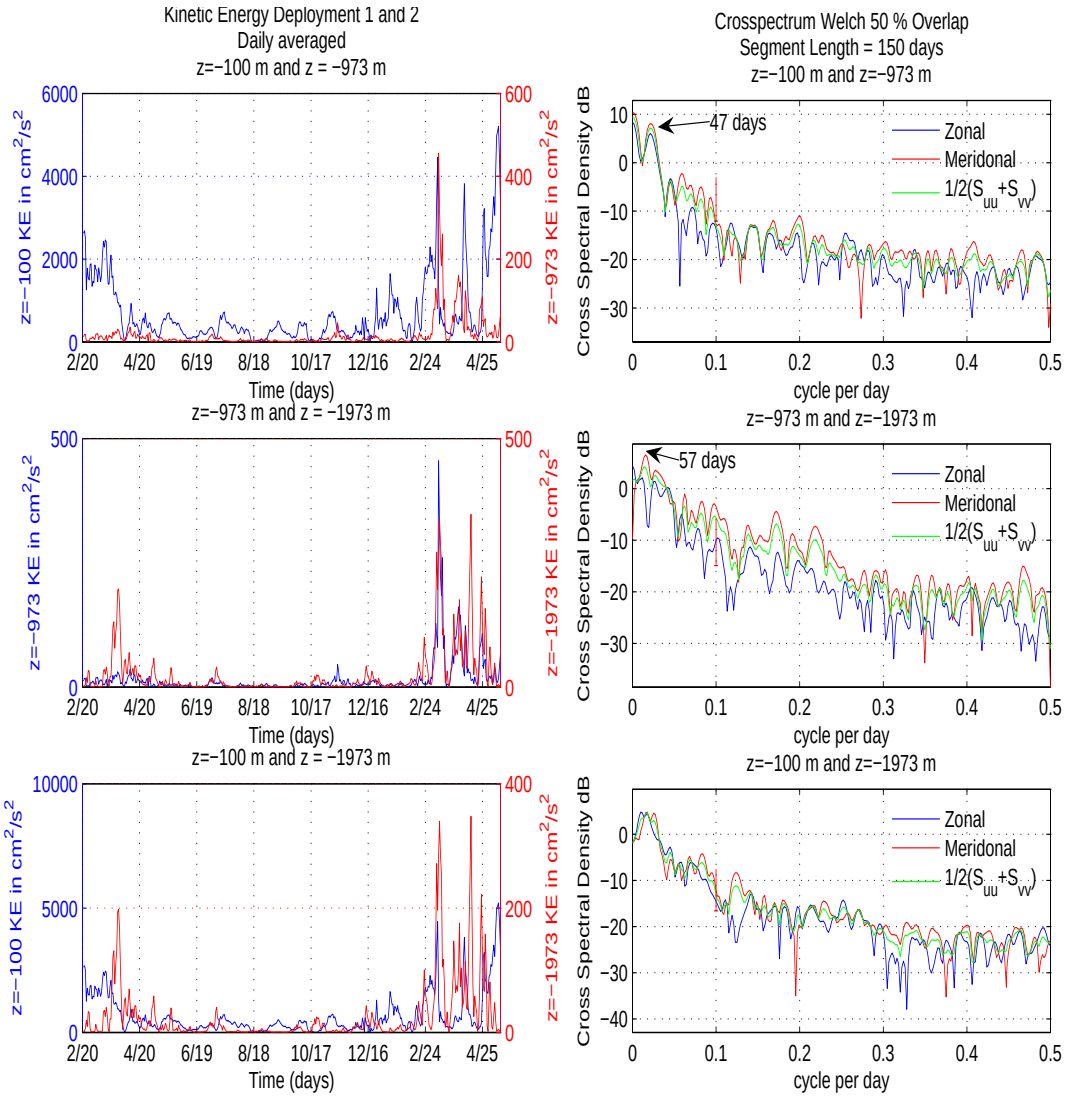

Figure 23. Cross-spectral analysis for Deployments 1 and 2.

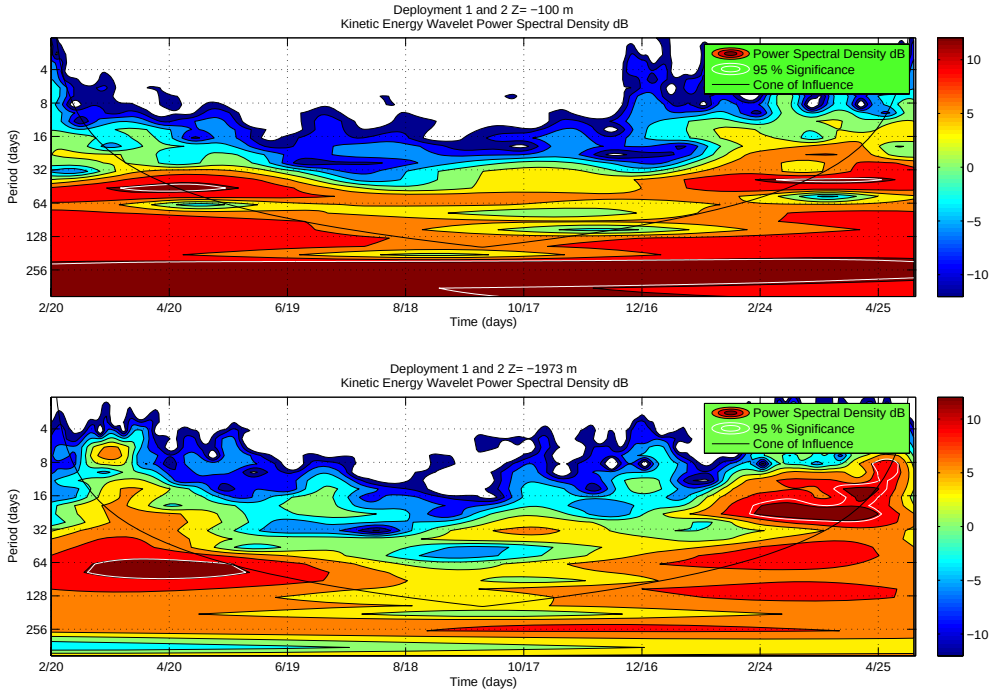

Figure 24. Wavelet analysis z = -100 m and z = -1973 m for Deployments 1 and 2.

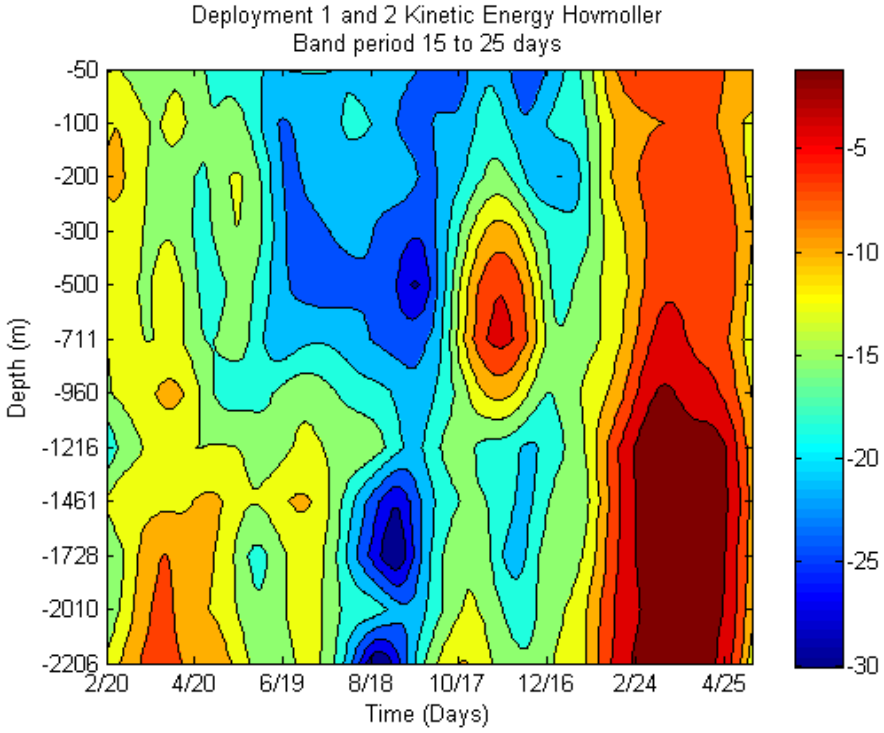

Figure 25. Hovmöller Deployment 1-2 for band period 15-25 days.

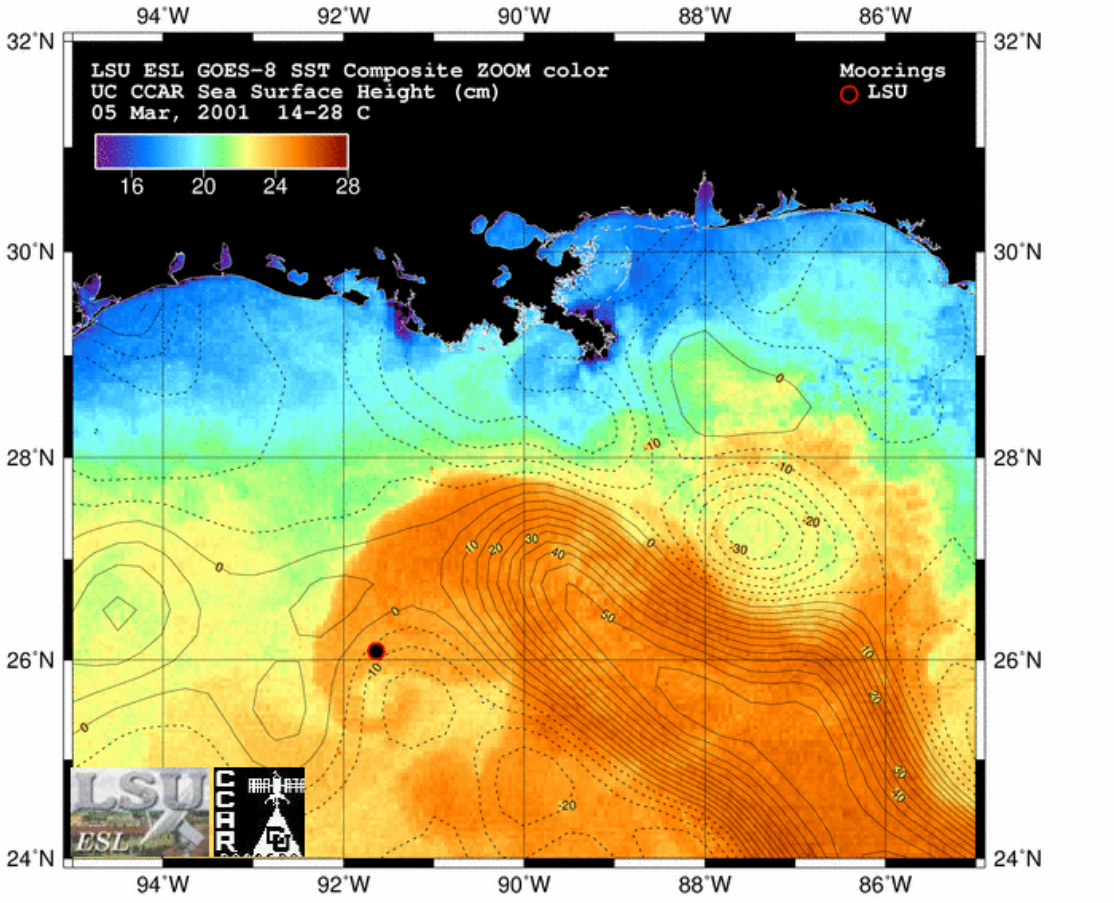

Figure 26. GOES SSH/SST image on March 5, 2001.

3.3 Evidence for Topographic Rossby Waves

Plotting the spectrum for the bottom 1000 m current meters showed no evidence at any frequency of a decrease in energy from the bottom as predicted by Rhines (1970) for TRW's. The bottom 1000 m does show good coherence in the vector plots along with the spectral plots, which is one indicator of a TRW. Others have noticed the lack of bottom trapping (Louis et al. 1982).

For Deployment 1-2 the principal axes in the lower 1000 m of water was close to 10^o as measured from east. This defines the wave vector $\vec{K}$ with a clockwise rotation of $\theta = 20^o$ from the steepest gradient of the slope. The maximum gradient of the bottom topography was estimated from Smith and Sandwell (1997) 2 minute DBD2 data to be $\nabla h = 0.025$. An average Brunt Väisälä frequency of N = 0.0005 Hz was determined from a CTD cast taken at the beginning of Deployment 1 for the bottom 500 m. The period of oscillation of a TRW using the above parameters (equation 3) was 17 days. This corresponds well with a weak 15-16 day signal seen in Figure 20. Rotary analysis showed a tendency for clockwise rotation between 25 and 50 days at depth. This analysis was for the whole time series, the determination of the transverse nature of TRW's in this area was inconclusive. Rotary wavelet analysis did show a transition

from CCW to CW at the beginning of the time series. This same rotary analysis showed a weak CCW rotation from surface to depth the last three months of the time series. This same analysis was mentioned above. The wavelength calculation is also inconclusive as there was no energy trapping seen in the multiple spectral plots. Deployments 1 and 2 data were band passed over three different frequencies. The higher frequency variance ellipses should align across slope with the lower frequencies variance ellipses rotating with the general trend being parallel to the isobaths. The direction of the variance ellipses were very sensitive to the width of the band-pass and no pattern of rotation in the variance ellipses was noticed. Evidence for TRW's for these two deployments was inconclusive.

4.0 MOORING LOCATION 2, DEPLOYMENT 3

4.1 Initial Conditions, Major Ocean Events, and CTD Data

In this section, water column currents and temperature are discussed in relationship to large-scale movements of Gulf water masses as revealed in satellite data as in Section 3.1. Color-enhanced time series of currents and temperatures in the upper 1200 m are depicted in Figure 27. Time-series of current speeds and current vectors are shown in Figure 28 and Figure 29. Satellite SST/SSH imagery for selected current events is displayed in Figure 30-37.

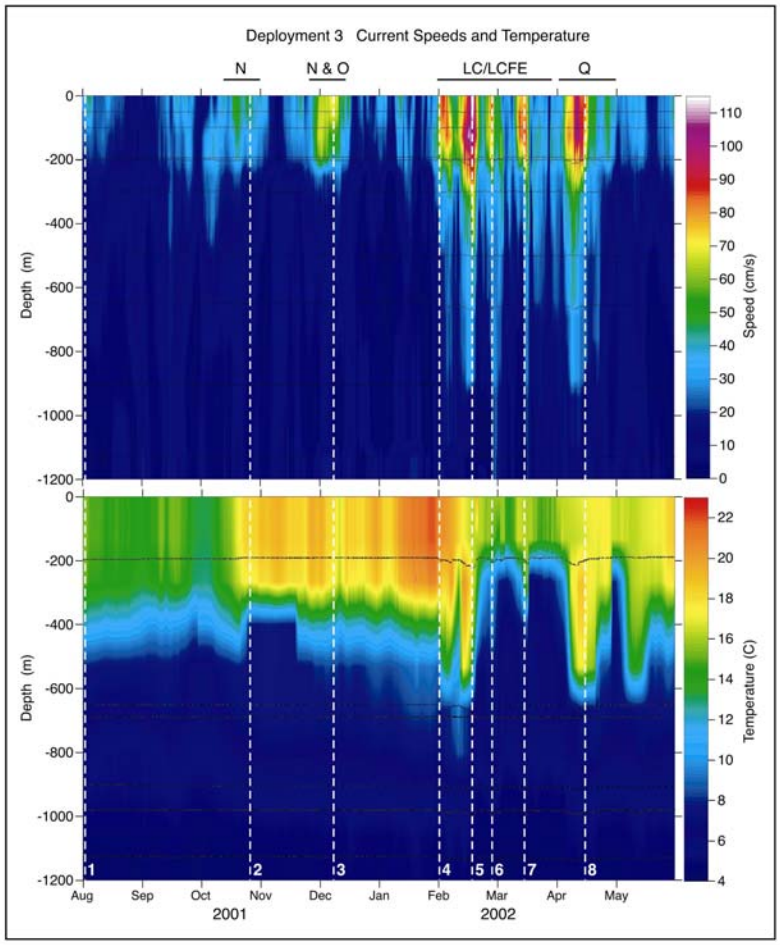

Figure 27. Color-enhanced LP current speed (cm/s) from 0-1200 m and temperature from 0-1200 m for Deployment 3. White lines depict case study events.

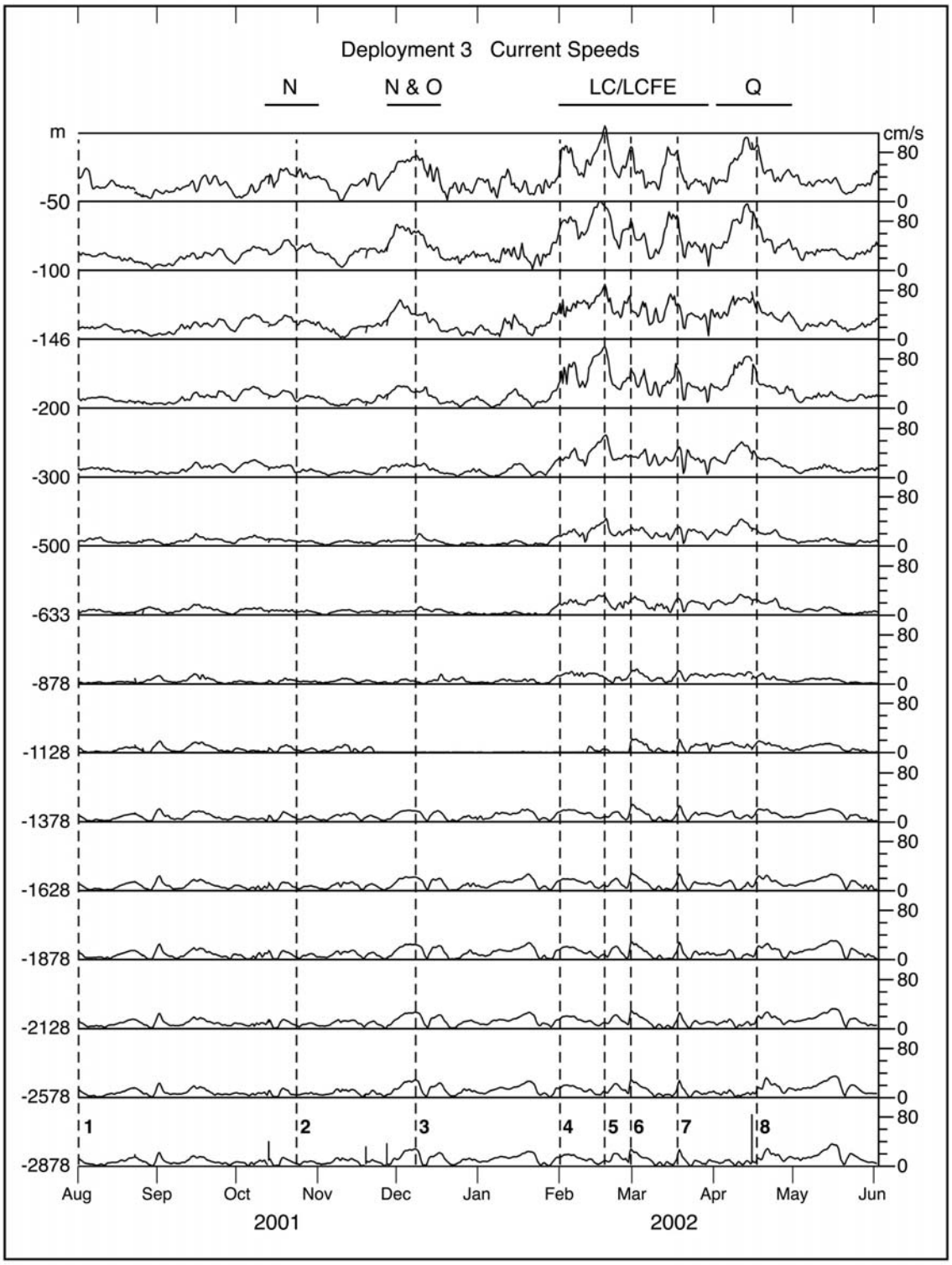

Figure 28. LP current speeds (cm/s) at 15 depths from near surface to near bottom for Deployment 3.

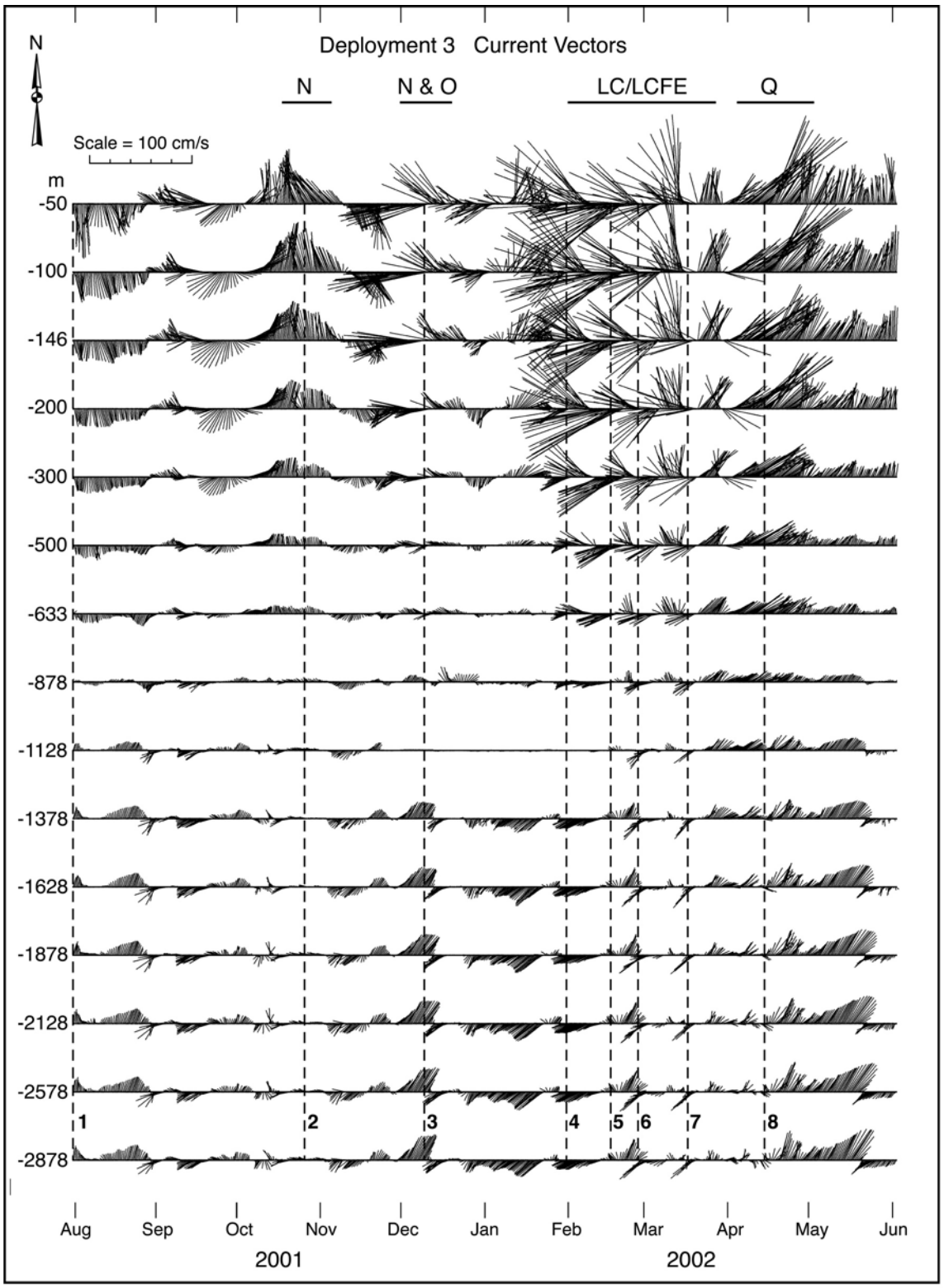

Figure 29. LP current vectors (cm/s) at 15 depths from near surface to near bottom for Deployment 3.

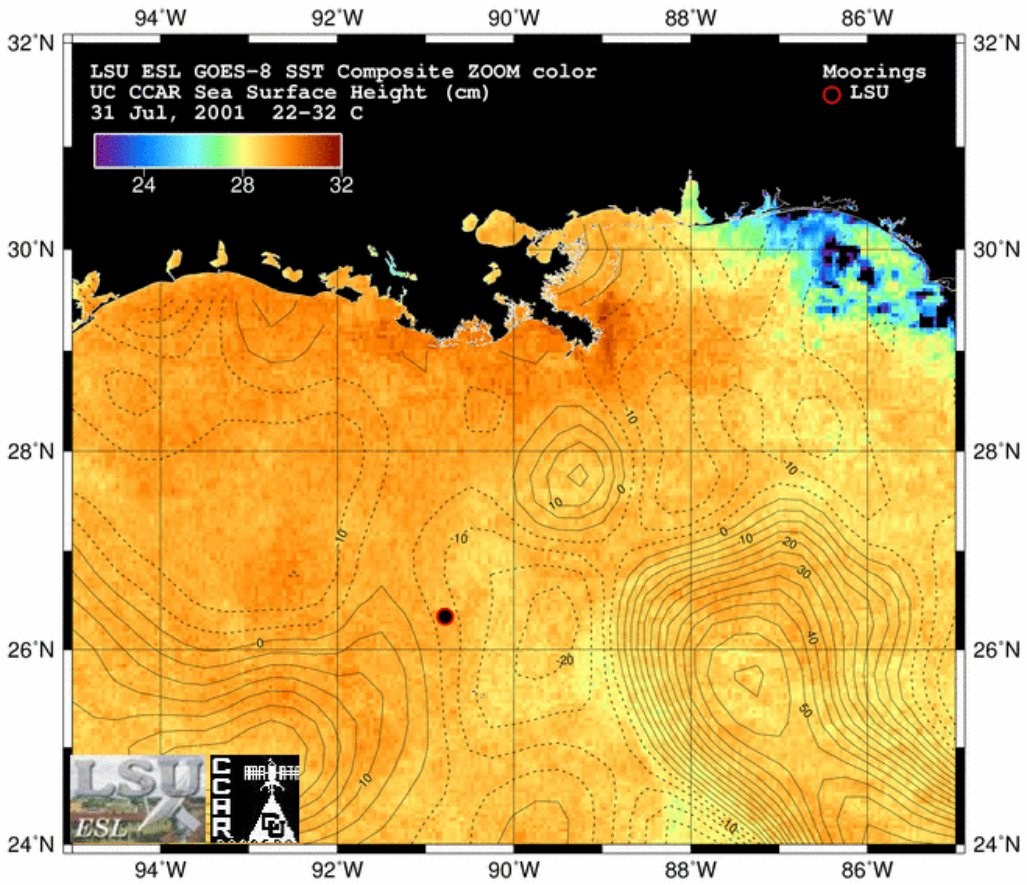

Figure 30. GOES night-time SST composites and SSH contours for Event 1 (31 July 2001).

The mooring was deployed on July 31, 2001 in ~2956 m of water close to the base of the Sigsbee Escarpment (Table 2, Figure 1). The deployment lasted ~10 months and the mooring was picked up on June 2, 2002. As during the previous deployment on the plateau, maximum currents throughout the water column were associated with the LC, detached WCE's and associated cyclonic circulations. Four WCE's affected the mooring over the 10-month period; Eddies N, O, P and Q. The January-April 2002 period exhibited five high velocity events during an extreme and abnormal northwestward intrusion of the LC. Leben (2005) showed that the LC surged abnormally far northwestward during January/February 2002. Based on altimetry, the LC intrusion reached 93º W. GOES SST imagery clearly revealed that LC water was advected by a LCFE cyclone beyond 96º W on February 24 (Figure 35). This abnormal westward intrusion led to the separation of Eddy P on February 28 followed by Eddy Q on March 15 (Figure 6). A more detailed description of the mooring currents associated with these energetic LC circulation events is presented later in this section.

The mooring was deployed between Eddy M (which was retreating westward) and a well-developed cyclone on the northwest margin of the LC (Figure 30, Event 1) resulting in southward surface currents ~ 60 cm/s. The cyclonic eddy affected the mooring until early

October during which time surface currents were relatively weak. In mid-October, Eddy N, a relatively small WCE, moved towards the mooring increasing near surface flow and temperature in the surface layer to about 300 m (Figure 27,Figure 31, Event 2). Another acceleration in surface flow occurred in late November until mid-December as Eddy Odessa approached from the northeast and merged with Eddy N in the vicinity of the mooring (Figure 27, Figure 32, Event 3). Currents in the upper 150 m reached maximum speeds of 50 cm/s during this eddy merger event. It is interesting to note that currents in the lower layer of the water column (below 1100 m) also increased in speed nearly simultaneously with those in the surface layers (Figure 27-Figure 29). Maximum bottom current speeds were 30 cm/s on December 5, 2001 (Figure 32, Event 3). Lower layer currents flowed towards the northeast while surface currents flowed northwest (Figure 29).

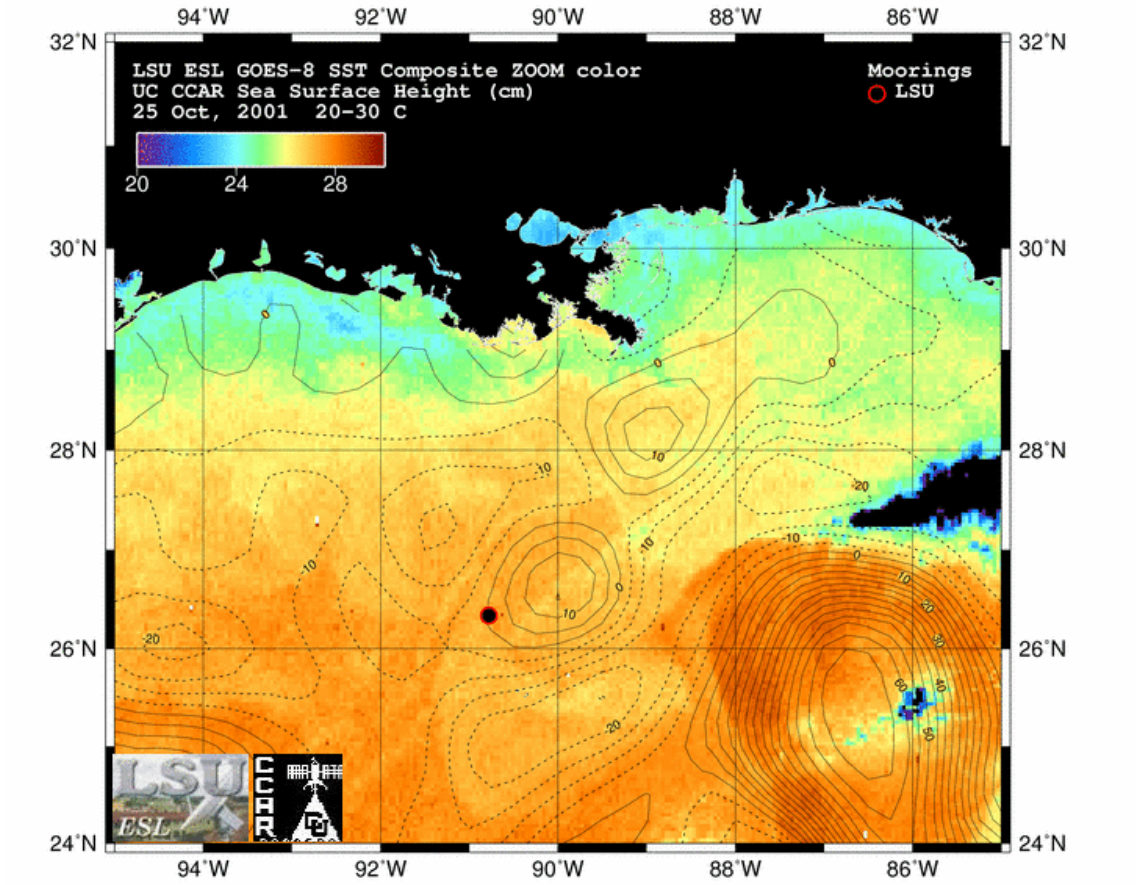

Figure 31. GOES night-time SST composites and SSH contours for Event 2 (25 October 2001).

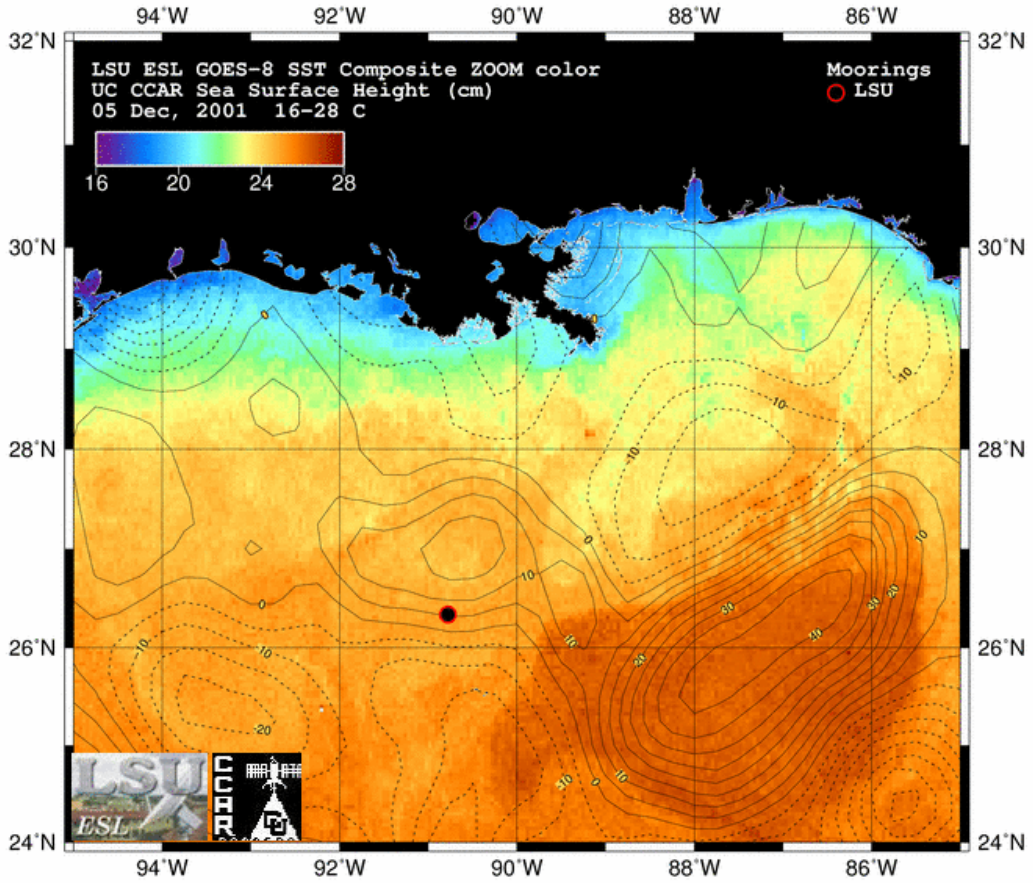

Figure 32. GOES night-time SST composites and SSH contours for Event 3 (5 December 2001).

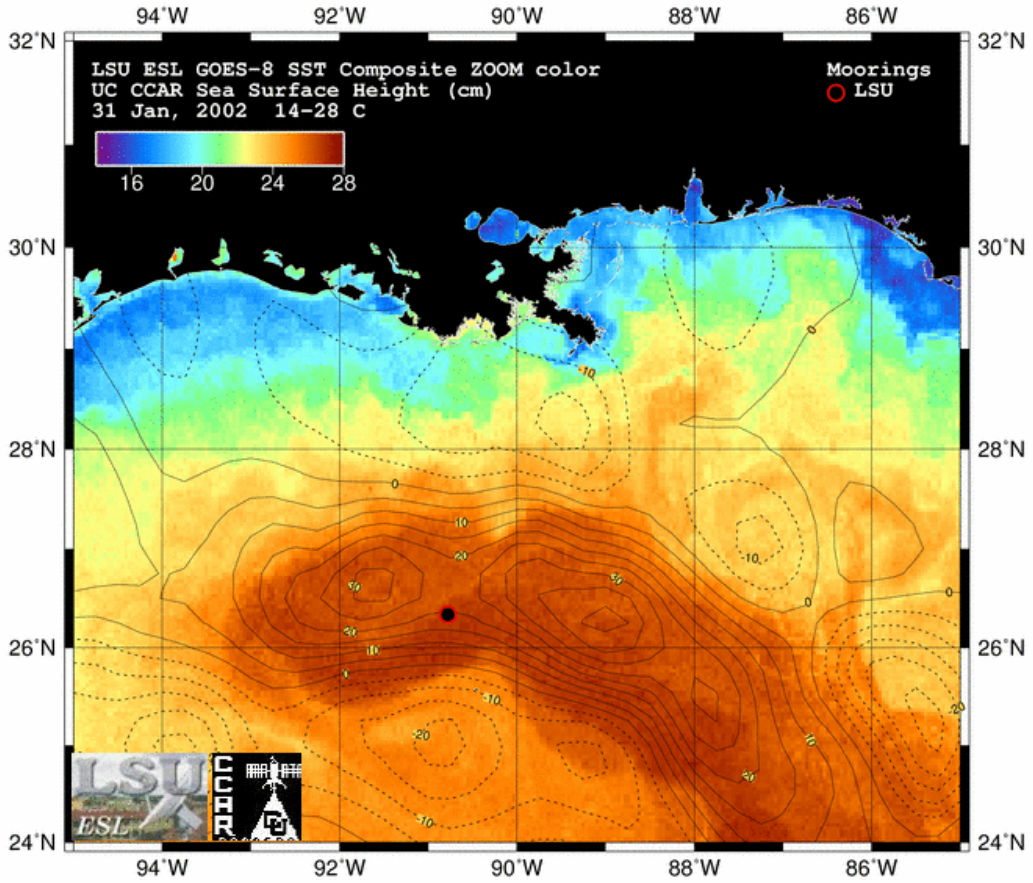

Figure 33. GOES night-time SST composites and SSH contours for Event 4 (31 January 2002).

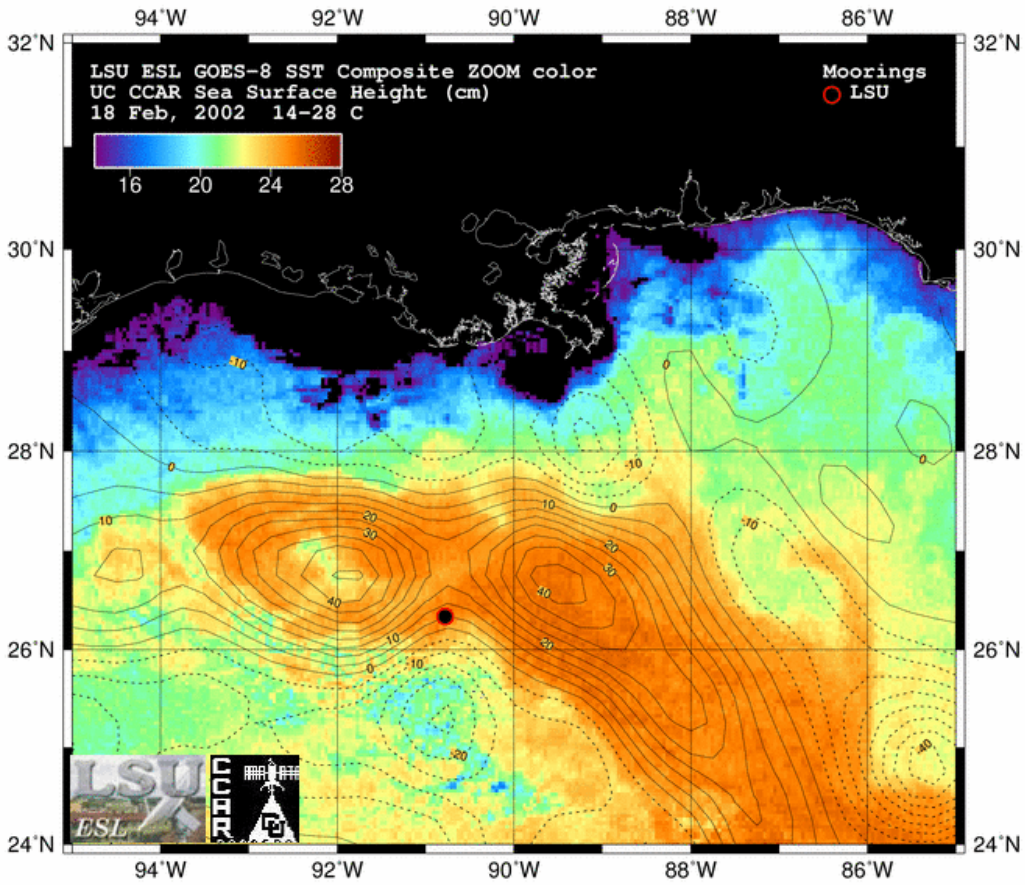

Figure 34. GOES night-time SST composites and SSH contours for Event 5 (18 February 2002).

Surface currents were relatively weak from mid-December 2001 through January 2002 (Figure 27-Figure 29). However in early January, the LC intruded rapidly towards the northwest close to the mooring site where its presence was initially manifest by high temperatures in the surface mixed layer during most of January (Figure 27). Four distinct surface current acceleration events occurred within a 6-week period from 31 January through mid-March 2002, which are all attributed to the LC, Eddies P and Q, and associated cyclones.

During the ~6-week LC intrusion episode, surface currents (at 50 m) exceeded 90 cm/s during each of the four events (Figure 27-Figure 29). The first event started January 31, 2001 and lasted about one week (Figure 27-Figure 29, Figure 33, Event 4). The LC continued to extend westward leading to maximum westward currents of 133 cm/s on February 17 near the surface when the axis of the LC was closest to the mooring site (Figure 27-Figure 29, Figure 34, Event 5). There was a notable warming to 600m associated with the LC event (Figure 27). Drifters, within the LC and Eddy P, reached speeds of 100-155 cm/s during this same time frame (Horizon Marine Inc, personal communication). Within this period of extreme LC activity over the mooring, the three-layer structure of currents typical of deep water (Hamilton, 1990; Hamilton

and Lugo-Fernandez, 2001) was replaced by flow which was coherent for periods of time from the surface to the bottom (Figure 28, Figure 29). Some of the bottom current events were short-lived (1-2 days) and others lasted a week or more. During the episodic LC intrusion and detachments of P and Q, three of the four surface current accelerations (>90 cm/s) were accompanied by southwest flow throughout the water column with bottom currents in excess of 20 cm/s (Figure 28, Figure 29). The two short-lived events (27-28 February and 18-19 March) exhibited weak bottom intensification. SST/SSH data are shown near the time of the two short-lived pulsed events (Figure 35, Figure 36, Events 6 and 7).

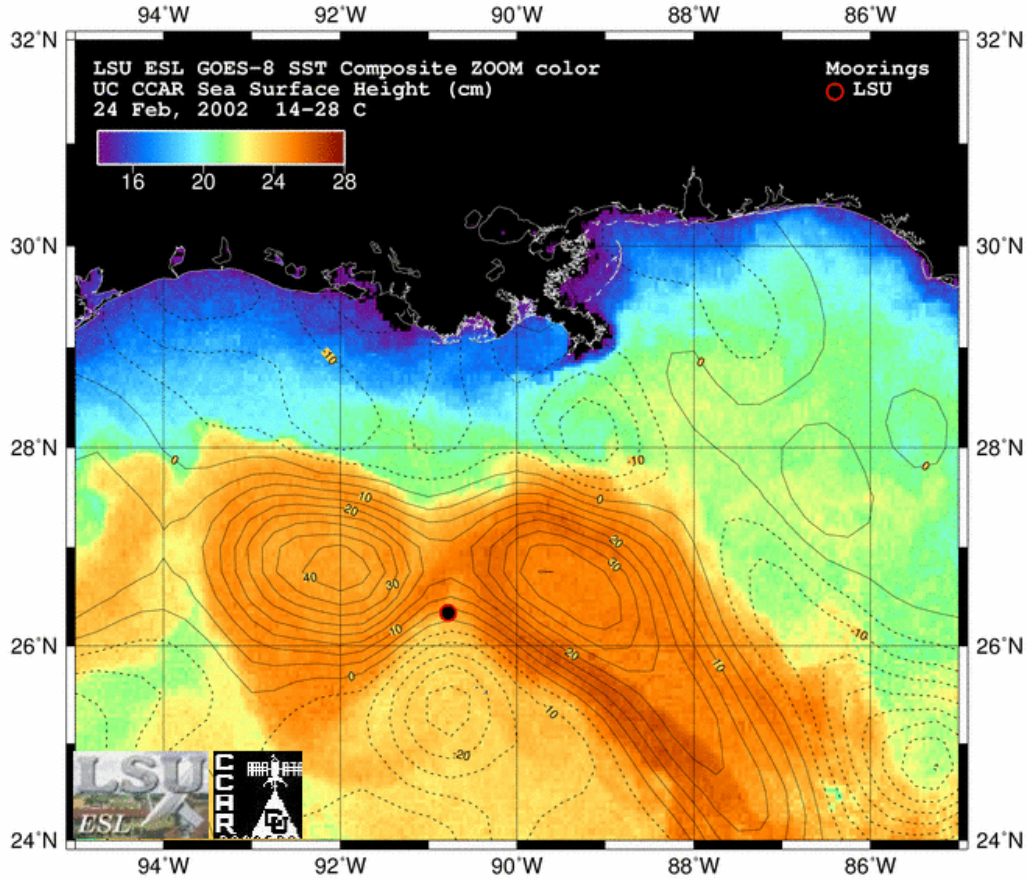

Figure 35. GOES night-time SST composites and SSH contours for Event 6 (24 February 2002).

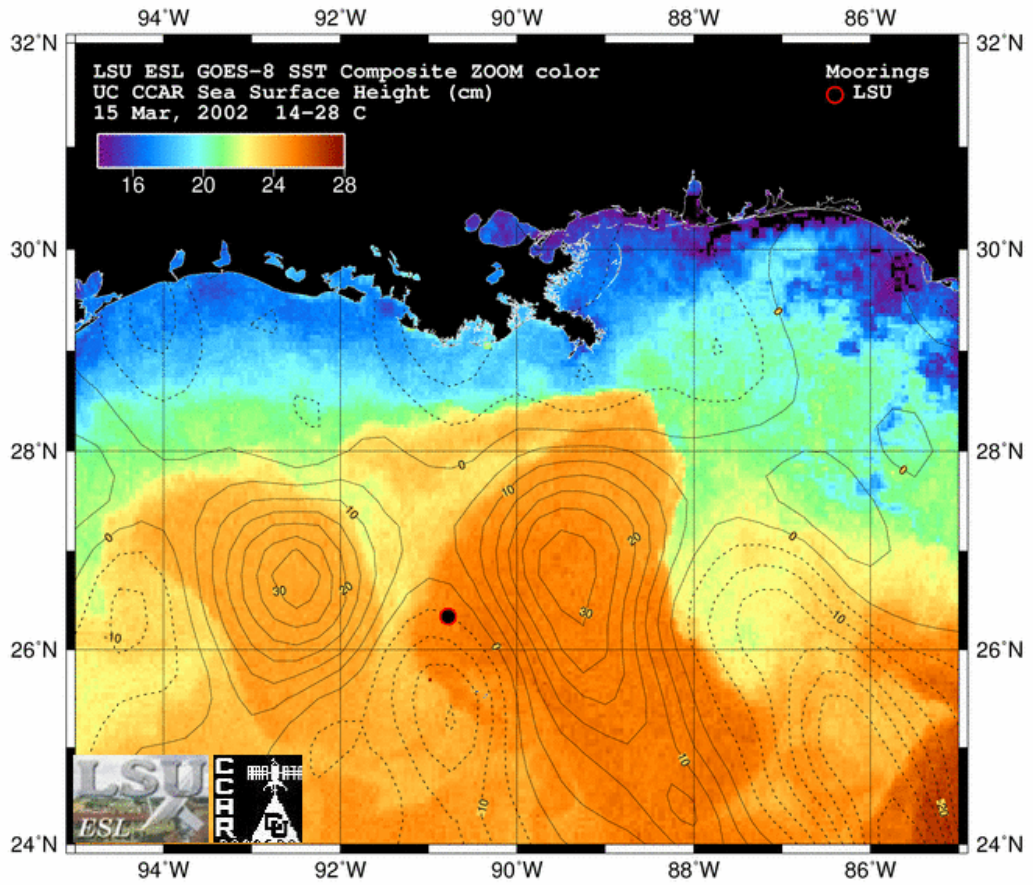

Figure 36. GOES night-time SST composites and SSH contours for Event 7 (15 March 2002).

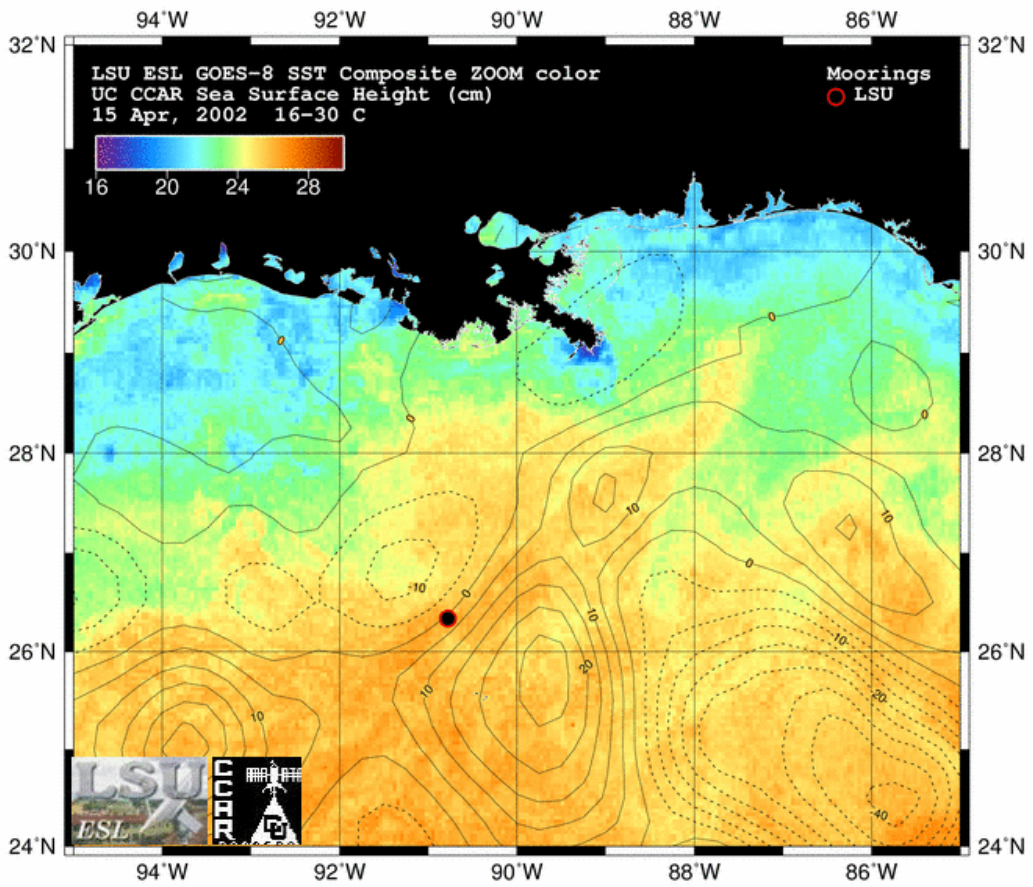

Figure 37. GOES night-time SST composites and SSH contours for Event 8 (15 April 2002).

These images and image animations (see http://www.esl.lsu.edu/research/CMI-GOES) revealed that the two short-lived pulsed bottom events were closely timed with LC intrusions towards the mooring and a rapid growth of LCFE's very close to the mooring location. During both events, the LCFE's moved into a region of pre-existing cyclonic circulation, based on the SSH data. Hamilton and Lugo-Fernandez (2001) also showed evidence of a LCFE cyclone over their mooring when they measured bottom currents exceeding 85 cm/s along the Sigsbee Escarpment approximately 70 km to the east. Temperature data confirms the presence of 2 consecutive cold-core cyclones at the mooring site during late February through March (Figure 27). One of these short pulsed events is described in more detail in Section 4.3.

The strongest surface acceleration on February 18 (Figure 34, Event 5) was not accompanied by strong currents throughout the water column. However, acceleration in lower layer currents occurred four days later when northeast flow exceeded 20 cm/s for three consecutive days. The northeast bottom flow reversed to southwest flow February 27 as one of the short-lived pulsed events, associated with LCFE activity over the mooring.

The strongest lower layer currents were associated with the westward movement of WCE's south of the mooring. From December 2-9, northeast flow of ~ 25 cm/s occurred as WCE O moved

westward (Figure 32, Event 3). Surface flow was westward, in opposition to the lower layer flow. Speeds between 300 m and 1128 m were weak, indicating little connection between surface and bottom circulation. From 23 March - 20 May, northeast flow prevailed from surface to bottom as WCE Q moved south of the mooring into the western Gulf (Figure 37, Event 8). Relatively strong currents were measured from the bottom at 2878 m to 878 m. The strong currents at 878 m were unusual since at this level currents are usually extremely weak. Strongest lower layer currents occurred on 21 April and 16 May, with the deployment maximum of 37 cm/s occurring in May at 2878 m. The time series of current vectors (Figure 29) reveals coherence of flow direction throughout the water column during April and May 2002 (Figure 28, Figure 29). The corresponding temperature time series (Figure 27) showed relatively warm temperatures typical of WCE's except for a cold-core cyclone which cooled waters within the upper water column (< 600 m) in late April (Figure 27).

4.2 Simple Statistics and Time Series Analysis

The basic current statistics for Deployment 3 are shown in Table 4. Similar to Deployments 1 and 2, the mean current velocity showed a net westward component of at all levels. Interestingly, Deployment 3 showed a significant northerly component at all levels whereas Deployments 1 and 2 did not. Also seen is the decrease in the mean current speed at the 1000 m. level. This decrease was also seen in Deployments 1 and 2 along with Deployment 4.

Table 4

Mean, Maximum, and Minimum Velocities for Deployment 3

Depth (m)	Mean (cm/s)			Max (cm/s)			Min (cm/s)			Standard Deviation (cm/s)		
	U	V	Speed	U	V	Speed	U	V	n	U	V	Speed
-50	-11.63	10.57	38.04	98.07	107.94	132.86	-115.63	-83.10	7336	29.96	27.84	21.74
-100	-7.64	10.01	37.84	93.33	99.96	119.58	-105.95	-76.30	7336	33.04	26.54	22.85
-148	-5.43	8.73	30.87	60.73	76.64		-82.60	-59.20	7336	26.21	21.22	
-200	-3.10	5.24	25.13	68.73	52.60	95.04	-82.60	-59.20	7336	23.04	17.59	15.68
-300	-2.11	3.17	19.41	52.25	44.25	73.90	-63.50	-44.35	7336	18.24	13.53	12.39
-500	-1.24	2.01	13.36	43.70	31.70	52.50	-45.40	-29.45	7336	12.94	9.12	8.82
-633	-1.26	1.98	11.07	31.20	26.02	37.42	-35.05	-23.50	7339	11.06	7.50	7.84
-878	-1.12	1.07	7.68	28.52	20.28	30.16	-27.36	-21.73	7340	7.79	5.21	5.59
-1128	-0.22	1.27	5.86	19.99	17.85	30.16	-28.79	-23.13	7339	6.44	4.85	5.69
-1373	-1.72	1.05	10.16	19.47	22.35	30.74	-23.85	-22.73	7339	8.41	7.85	5.75
-1628	-1.77	1.15	10.66	22.84	25.34	31.32	-24.15	-25.30	7339	8.82	8.68	6.63
-1878	-2.15	1.62	11.10	23.52	27.40	32.19	-25.70	-22.47	7340	9.50	8.80	7.19
-2128	-2.07	1.77	11.59	23.01	30.34	33.36	-24.63	-21.54	7336	9.26	9.29	6.71
-2578	-2.14	1.59	11.33	23.17	29.46	36.04	-23.71	-22.31	7339	9.09	9.44	7.11
-2878	-2.82	1.47	11.08	23.09	30.86	37.39	-24.14	-20.97	7339	8.38	9.47	6.87

The particle motion variance at depth paralleled the bathymetry with the mean flow tending to flow across the isobaths. The variance ellipses and mean current vectors show this in Figure 38. From 878 m to depth there was a counterclockwise rotation of the principal axes of the variance ellipses. The area of the ellipses also increased with depth which indicates an increase in energy with depth. The top 800 m showed the variance ellipses rotating in a clockwise direction from the surface to 500 m. The largest amounts of energy are at the surface, decreasing with depth. The mean flow below 1000 m showed a net increase in speed with depth with no general trend in rotation seen.

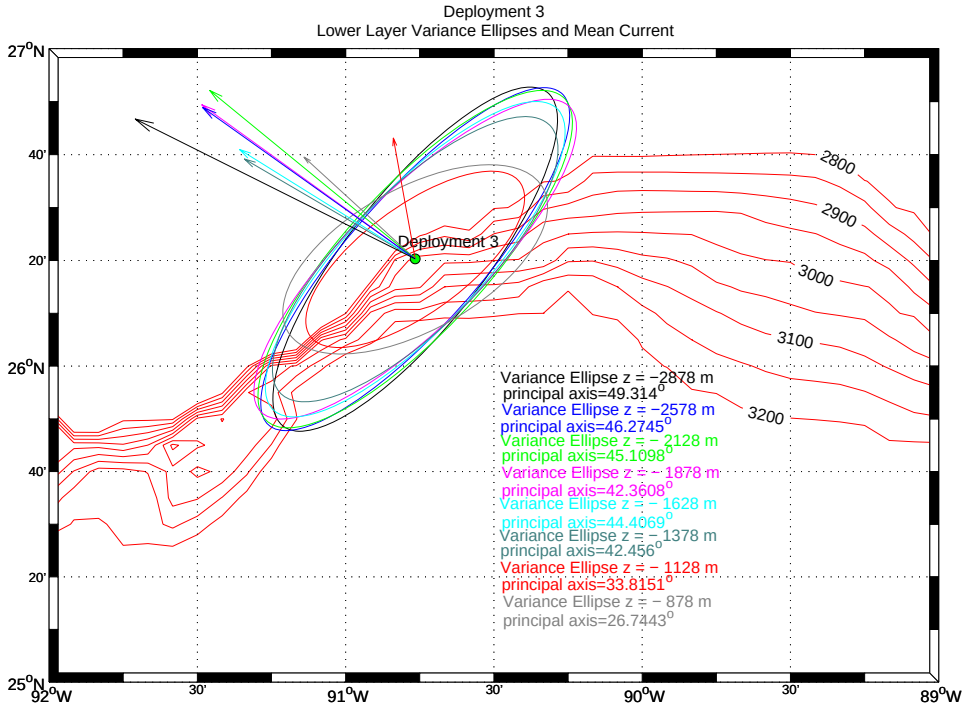

Figure 38. Lower layer variance ellipses and mean current vectors for Deployment 3.

Spectral analyses of wind from NDBC 42001 buoy over the same time period as Deployment 3 showed robust signals at 4.7, 9 and 16 days, with weak signals at 22 and 51 days. The first and second half of the buoy time series showed a strong 8-9 day signal. The second half of the time series also showed a strong 50 day signal (figure not shown).

The upper 1000 m of the water column showed a robust 17 day signal. Both wavelet analyses (Figure 43) along with standard spectral methods (Figure 39 and Figure 41) showed this signal to be dominant in the second half of the time series. This signal occurred when the LC and eddy P were over the mooring. The surface north-south current can be seen fluctuating between 13 and 17 days after January 27 until a little before March 28 (Figure 39).

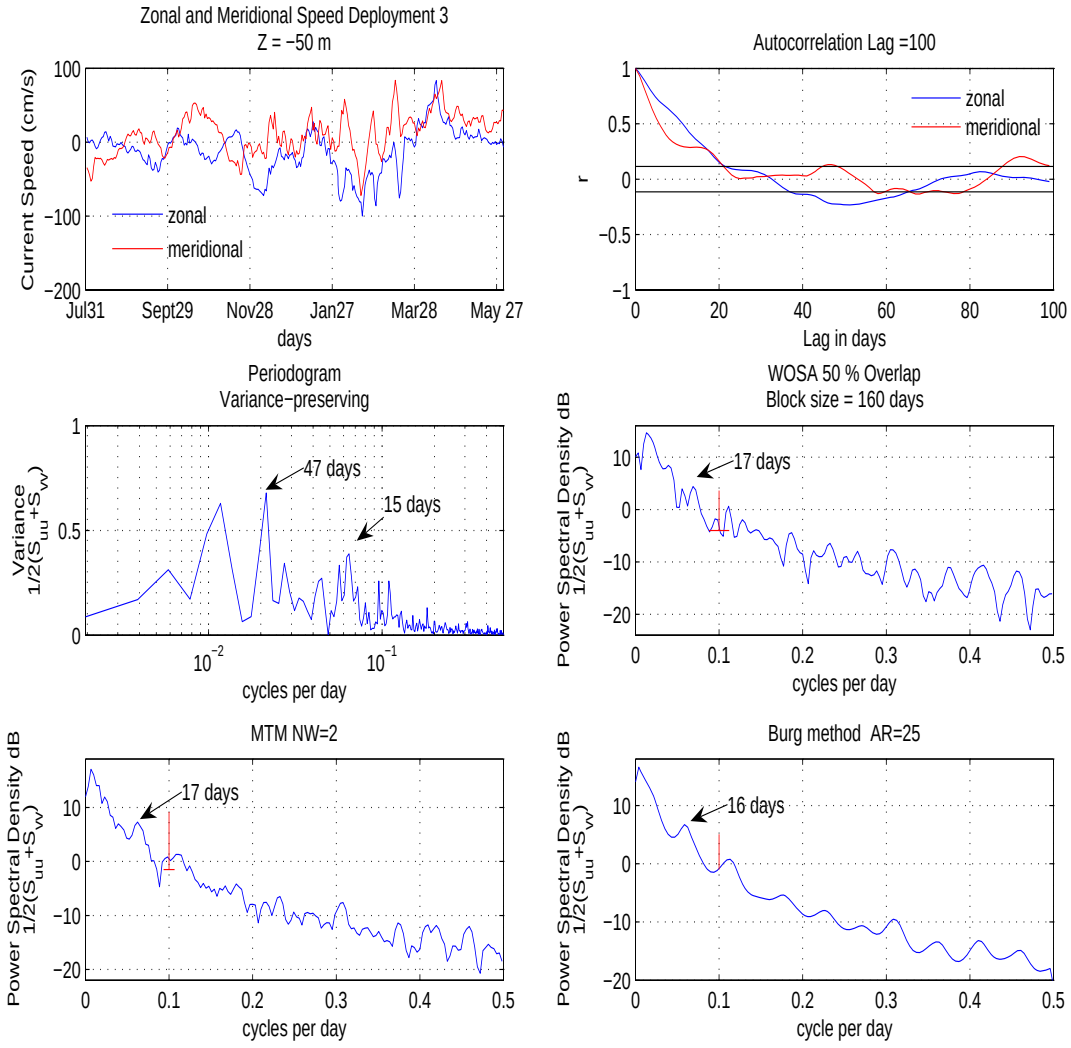

Figure 39. Multiple methods of spectral analysis z = -50 m for Deployment 3.

The first half of the surface time series showed a strong 50 day signal (Figure 41). There was a dipole eddy affecting the mooring during September and early October which may be related to this signal. A strong 15 day signal was seen in the second half of the time series at z = -878 m. A weak 28 day signal was also present in the second half of the time series. This signal was present in the time series from the end of December through the second week of February. During the beginning of this time period eddy N/O was affecting the mooring with the LC/Eddy P impinging on the mooring in the middle to later part of January (Horizon Marine Eddy Track, GOES video, http://www.esl.lsu.edu/reserach/CMI-GOES) A weak 10, 17 and 27 day signal was seen in the lower water column, depths greater than z = - 1378 m. Wavelet analysis (Figure 43) showed a statistically significant 16 day signal near the end of February at this level. Correlation analysis showed no significant correlation between the surface and depth for the months of February and March (Figure 45). At z = -2578 m wavelet analysis showed a 28 day

signal in mid January changing to 16 days in mid February. Wavelet Hovmöller, band-passed between 15-25 days showed a continuous signal from the surface to depth during the later part of February 2002 (Figure 44). Figure 35 shows a GOES SST/SSH, again as in Deployment 1-2, with the mooring between the LC with a LCFE during this same time. A strong connection is evident between the surface and depth for areas between a LCFE and the LC.

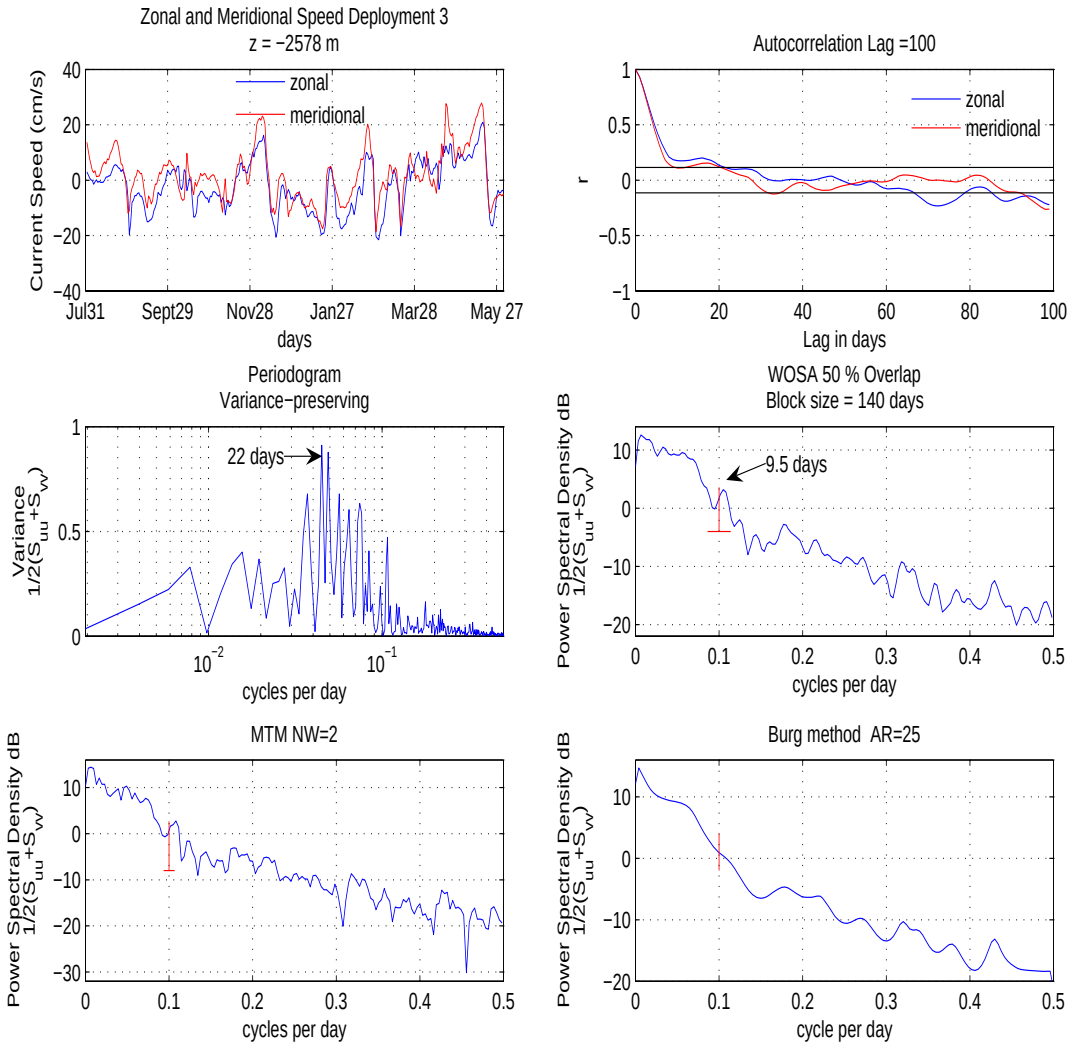

Figure 40. Multiple methods of spectral analysis z = -2578 m for Deployment 3.

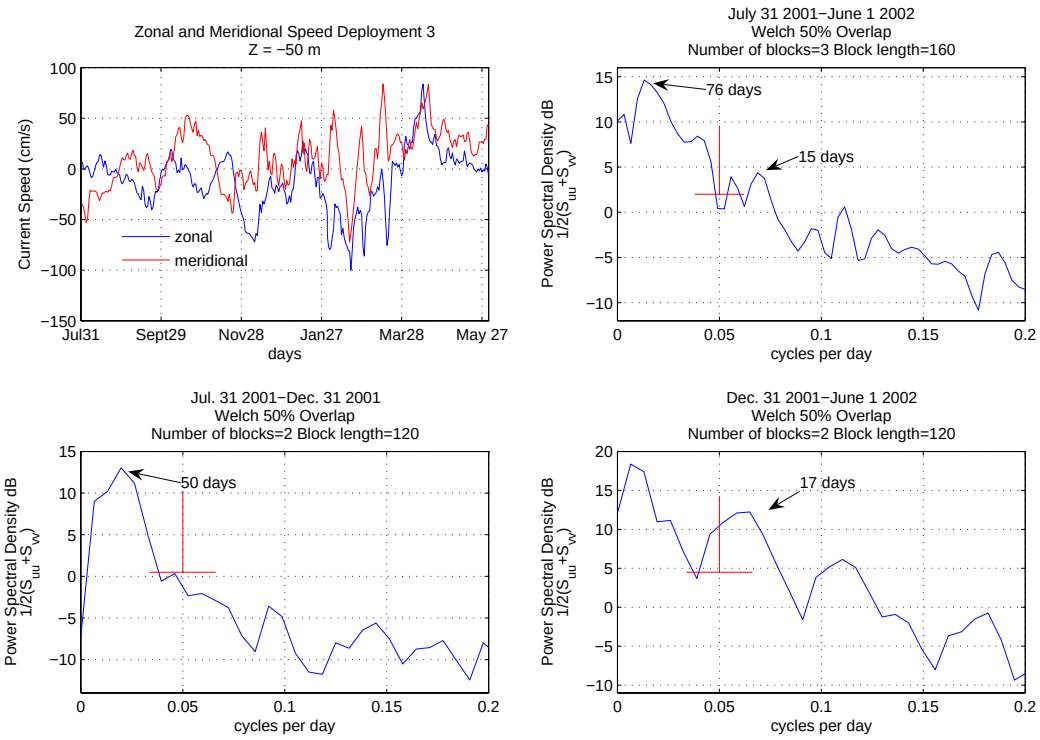

Figure 41. WOSA first and second half of time series z = -50 m for Deployment 3.

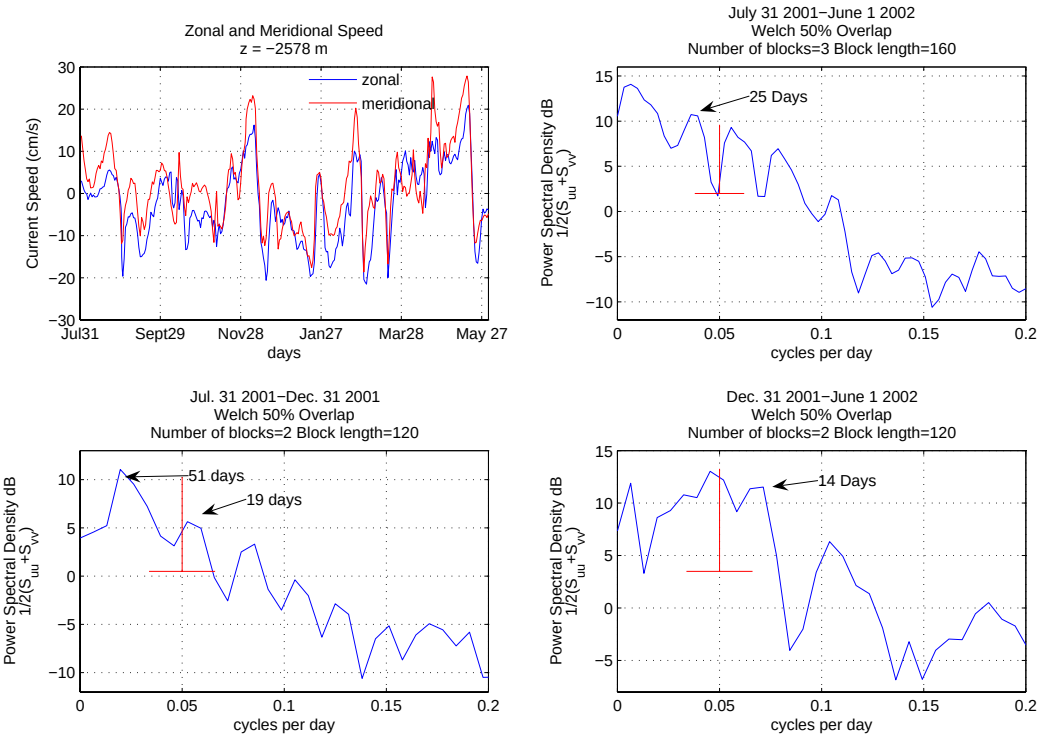

Figure 42. WOSA first and second half of time series z = -2578 m for Deployment 3.

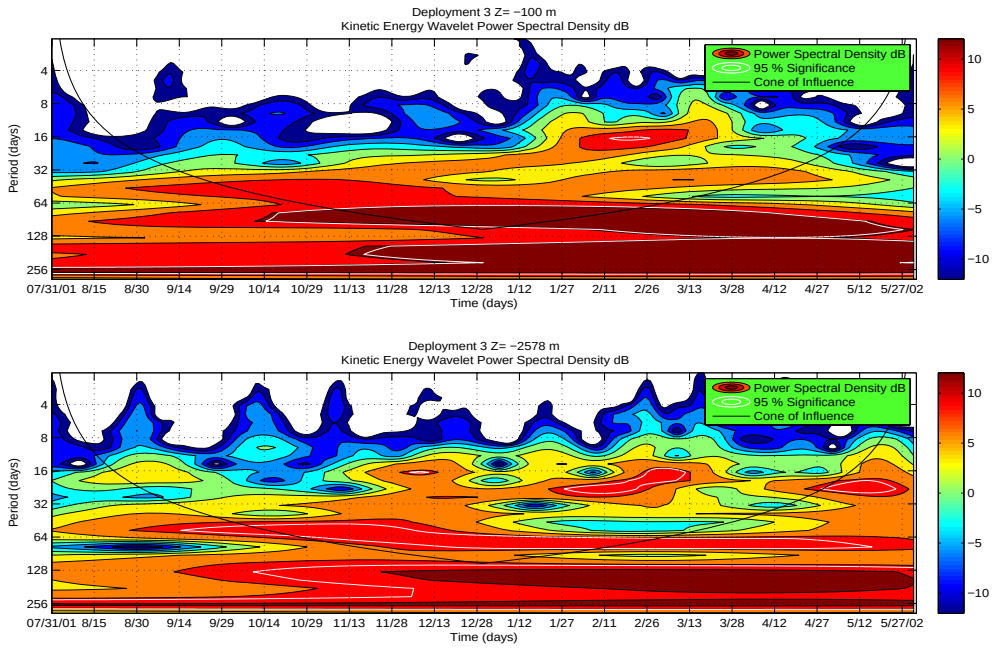

Figure 43. Wavelet analysis z = -100 m and z = -2578 m for Deployment 3.

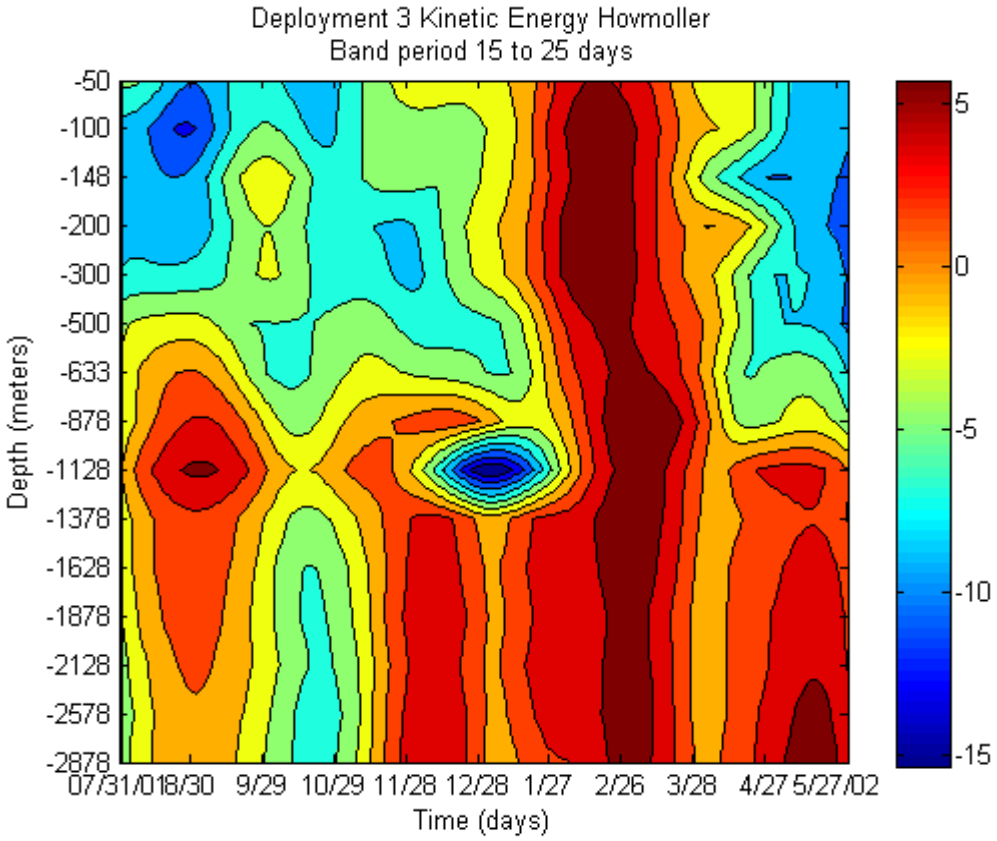

Figure 44. Hovmöller Deployment 3 for band period 15-25 days.

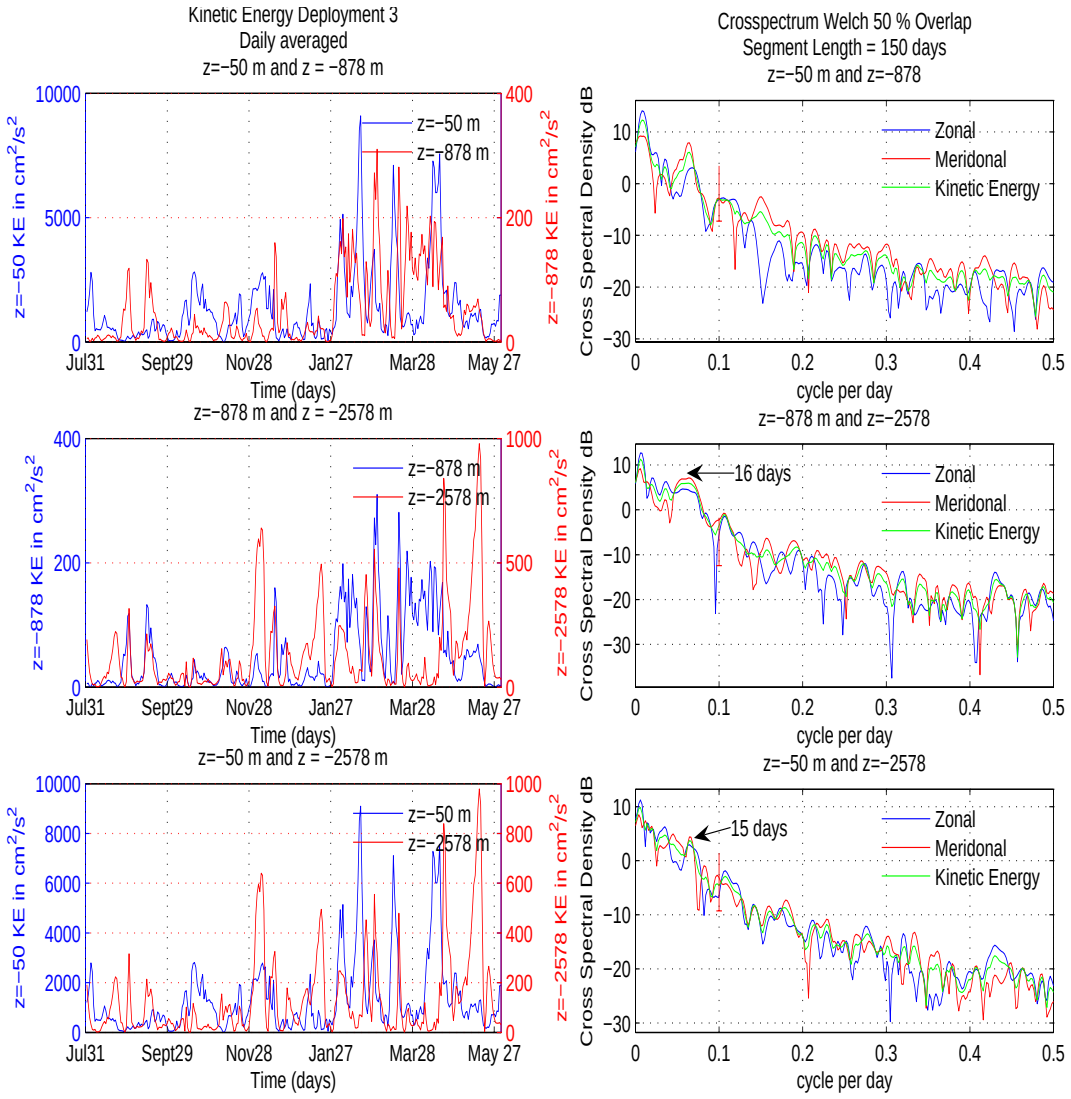

Figure 45. Cross spectral analysis for Deployment 3

4.3 Case Study

During Deployment 3, two distinct short-lived bottom current events were observed in the time series from 27 February to 1 March 2002 and 17-18 March 2002. Both events coincided with energetic meandering of the LC and rapid growth in LCFE cyclones in close proximity and slightly east of the mooring. During these two events (see also Section 4.1, Figure 35 and Figure 36), currents became suddenly energized throughout the water column and even within the normal transition zone where currents are typically near zero (near 1000 m). Current direction throughout the water column below ~200 m was also coherent and flow was directed along the escarpment towards the southwest in both cases. Although as pointed out by Donahue et al. (2006), such current coherency throughout the water column could be a mere coincidence, the two pulsed events during Deployment 3 present an opportunity to explore the possible connections between surface events and water column currents in more detail.

The second event was better revealed in satellite imagery as skies were clearer. A time sequence of GOES SST night-time composite images is shown in Figure 46 and Figure 52, spanning the time period 13 to 19 March 2002. At this time, both Eddies P and Q were detached from the LC which had retreated south of 26º N. The GOES SST imagery reveals that the mooring was situated just to the west of the western flank of Eddy Q. The time sequence of GOES imagery clearly shows the growth of a LC meander and associated LCFE along the northwestern quadrant of Eddy Q directly over the mooring. Unfiltered currents, averaged over 24 hours, at 50m, 1128m and 2878m have been color-coded and superimposed on the satellite imagery. Note that the 50m currents are shown at 50% scale since they are stronger. On 13-14 March, surface currents were strong and northward while bottom currents flowed northeast along the escarpment. As the LCFE grew in size on 15 and 16 March, surface currents rotated counter-clockwise and bottom currents switched direction from northeast to southwest by 16 March. By 17 March, bottom current speeds had intensified further and by 18 March the 1128 m currents were similar in magnitude to those at the bottom. Inspection of currents at all levels (Figure 27-Figure 29) reveals coherency throughout the water column on 18 and 19 March. The short-lived bottom current event to the southwest is consistent with intensification of cyclonic flow at depth, trapped by the escarpment and also with the direction TRW movement.

SSH data shows an area of cyclonic circulation situated between Eddies P and Q several weeks prior, a situation which affected the growth of the LCFE as it moved over it. Similar whole water column current events were observed in late February 2002 as well as during Deployment 4 (1 August 2003) and Deployment 1 (March 2001).

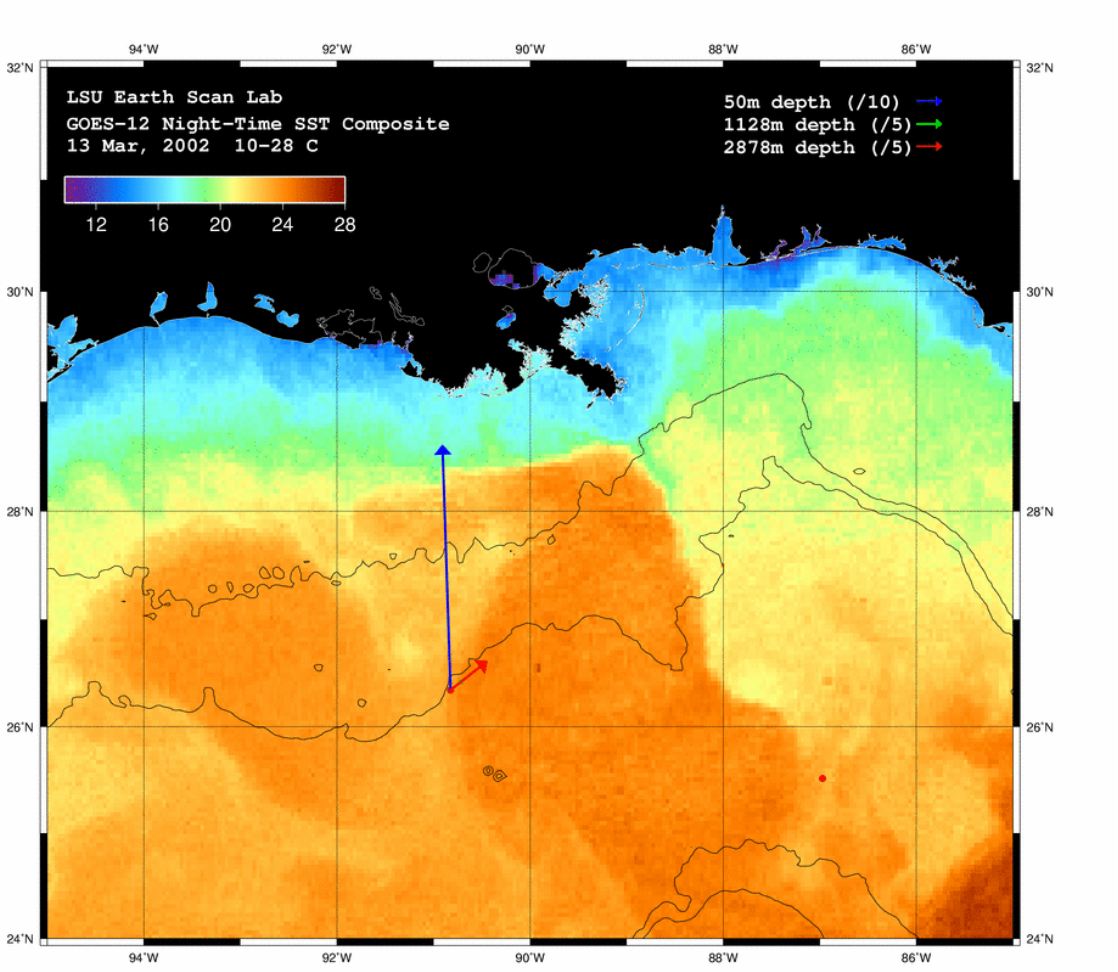

Figure 46. GOES night-time SST composites with mean currents for March 13, 2002.

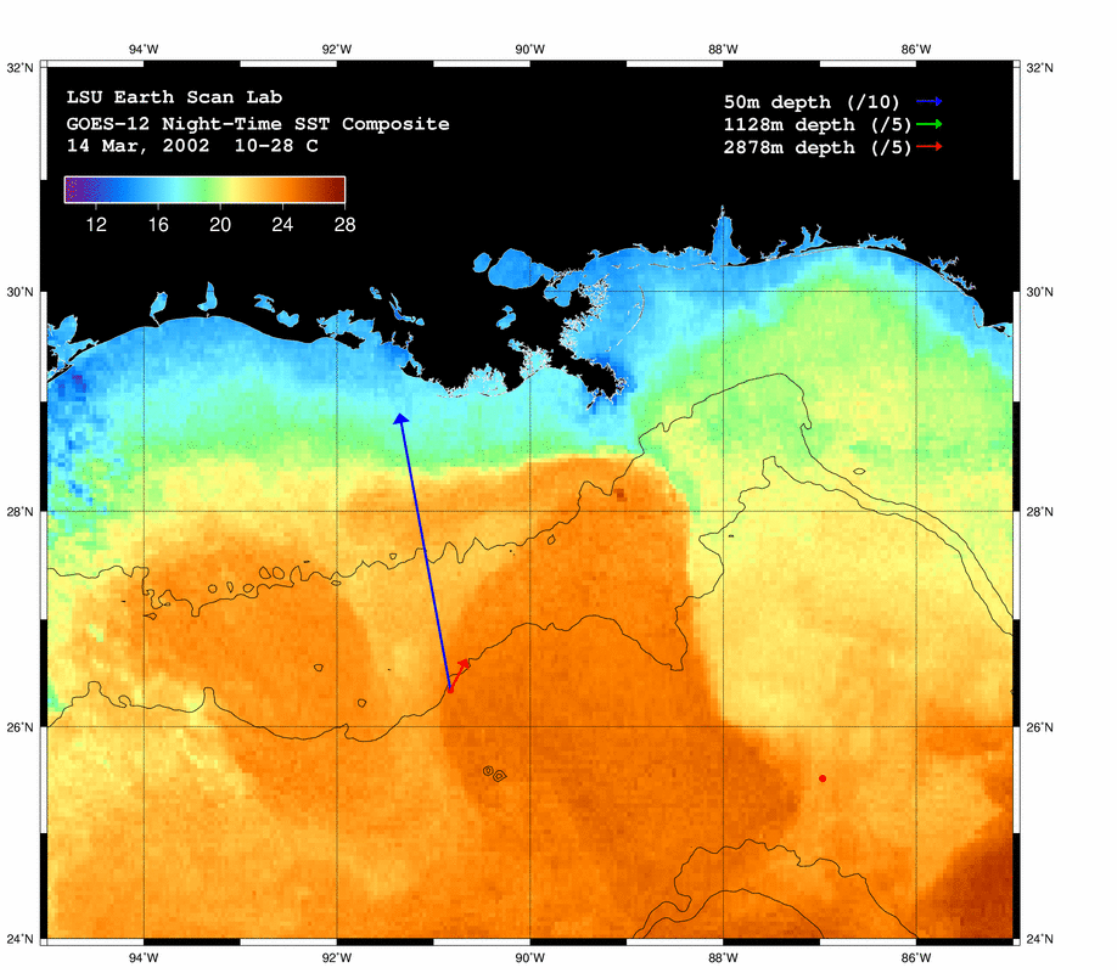

Figure 47. GOES night-time SST composites with mean currents for March 14, 2002.

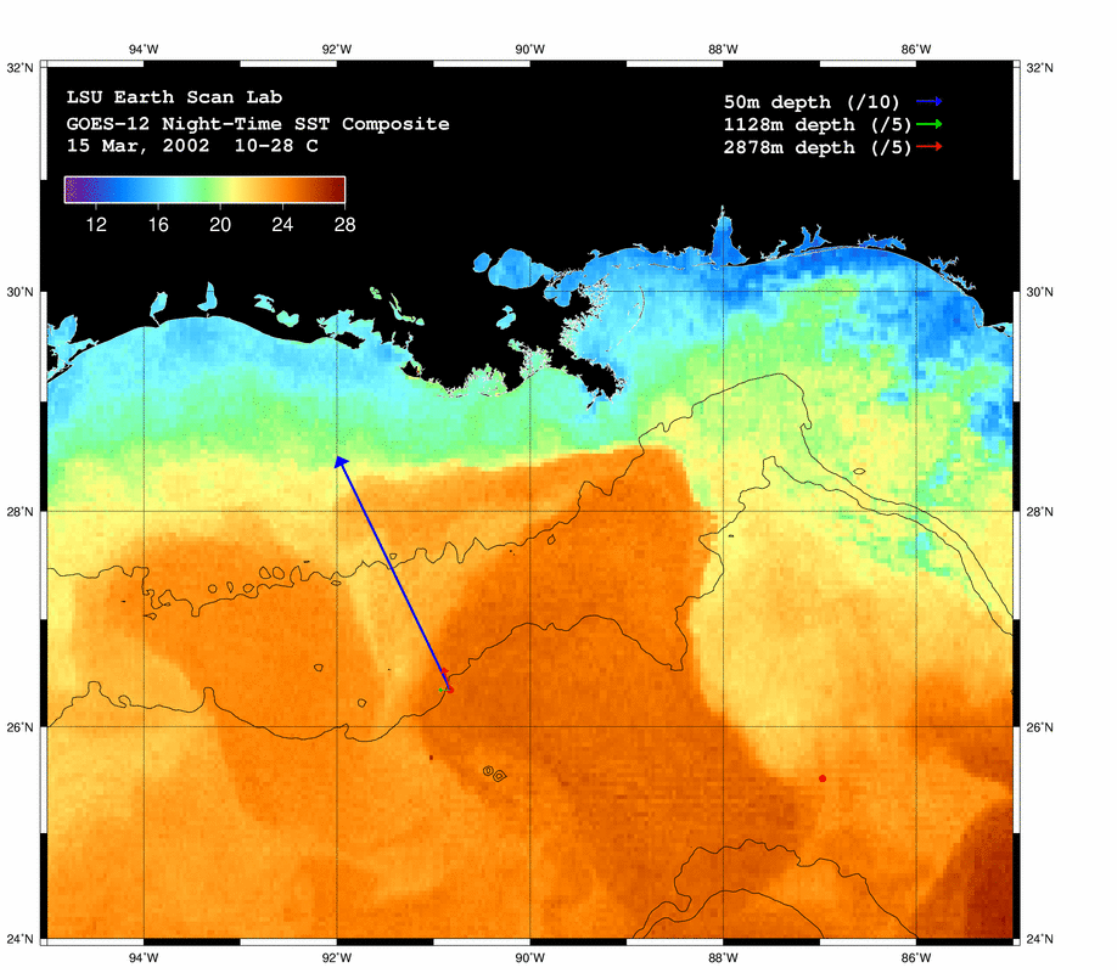

Figure 48. GOES night-time SST composites with mean currents for March 15, 2002.

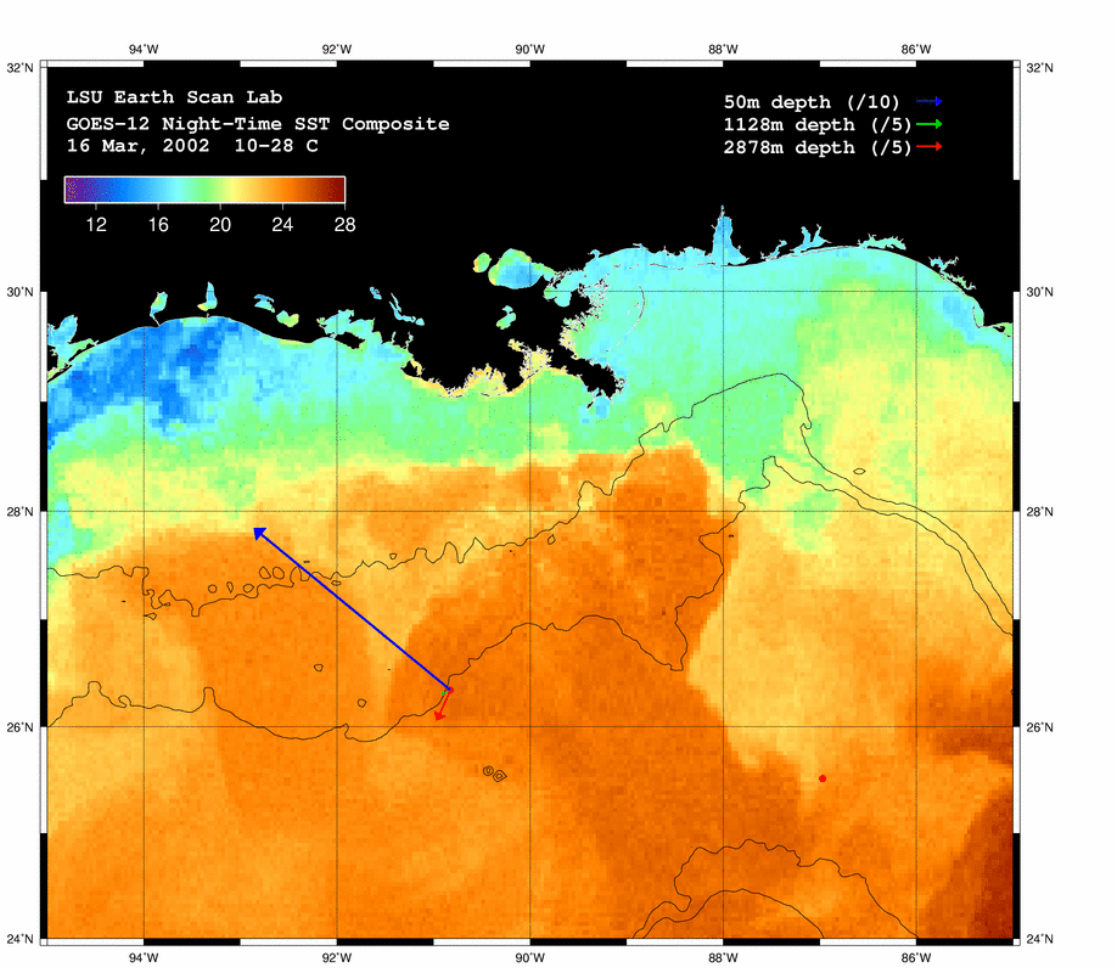

Figure 49. GOES night-time SST composites with mean currents for March 16, 2002.

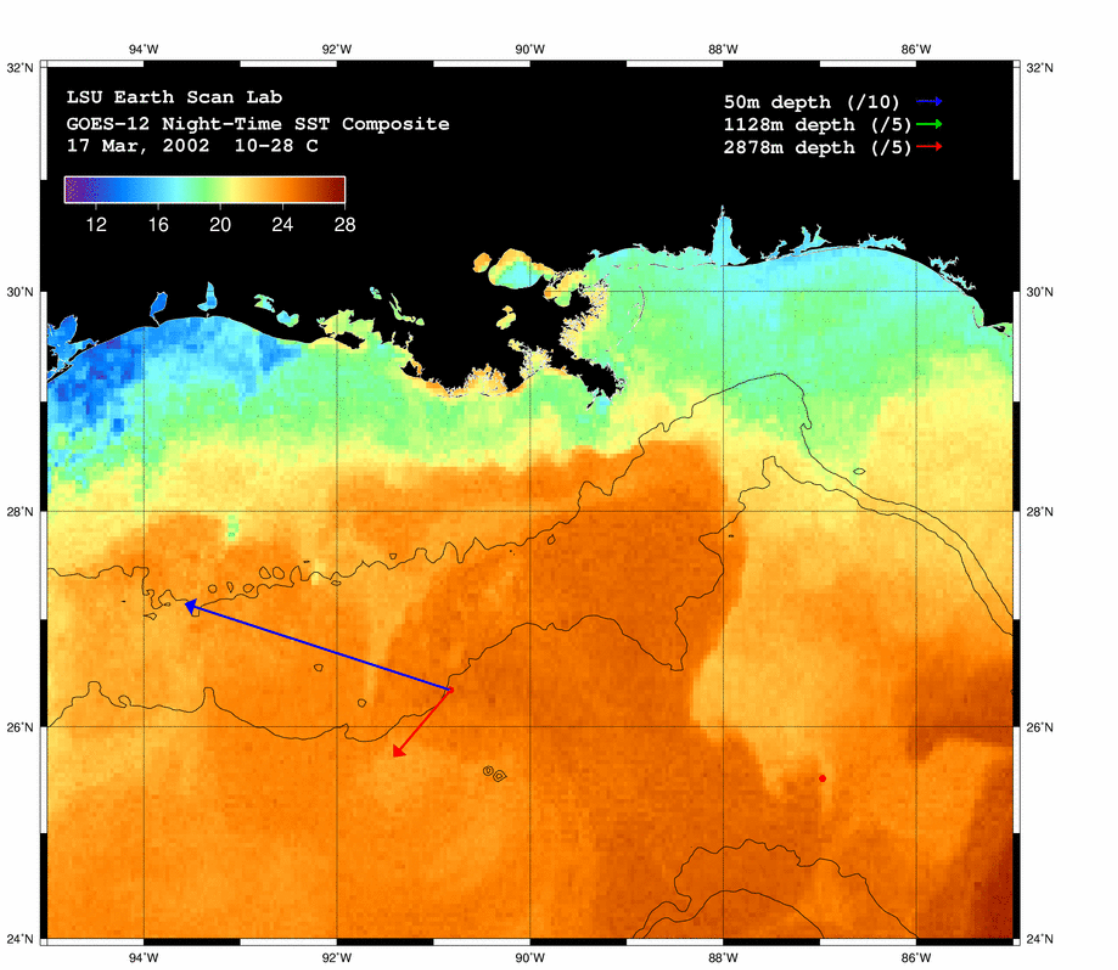

Figure 50. GOES night-time SST composites with mean currents for March 17, 2002.

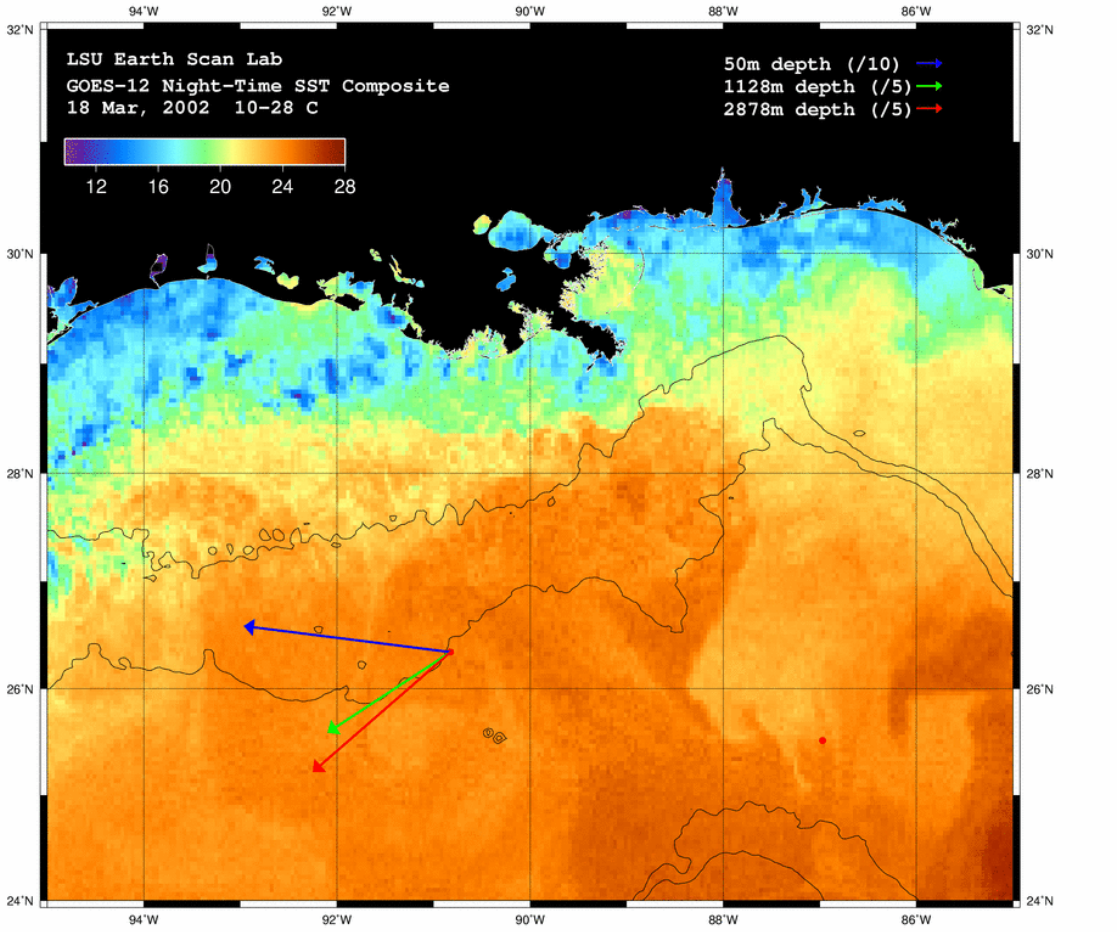

Figure 51. GOES night-time SST composites with mean currents for March 18, 2002.

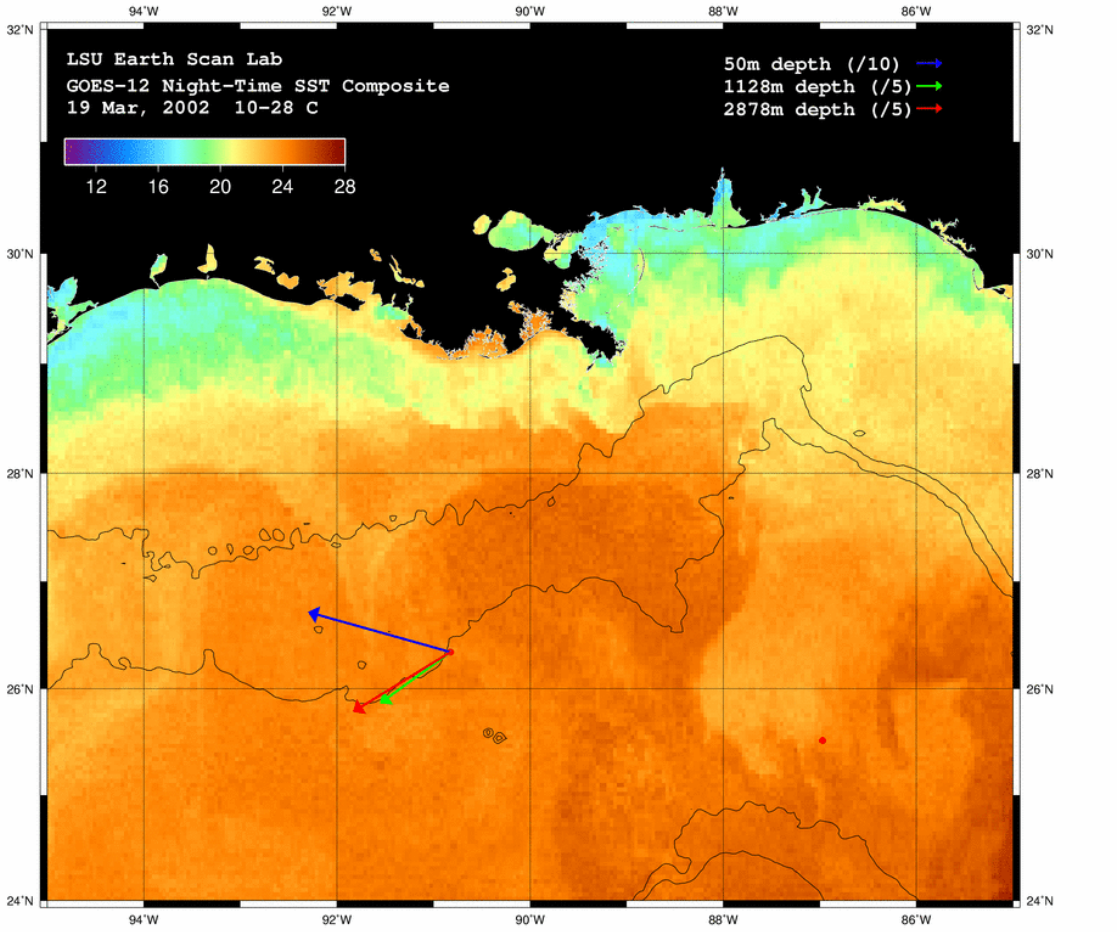

Figure 52. GOES night-time SST composites with mean currents for March 19, 2002.

5.0 MOORING LOCATION 3, DEPLOYMENT 4

5.1 Initial Conditions, Major Ocean Events, and CTD Data

In this section, water column currents and temperature are discussed in relationship to large-scale movements of Gulf water masses as revealed in satellite SST and SSH data. Color-enhanced time series of currents and temperatures in the upper 1200 m are depicted in Figure 53. Time-series of current speeds and current vectors are shown in Figure 54 and Figure 55. Satellite SST/SSH imagery for selected current Events are displayed in Figure 56-Figure 68.

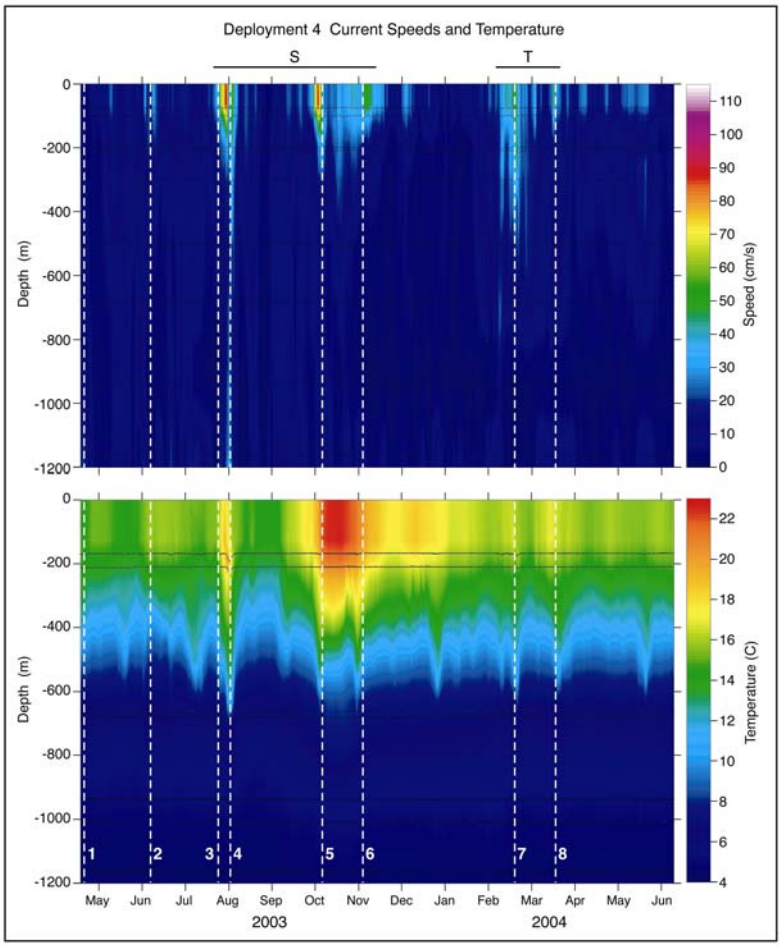

Figure 53. Color-enhanced LP current speed (cm/s) from 0-1200 m and temperature from 0-1200 m for Deployment 4. White lines depict case study events.

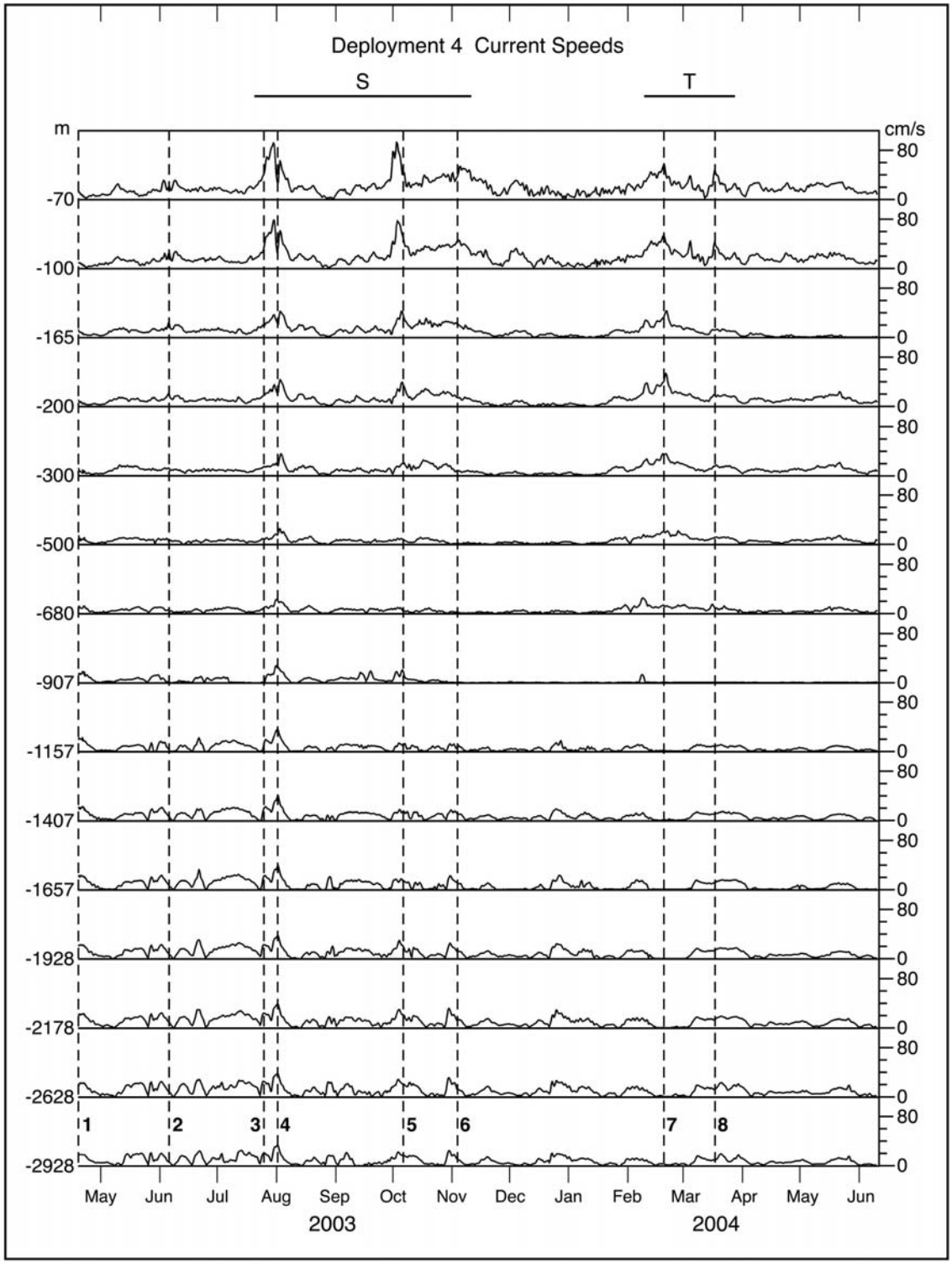

Figure 54. LP current speeds (cm/s) at 15 depths from near surface to near bottom for Deployment 4.

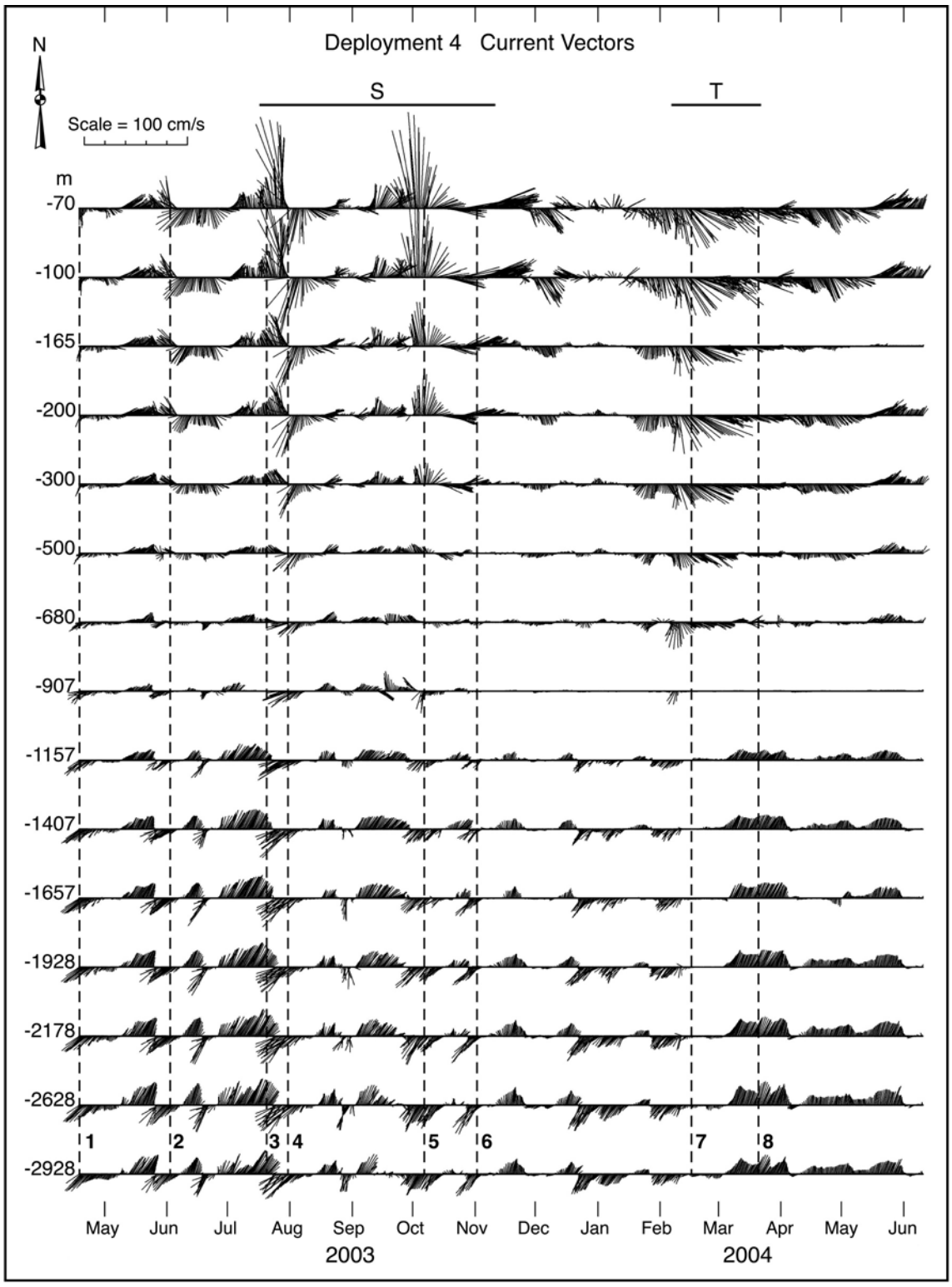

Figure 55. LP current vectors (cm/s) at 15 depths from near surface to near bottom for Deployment 4.

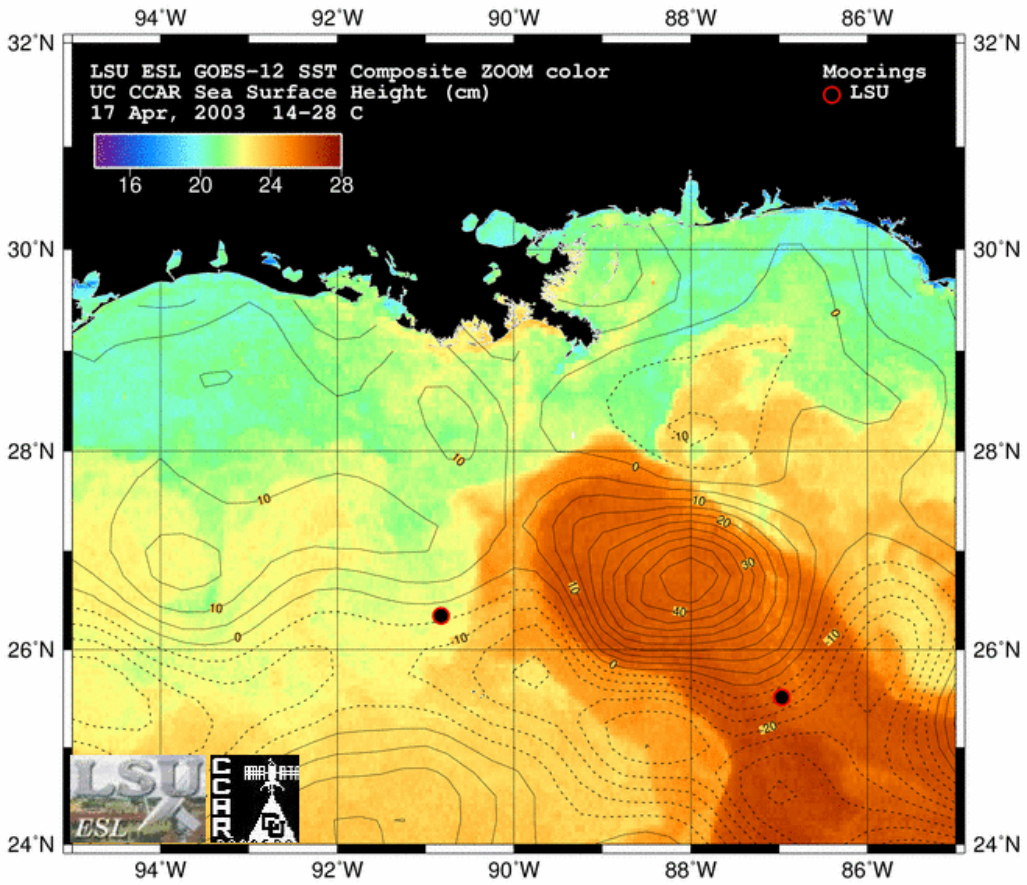

Figure 56. GOES night-time SST composites and SSH contours for Event 1 (17 April 2003). The LC mooring of Inoue et al. (in preparation) is also shown.

This full water column mooring was deployed on April 17, 2003 in 3028 m of water slightly west of the previous mooring at the base of the Sigsbee Escarpment (Figure 53, Figure 1, Table 2). This change in mooring location was requested by SAIC at the last minute, before deployment, as they feared that our mooring and theirs might interfere with one another. This mooring site was a little closer to the Sigsbee Escarpment (~3 km) than the previous mooring. In March and April, before the deployment, LC activity increased east of the mooring as it surged northwards. At the time of deployment, the LC was east of the mooring and its northern flank as revealed by SST imagery was near 28ºN (Figure 56, Event 1). SSH data revealed that the mooring was located in a region of cyclonic circulation associated with a LCFE cyclone on the northwest margin of the LC. Surface currents were initially very weak. East of 90º, LC and LCFE activity increased in May and June and Eddy S began to form. By early June, the LC was elongated west to east (90º to 86º W) and a LCFE moved close to the mooring, where a cold core cyclone was still the dominant feature (Figure 57, Event 2). Surface flow switched rapidly from northward to southward as the LCFE moved northwestward over the mooring on June 3-4 (Figure 57, Event 2). It is interesting to note that the bottom currents were relatively strong (~25 cm/s) and alternated from northeast to southwest, with flow reversals every ~10 to 14 days in

May and June when LCFE activity was present close to the Sigsbee Escarpment east of the mooring (Figure 58). This may indicate the presence of stronger than usual TRW activity initiated east of the mooring and traveling westward past the mooring.

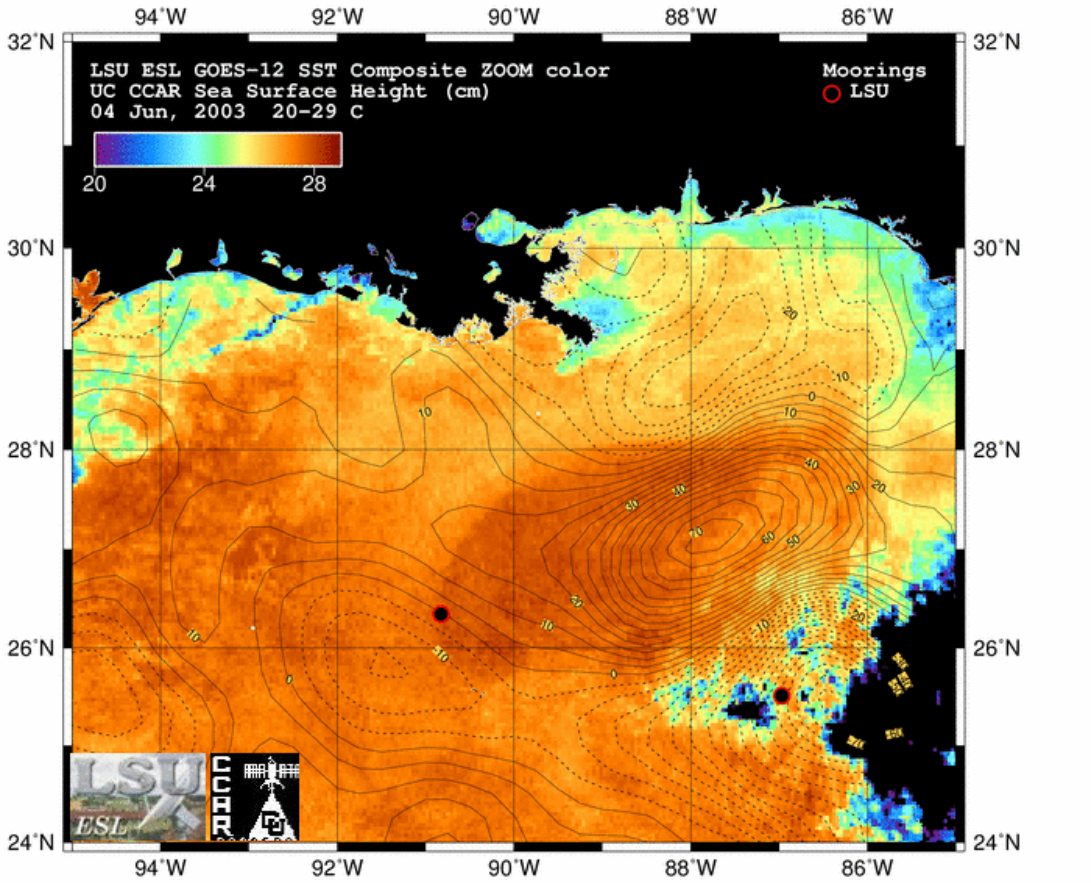

Figure 57. GOES night-time SST composites and SSH contours for Event 2 (4 June 2003). The LC mooring of Inoue et al. (in preparation) is also shown.

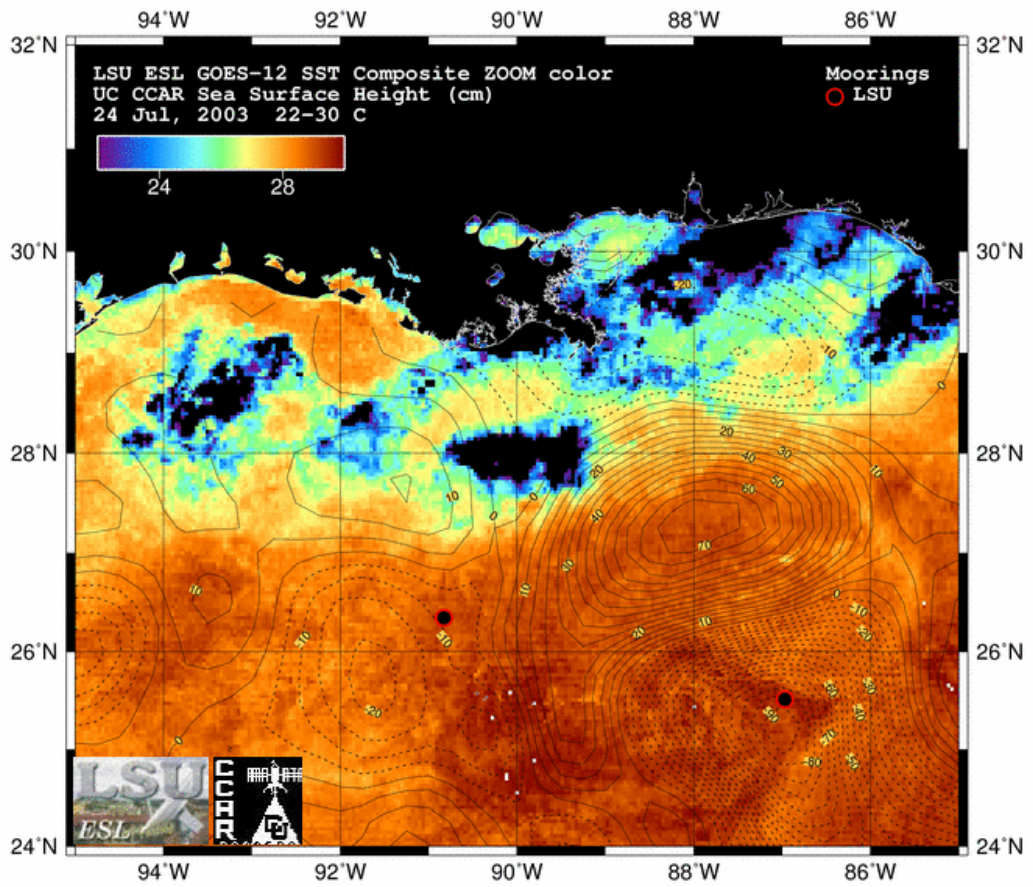

Figure 58. GOES night-time SST composites and SSH contours for Event 3 (24 July 2003). The LC mooring of Inoue et al. (in preparation) is also shown.

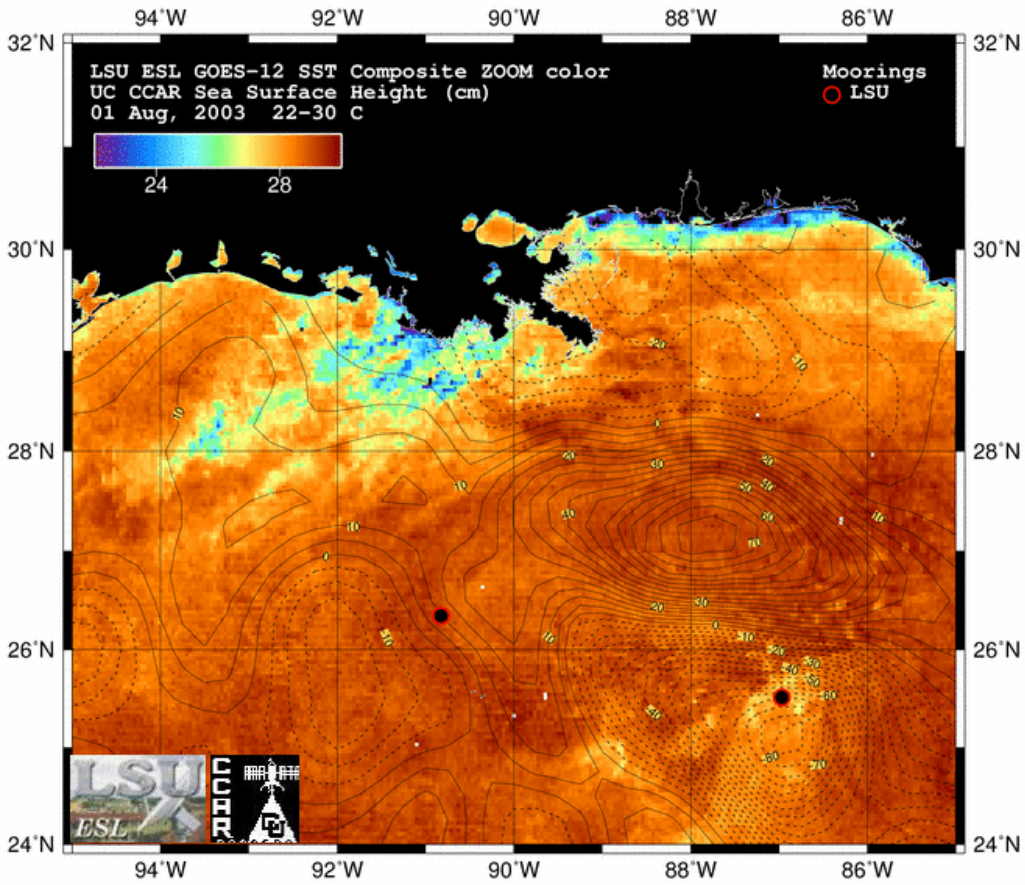

Figure 59. GOES night-time SST composites and SSH contours for Event 4 (1 August 2003). The LC mooring of Inoue et al. (in preparation) is also shown.

The strongest current event of the deployment occurred in late July/early August and this event affected the entire water column (Figure 54, Figure 55). The current records reveal that on July 25, northward surface flow began to increase to a maximum of near 100 cm/s on 29 and 30 July (Figure 53-Figure 55). A reversal in bottom flow to the southwest occurred on July 23, several days before the surface current acceleration, an event which could have been initiated along the escarpment east of the mooring. Southwestward bottom flow was sustained for two weeks with maximum speeds of ~30 cm/s on July 31 (Figure 54, Figure 55). On August 1, surface flow changed direction rapidly to southwestward, increasing to a speed maximum of 60 cm/s on August 3. The time series of current speeds at all depths (Figure 54) clearly reveals acceleration of the entire water column from July 31- August 5 with coherency of flow to the southwest throughout the water column. Evidence of mooring blow-over was observed in the pressure records to 1200 m water depth (Figure 53). SSH data at that time revealed a LCFE cyclone had developed along the northwest flank of Eddy S, which was still attached to the LC (Figure 58-Figure 59, Events 3 and 4). Unfortunately the GOES SST data revealed little temperature information that could assist in tracking Eddy S and LCFE cyclones during this event. During mid-summer infrared measurements of SST are not often useful as surface temperature gradients

are non-existent. In addition, when features move very fast, as they did during this event, SSH data does not always provide accurate feature information. However, an analysis of MODIS chlorophyll *a* satellite imagery performed by Bob Leben has enabled re-creation of the major events that transpired from July 9 through early August (See Fig 4.1-13 in Donohue et al., 2006). Since LC water is deficient in chlorophyll *a*, it can be distinguished from LCFE cyclones which are relatively rich in chlorophyll *a* due to the upwelling of nutrients which cause phytoplankton blooms. The MODIS time series demonstrated that in mid-July, a LCFE cyclone traveled clockwise south of the southern flank of Eddy S, initiating the separation of Eddy S from the LC. This cyclone continued to move westward, and it cut Eddy S (which was an odd elongated shape) into two parts by early August. The southern part became a separate WCE, but was never named by Horizon Marine Inc. The strong surface currents at the mooring on July 24 and the subsequent coherence in flow throughout the water column (July 31-Aug 5) can be attributed to effects from this LCFE. Figure 53 reveals that the strongest surface flow late in July 2003 was accompanied by a surge of warm water, traceable to 600 m in depth. Close inspection of the MODIS time series (Donohue et al., 2006) indicates that the warm filament may have been pushed over the mooring (from east to west) by the approaching LCFE (the one that later separated Eddy S into 2 parts). The warm water event was short-lived at the mooring as the temperature time series reveals that much cooler water moved in several days later and persisted through September (Figure 53). It is likely that the cool water was associated with the cyclone that split Eddy S into parts, giving birth to the un-named WCE. As a result of the very rapid movements of this LCFE cyclone, the SSH data demonstrated in July 24 and July 31 images (Figure 58 and Figure 59) are not considered very accurate.

Further investigation of the time history of this unique event was pursued using Oceansat-1 OCM chlorophyll *a* images as well as image composites over 3-day periods. As the images are available every other day, combining two yields a 3 day composite. These images have the potential of providing both more spatial and temporal detail. A sequence of selected clearest sky 3-day composites are shown in Figure 60-Figure 64 spanning the time period, 8/10 July to 30 July/1 August 2003. Annotations of features are provided to assist the reader.

The July 8/10 composite shows Eddy S, which is entraining shelf water along its eastern margin towards a well-developed circular-shaped cyclone near 26º N, 89º W. The composite of July 12/14 reveals passage of Hurricane Claudette towards Louisiana. When the skies cleared on 18/20 July, the cyclone (indicated with relatively high chlorophyll *a)* had moved between the LC and Eddy S and was now positioned south of Eddy S which had become elongated and indented on the southern flank. It is interesting to speculate on the possible influence of hurricane-force winds in this event. Walker et al. (2005) showed that circulation and upwelling within LCFE cyclones can be greatly intensified during hurricane passages. The July 24/26 composite reveals that the cyclone was continuing to move around Eddy S with the leading edge positioned near 26.4º N, 90º W. By July 30/August 1, the leading edge of the cyclone had reached LSU's mooring. A short-lived whole water column event, characterized by southwest flow from 70m to the bottom, was experienced on August 1, coinciding with the arrival of this energetic cyclone. The temperature signal reinforces the satellite observations as the warm water observed at the mooring due to Eddy S was quickly replaced by cooler water when the cyclone reached the mooring in early August 2003.

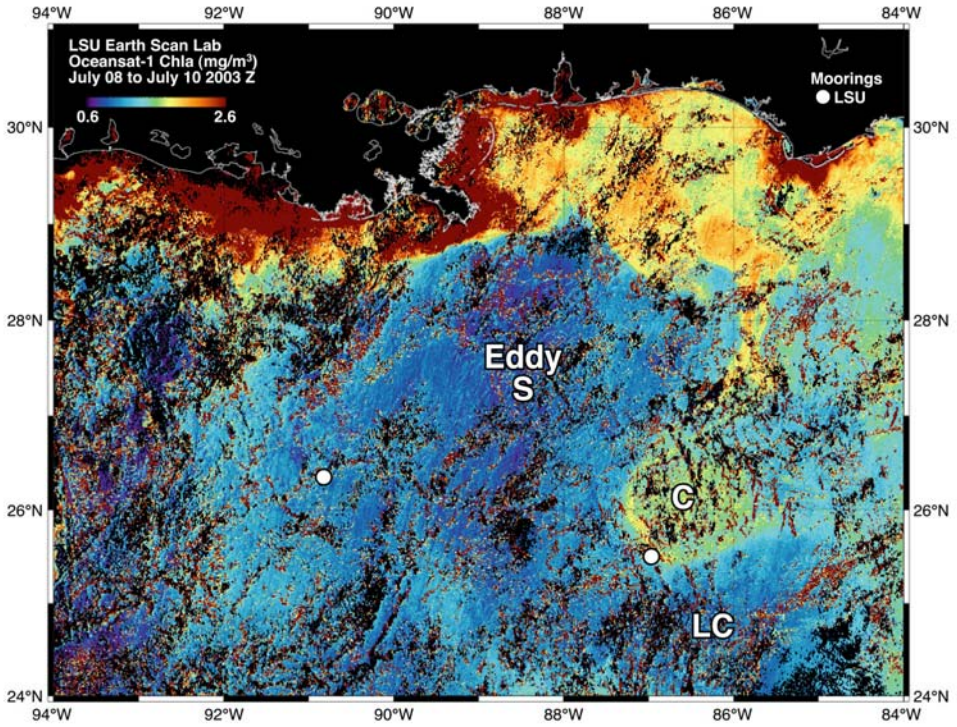

Figure 60. Oceansat-1 OCM Chlorophyll *a* July 8-10 2003. The LC mooring of Inoue et al. (in preparation) is also shown.

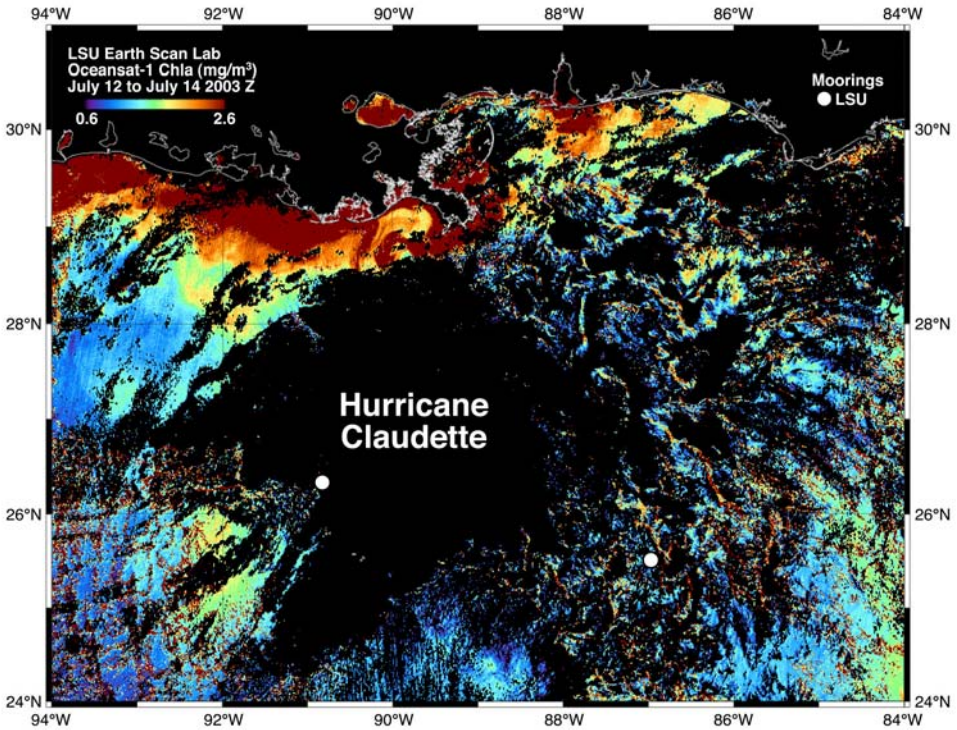

Figure 61. Oceansat-1 OCM Chlorophyll *a* July 12-14 2003. The LC mooring of Inoue et al. (in preparation) is also shown.

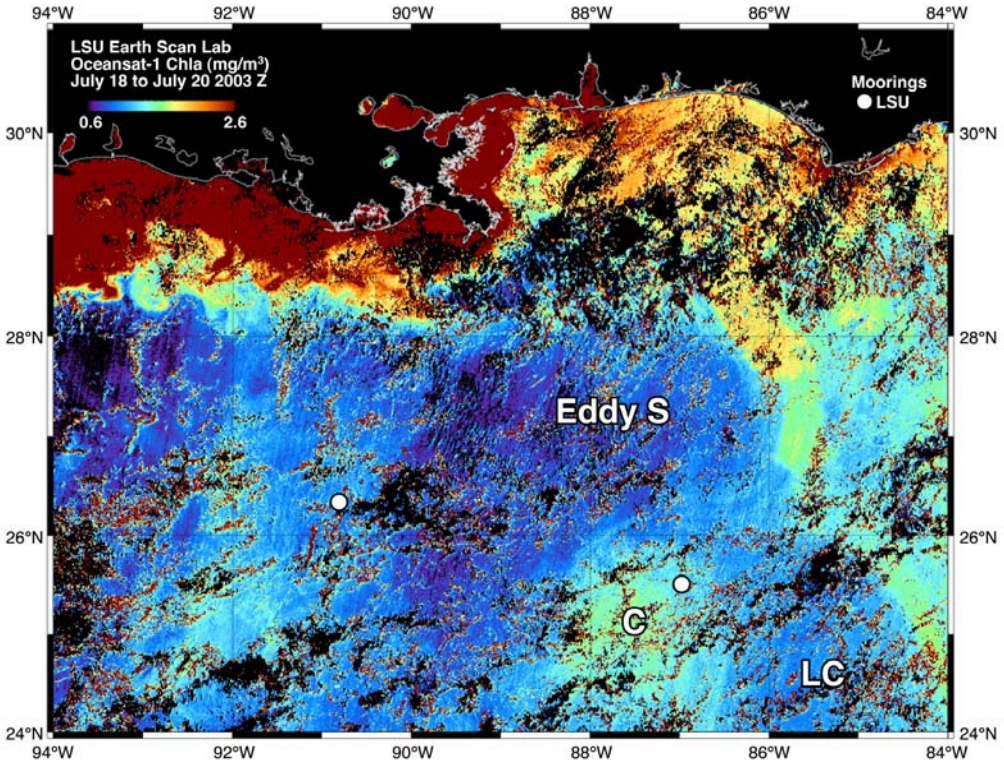

Figure 62. Oceansat-1 OCM Chlorophyll *a* July 18-20 2003. The LC mooring of Inoue et al. (in preparation) is also shown.

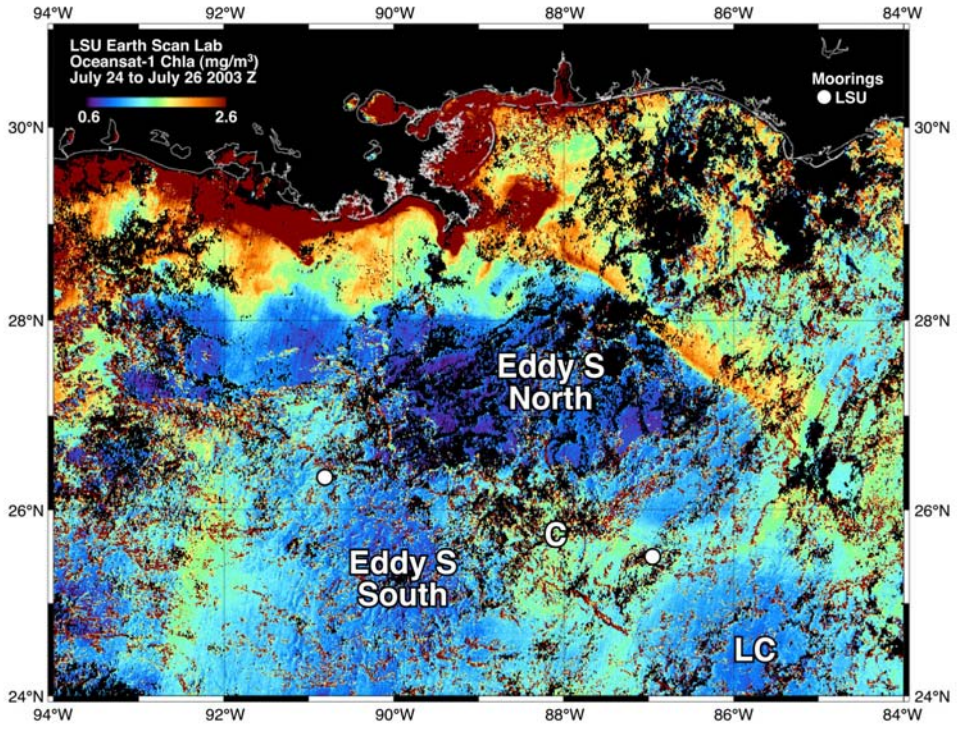

Figure 63. Oceansat-1 OCM Chlorophyll *a* July 24-26 2003. The LC mooring of Inoue et al. (in preparation) is also shown.

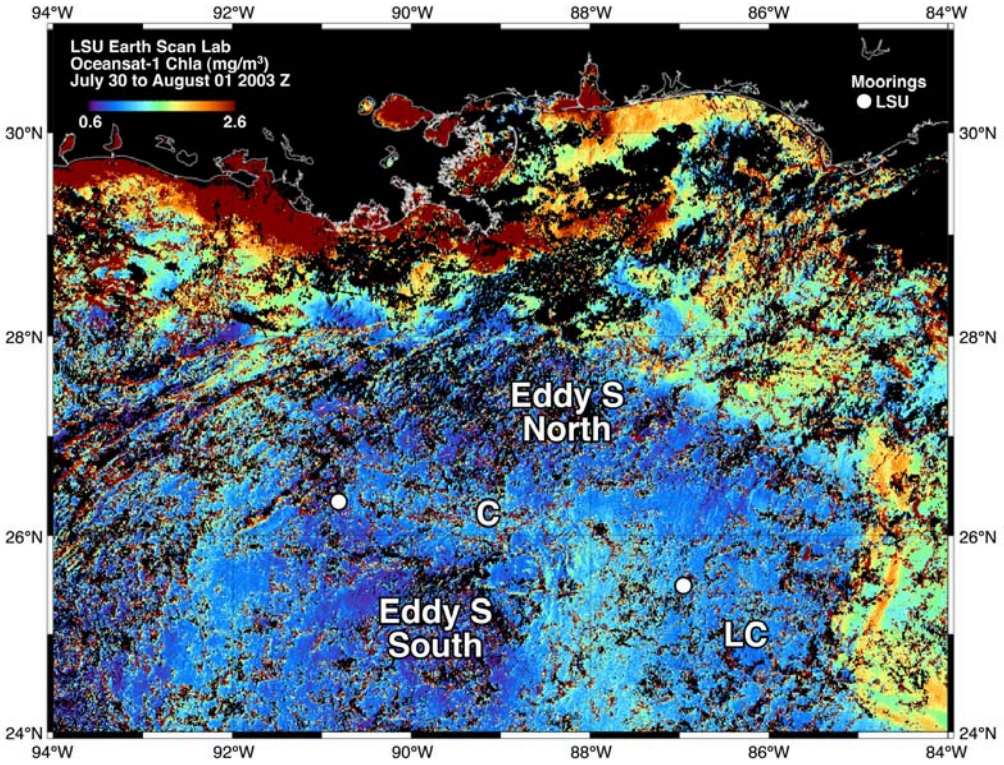

Figure 64. Oceansat-1 OCM Chlorophyll *a* July 30-August 1 2003. The LC mooring of Inoue et al. (in preparation) is also shown.

The next surface current acceleration at the mooring occurred from September 30 to October 6 (Figure 53-Figure 55), followed by relatively warm temperatures from late September through December 2003 (Figure 53). The surface current acceleration occurred as Eddy S moved southwestward towards the mooring (Figure 65, Event 5). Eddy S moved directly over the mooring, and event that is reflected in the surface temperatures which exceeded 22º C during the month of October. A second acceleration in surface currents occurred as the northern flank of Eddy S moved across the mooring in early November (Figure 66, Event 6). It is interesting to note that current speeds increased from the surface to the bottom during these two time periods, associated with the southwestern and northern flanks of Eddy S (Figure 54). During both current events, lower layer flow associated with Eddy S was directed to the southwest (Figure 55).

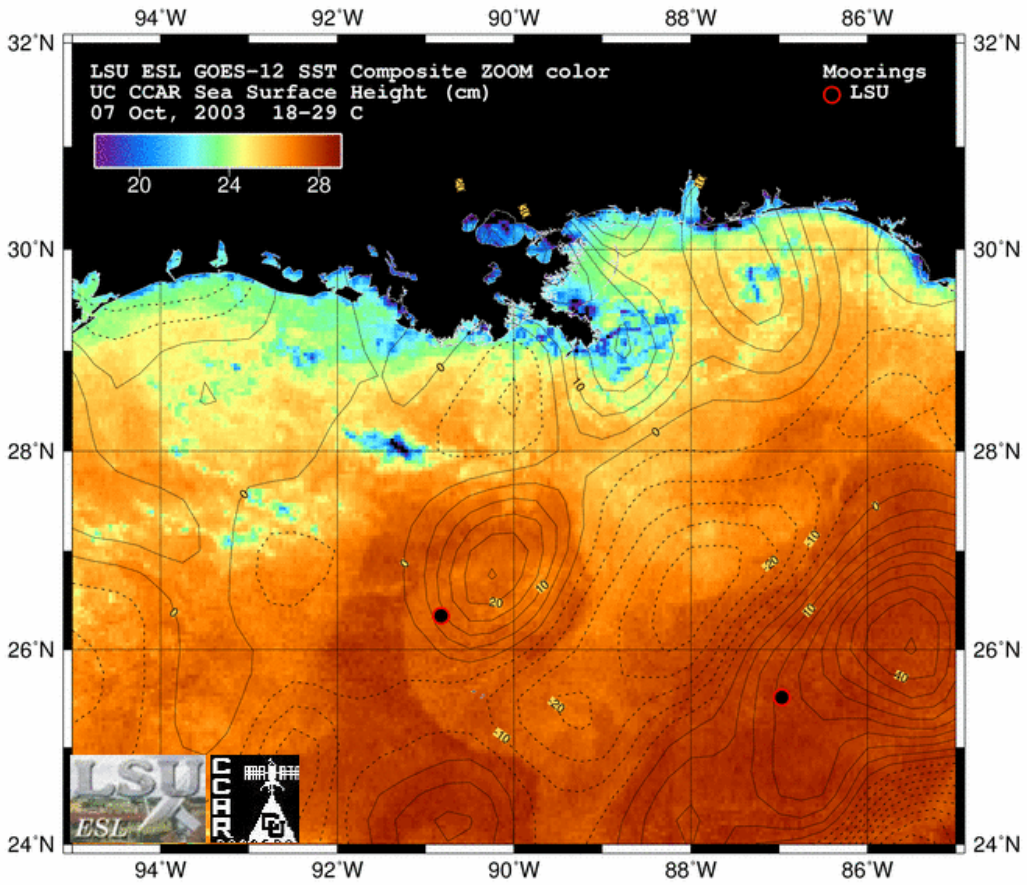

Figure 65. GOES night-time SST composites and SSH contours for Event 5 (7 October 2003). The LC mooring of Inoue et al. (in preparation) is also shown.

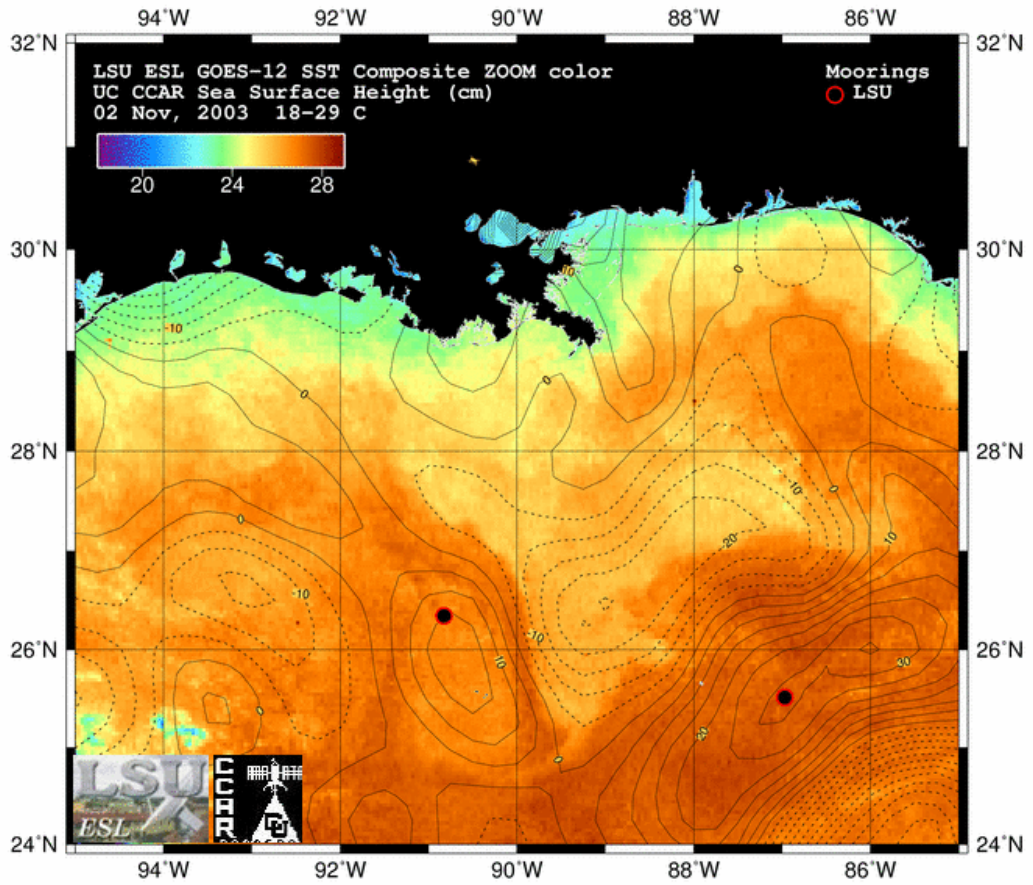

Figure 66. GOES night-time SST composites and SSH contours for Event 6 (2 November 2003). The LC mooring of Inoue et al. (in preparation) is also shown.

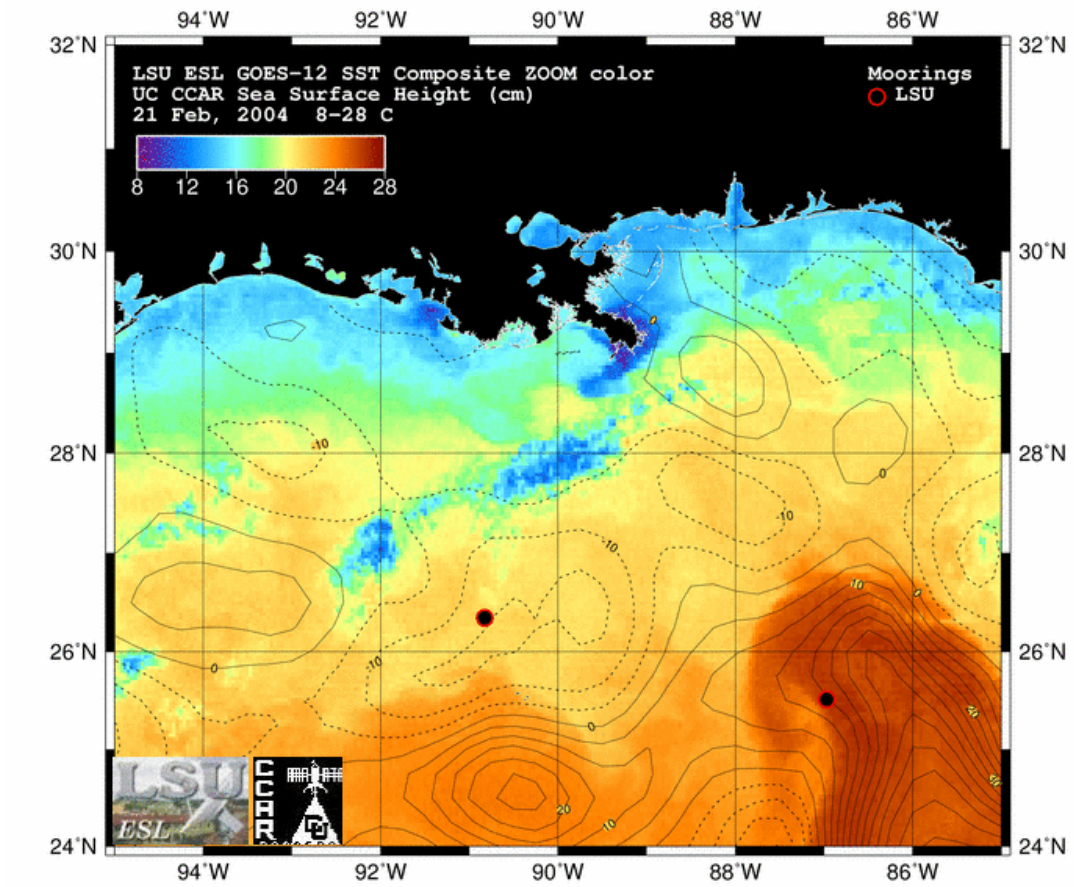

Figure 67. GOES night-time SST composites and SSH contours for Event 7 (20 February 2004). The LC mooring of Inoue et al. (in preparation) is also shown.

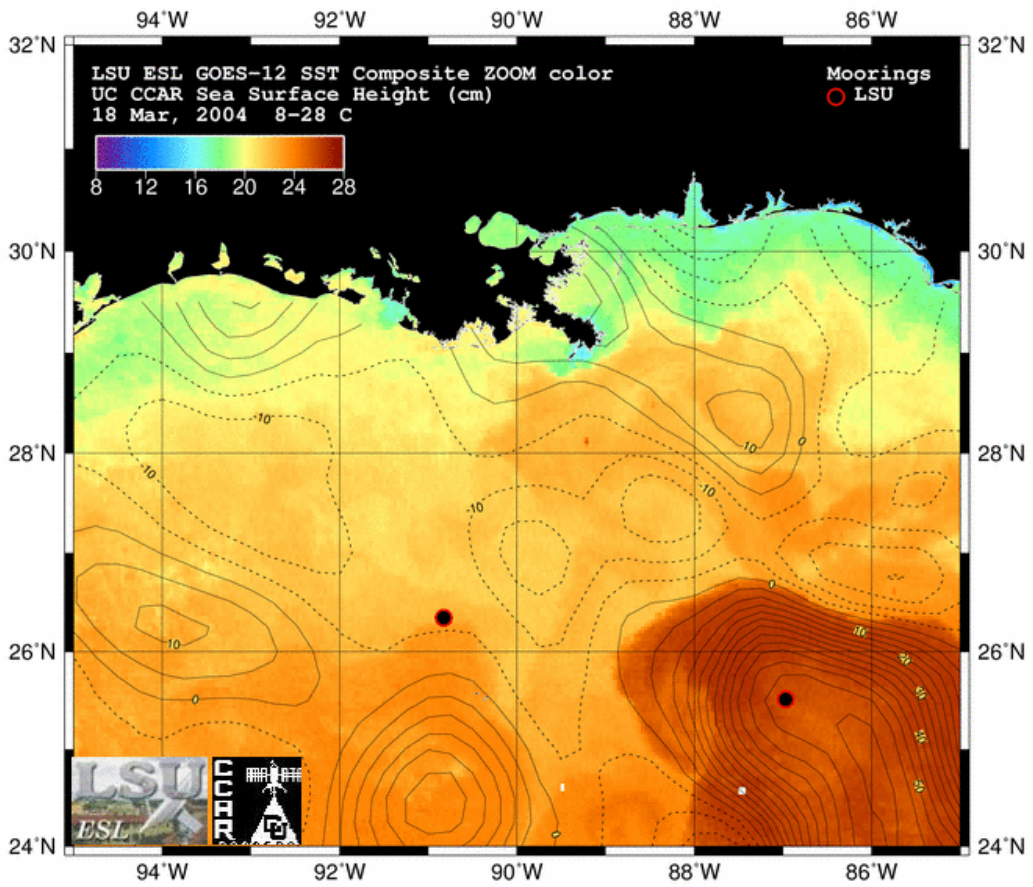

Figure 68. GOES night-time SST composites and SSH contours for Event 8 (18 March 2004). The LC mooring of Inoue et al. (in preparation) is also shown.

Thereafter, surface currents at the mooring were relatively weak until Eddy T moved south of the mooring in mid-February 2004 (Figure 53-Figure 67, Event 7). Maximum surface currents near 60 cm/s occurred on February 20 when the new WCE, Eddy T, passed south of the mooring, although the mooring was then in a region of cyclonic circulation (Figure 59, Event 4). This indicates that surface circulation in general was intensified by approach of the eddy. Eddy T remained south of the mooring during March and caused two additional accelerations in surface flow, the strongest of which occurred on 15-17 March (Figure 68, Event 8) when near surface speeds reached 50 cm/s (Figure 53-Figure 55). Flow in the bottom layer (1160-2928 m) was directed to the northeast during March, April and May and appeared unrelated to surface events (Figure 55). Although the LC again surged northwards in March and April to 27º N, the LC current and LCFE's remained east of 89º W where they had minimal influence on circulation at the mooring for the rest of the deployment period.

5.2 Simple Statistics and Time Series Analysis

Basic current statistics for Deployment 4 are shown in Table 5. Deployment 4 differed from the other deployments in that the western component of the velocity only dominated the lower 1000 m. The northerly component was similar to what was seen in Deployments 1 and 2. Both showed a net northerly component in the bottom 1000 m.

Table 5

Mean, Maximum, and Minimum Velocities Deployment 4

Depth (m)	Mean (cm/s)			Max (cm/s)			Min (cm/s)			Standard Deviation (cm/s)		
	U	V	Speed	U	V	Speed	U	V	n	U	V	Speed
-76	10.06	1.14	22.51	69.25	102.00	102.21	-41.00	-78.00	10073	15.78	19.25	14.68
-100	9.03	0.35	20.22	63.05	88.00	88.45	-33.53	-67.50	10073	14.48	16.82	12.85
-165	4.22	.25	11.78	51.15	48.98		-29.14	-44.77	10073	9.85	10.11	
-200	6.00	-0.44	13.38	58.25	48.67	64.20	-31.93	-48.67	10073	10.22	10.38	8.31
-300	4.85	-0.49	11.32	43.77	32.00	46.83	-23.63	-38.67	10073	8.93	8.21	6.55
-500	2.73	-0.43	8.49	30.45	23.00	34.17	-27.70	-27.33	10072	7.26	5.97	4.90
-662	1.31	-0.06	7.40	22.60	21.27	31.90	-31.90	-31.30	10074	6.70	5.55	4.76
-907	-0.27	0.05	3.77	16.50	20.48	32.19	-30.00	-25.51	10074	4.54	3.94	4.68
-1157	-0.35	1.51	7.08	16.01	18.21	41.78	-36.85	-22.97	10074	6.38	6.14	5.54
-1407	-0.99	1.92	8.97	14.31	21.33	43.53	-33.19	-30.53	10074	6.86	8.16	6.15
-1657	-0.61	1.10	8.59	16.64	26.46	44.11	-31.94	-31.90	10074	6.98	8.79	7.33
-1928	-1.03	1.93	10.52	14.88	26.99	38.88	-32.94	-28.34	10074	7.83	9.60	6.89
-2178	-1.07	1.69	11.28	15.44	28.36	40.33	-34.07	-32.75	10074	7.91	10.57	7.14
-2628	-1.44	1.27	11.53	15.09	31.63	39.17	-33.45	-31.82	10074	7.16	11.59	7.51
-2928	-1.07	0.72	9.58	19.54	28.29	36.66	-29.85	-27.32	10074	6.38	9.39	6.22

From the surface to depth all the variance ellipses rotated in a counter clockwise direction. This was contrary to Deployment 3 where the top 500 m showed a clockwise rotation with increasing depth, and the bottom 1500 m showed a counter clockwise rotation, also with increasing depth (Figure 69). The bottom 1500 m showed energy increasing with depth, with a decrease in energy occuring in the bottom current meter. This is indicative of a TRW with the bottom of the mooring being affected by the boundary layer. The net zonal velocity in the top 600 m was to the east which is opposite of what was seen in Deployment 3. The net meridional velocity from z = -200 m to z = -662 m was southerly, again opposite to what was seen in Deployment 3. The bottom 1500 m showed the the mean current was close to perpendicular to the isobaths (Figure 69). This was similar to what was seen in Deployment 3.

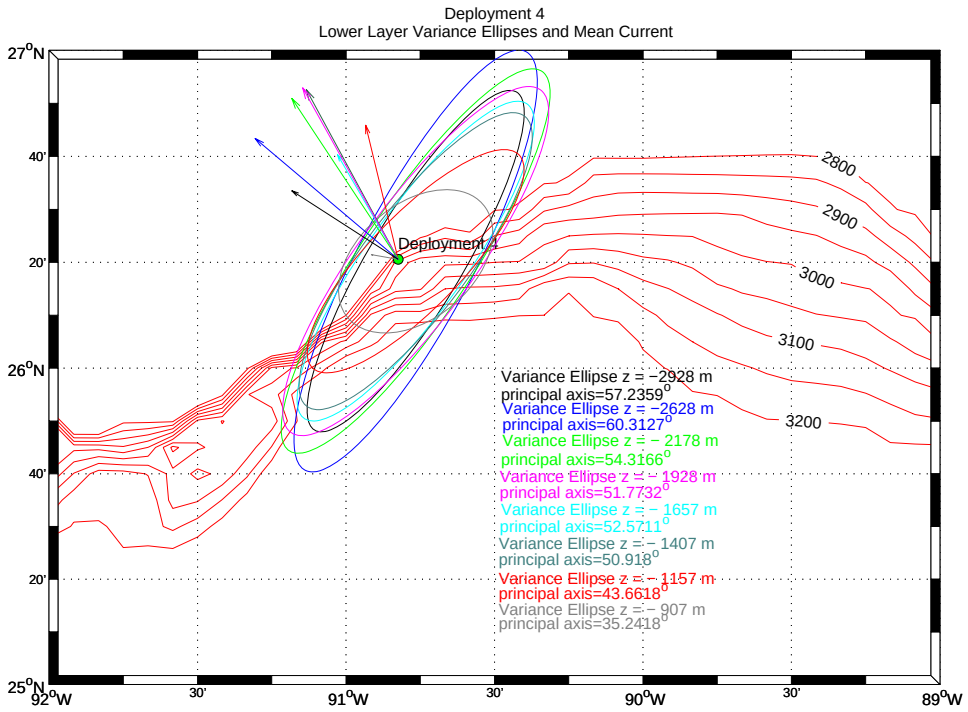

Figure 69. Lower layer variance ellipses and mean current vectors for Deployment 4.

The top mooring, z = -76 m showed a weak but robust signal at 25 days (Figure 70). The autocorrelation showed a weak but significant signal at 22-23 days, and three of the four spectral methods showed the weak 25 day signal. The periodogram showed possible signals at 39 and 64 days, but neither of these signals were found in the other spectral methods. The autocorrelation does have a significant signal between 43 and 56 days and one around 70 days. The NDBC buoy 42001 wind showed some weak signals at 6-7 days, 15 days, and 21 days. It should be kept in mind that two large events affected this time series. Hurricane Claudette, towards the end of July and Eddy S near the first of October. It is possible that these large signals affected the spectral analyses due to their large influence on the mooring. Wavelet analysis may give a better picture of the signals in this time series.

With the surface time series was broken up into two equal pieces, a 25 day and 14 day signal were found in the first and second half of the time series. A 52 day signal was seen in the first half, but not the second.

At z = -662 m a longer period 50-60 day signal was found in all methods, with a weak 22 day signal found in three methods, and a weak 12 day signal found in all four methods. A 52 day signal was seen in the first half of this time series along with a 21 day signal. The second half of the time series showed a broad band signal around 18 days, but no 50 day signal. An 11-12 day signal was seen in both the halves of the time series.

The z = -1157 m current meter showed a weak 32 day signal, and a week 22 day signal. A possible 50-60 day signal was also seen. The WOSA and MTM methods did not resolve the two signals but did show a 60 day signal. The periodogram resolved a 50 and 60 day signal while the AR method showed the time series to have a 50 days signal. The WOSA method showed a 50 day signal in the first half of the time series, and only a weak 20 day signal in the second half of the time series.

For the z = -1928 m the signals were the same as z = -1157 m meter. The power in the spectrum was greater at 32 days than at -1657 m and -1157 m which is indicative of TRW's. This was not the case at the 50-60 day peaks. The 20 day to 16 day part of the spectrum did show this increase in energy with depth. One interesting difference was a 32-day signal found in the first half of this time series which was not seen in the z = -1157 m time series.

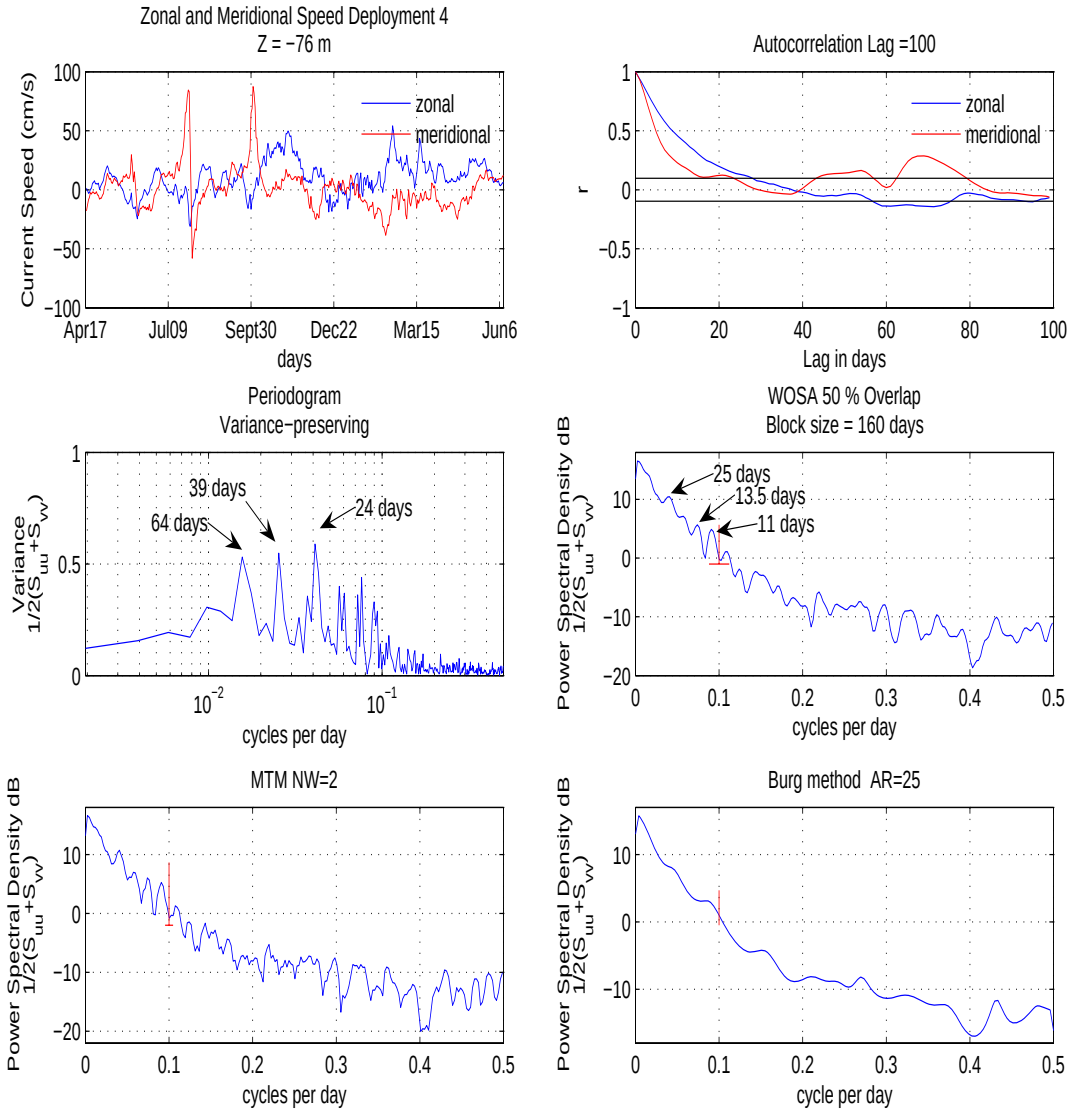

Figure 70. Multiple methods of spectral analysis z = -73 m for Deployment 4.

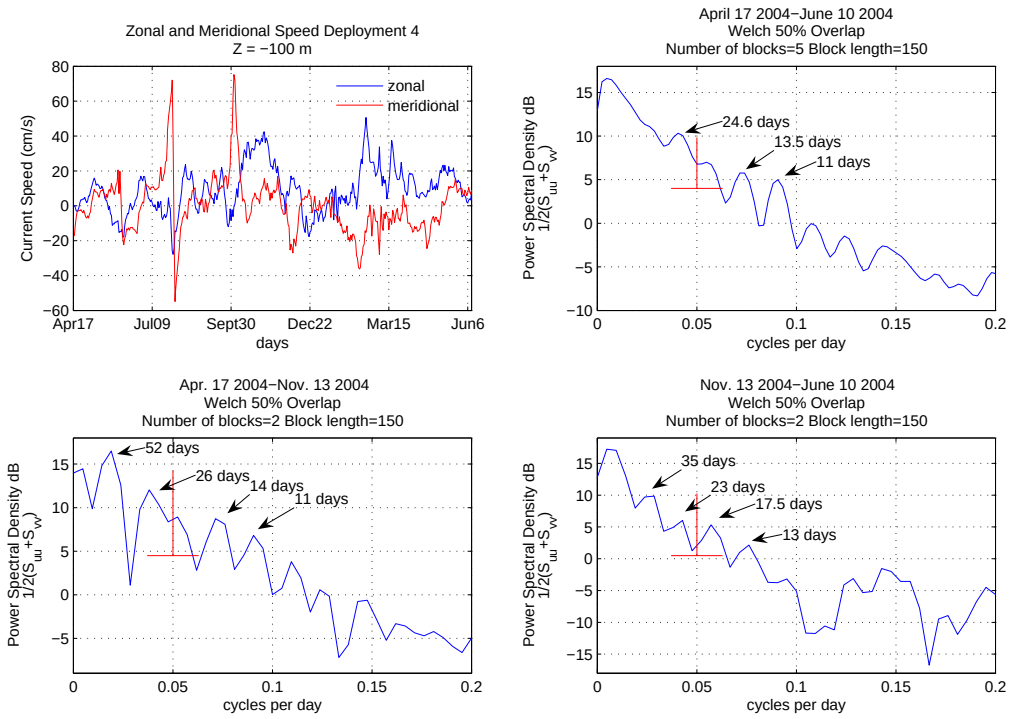

Figure 71. WOSA first and second half of time series z = -100 m for Deployment 4.

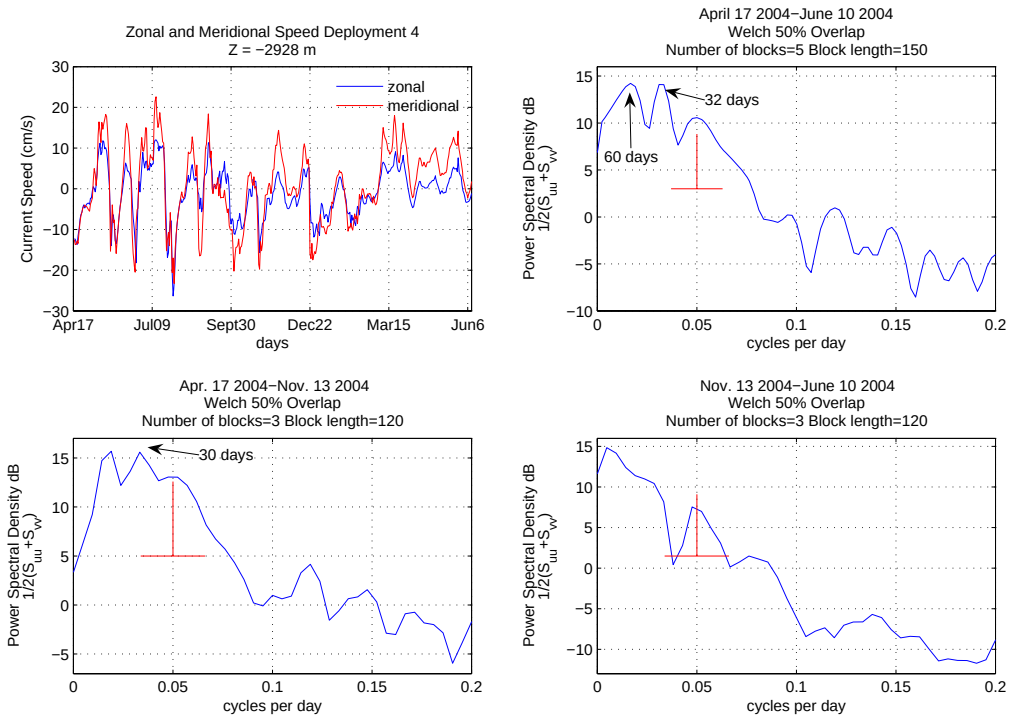

Figure 72. WOSA first and second half of time series z = -2928 m for Deployment 4.

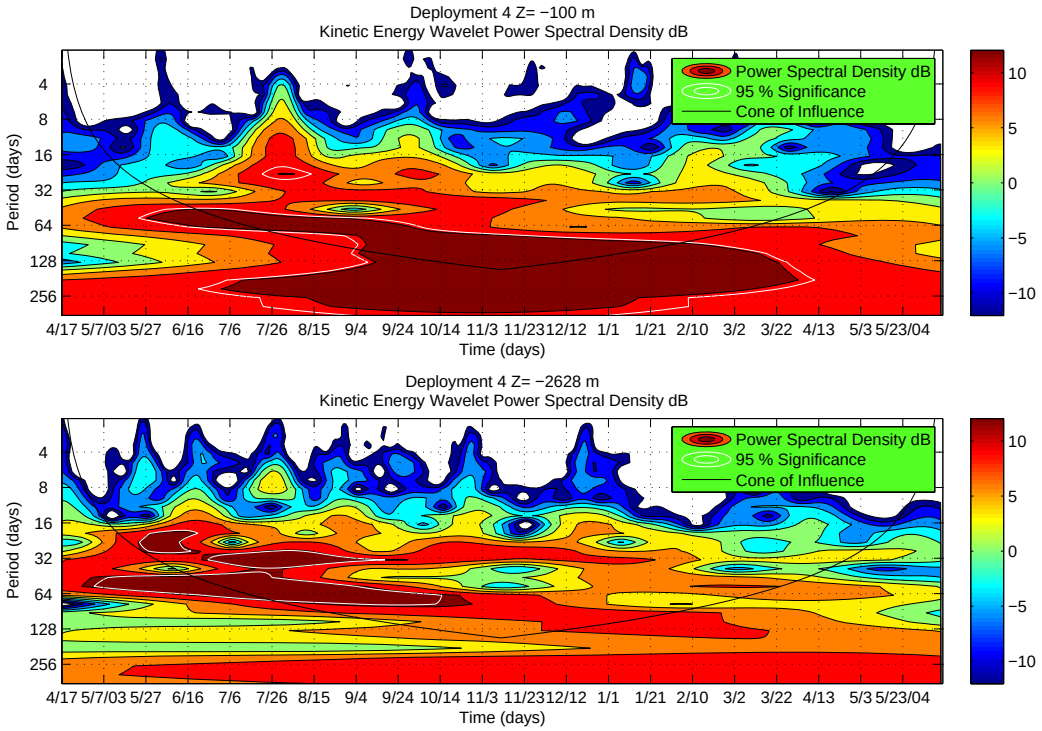

Figure 73. Wavelet analysis z = -100 m and z = -2628 m for Deployment 4.

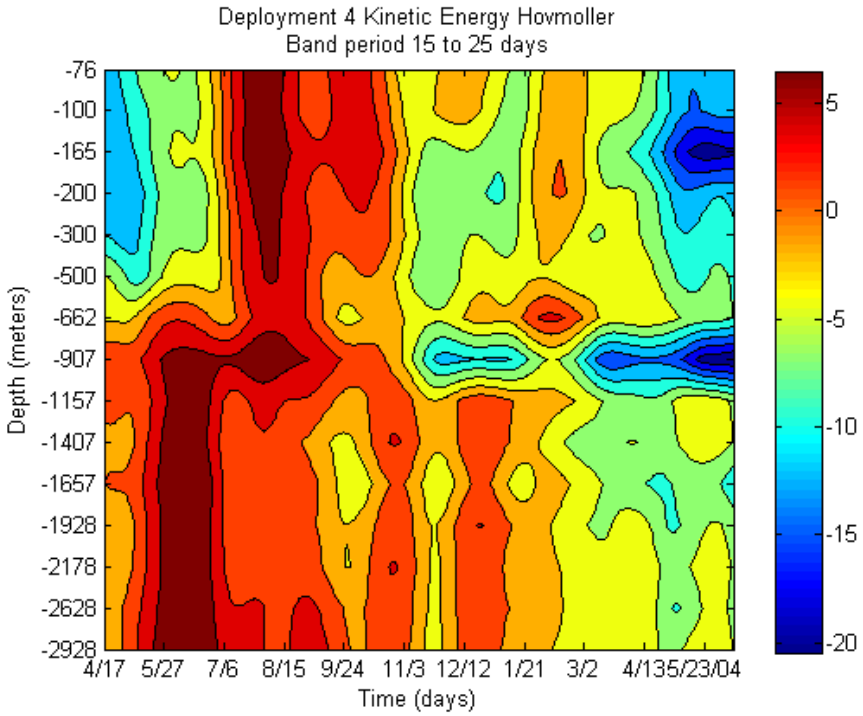

Figure 74. Hovmöller Deployment 4 for band period 15-25 days.

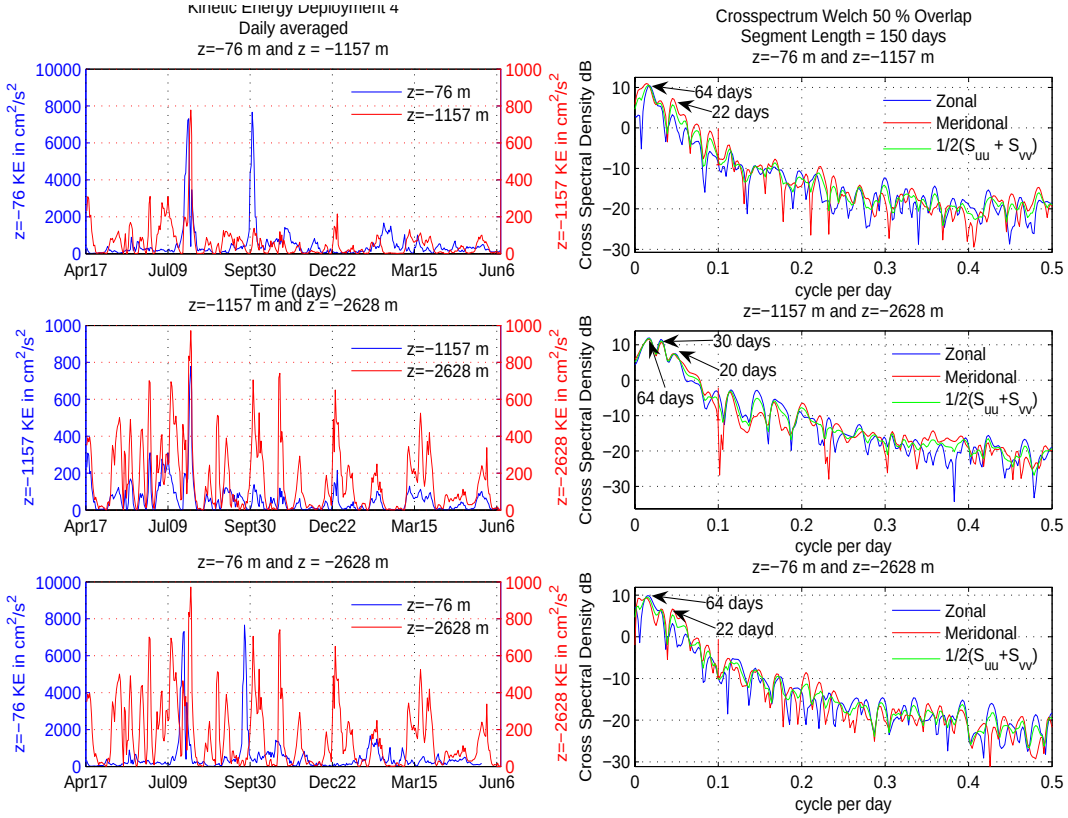

Figure 75. Cross-spectral analysis for Deployment 4.

spectral plot for the bottom current meter z = -2928 m is shown in Figure 5. Its peaks were similar to the ones found in -1157 and -2178 m.

Cross-spectral analysis did show a weak 60 day signal between the surface and z = -2929 m, Figure 75. The bottom 1500 m showed good correlation at 60 and 32 days. The surface and z = -1157 m showed some correlation at 60 and 22 days. Wavelet analysis showed that the 60 days signal was significant in the first half of the time series, mid May through late October or early November (Figure 73). This was the time frame when the unnamed Eddy and Eddy Sargassum were affecting the surface.

Rotary spectral analysis showed in the 50-70 day band little rotation in the bottom 1500 m of the water column and strong cyclonic motion in the top 1000 m.

Wavelet analysis (Figure 73) did reveal a significant signal at the surface and depth signal towards the end of July. The signal was in the 15-25 day period. Wavelet Hovmöller analysis also confirmed this (Figure 74). The mooring during this time was again found between the LC and a LCFE. During this same time period, LSU had another mooring southeast of Deployment 4. This mooring was also at the edge of the loop current. Using a wavelet Hovmöller analysis, a surface to depth signal was also seen in the 15-25 day.

Complex EOF was used to try and map moving waves in the SAIC array which was deployed during the same time period as Deployment 4. The analysis was very dependent on how the data was bandpassed, and no conclusive evidence was seen regarding moving waves along the escarpment in the time period.

6.0 SUMMARY

LSU deployed four full water column moorings starting in February of 2000 and removed the last mooring in June 2004. These moorings were designed to measure current, along with temperature and salinity at various depths throughout the water column. Full water column plots of current speed for all four deployments are shown in Figure 76. The first two moorings were located on top of the Sigsbee Escarpment on a plateau in approximately 2200 m of water. The last two mooring were deployed at the base of the Sigsbee escarpment in approximately 3000 m of water (Figure 1). The characterization of the long term currents above and below the Sigsbee Escarpment was one of the main objectives of this project. This was carried out by using multiple methods of spectral analysis, wavelet analysis along with basic statistical analysis. The maximum and mean current speeds are shown in Figure 77 and Figure 78. Another major component of this study was the analysis of the surface variability in the GoM. This included but was not limited to the Loop Current, Loop Current warm core eddies, and Loop Current frontal eddy cyclones, as well as additional mesoscale cyclonic and anticyclonic eddies. GOES-8 and GOES-12 SST imagery as well as chlorophyll *a* estimates from Oceansat-1 OCM were used extensively in the analysis. SSH data were often integrated with the SST data to better resolve ocean features of interest.

Using GOES night-time SST/SSH composite images, along with current and temperature measurements, 8 major circulation events (including several full water column events) were analyzed in each of the three time series. The color enhanced currents shown in Figure 76 enable visual comparisons between the three deployments. Surface events were strongest in Deployment 3 when the LC had a direct effect on the mooring for an extended period of time and shed two WCE's in the process. This abnormal northwestward intrusion was long-lasting and is most likely the reason that Deployment 3 exhibited the highest mean current speeds at least at the surface (Figure 78). Deployments 1-2 on the plateau exhibited the lowest mean current speeds at the surface and the bottom. However, Deployment 1-2 did experience short-lived strong surface flow from WCE's and maximum surface currents of 140 cm/s resulted (Figure 77). Surface currents during Deployment 4 were relatively weak in comparison to the prior two time periods.

During a few time periods, current speeds increased from the surface to the bottom nearly simultaneously. The main events occurred in late February 2001, late February 2002, mid-March 2002, and late July/early August 2003 and were described in detail in the preceding sections. These events are apparent in Figure 76 as the normally quiescent layer (around 1000 m) becomes notably energized. Our analyses of satellite information clearly showed a link between these full water column events and the proximity of LC meanders and associated LCFE cyclones. The combined use of SST data and SSH data maximized information concerning these events. In all cases, the SSH data suggests that the LCFE's moved into areas of pre-existing cyclonic circulation, where rapid growth in spatial extent of LCFE's was revealed by the GOES SST data. The growth of a LCFE cyclone over the LSU mooring was best revealed in the March 2002 Case

Study, Section 4.3), an event which coincided in time with a full-water column event. Hovmöller analyses of kinetic energy for Deployment 1-2, 3 and 4 all clearly revealed energy in the 15-25 day period for periods of 6-8 weeks, surrounding these surface to bottom events. This frequency band corresponds to the observed frequency of LCFE movements along the west flank of the LC (Walker et al., 2007).

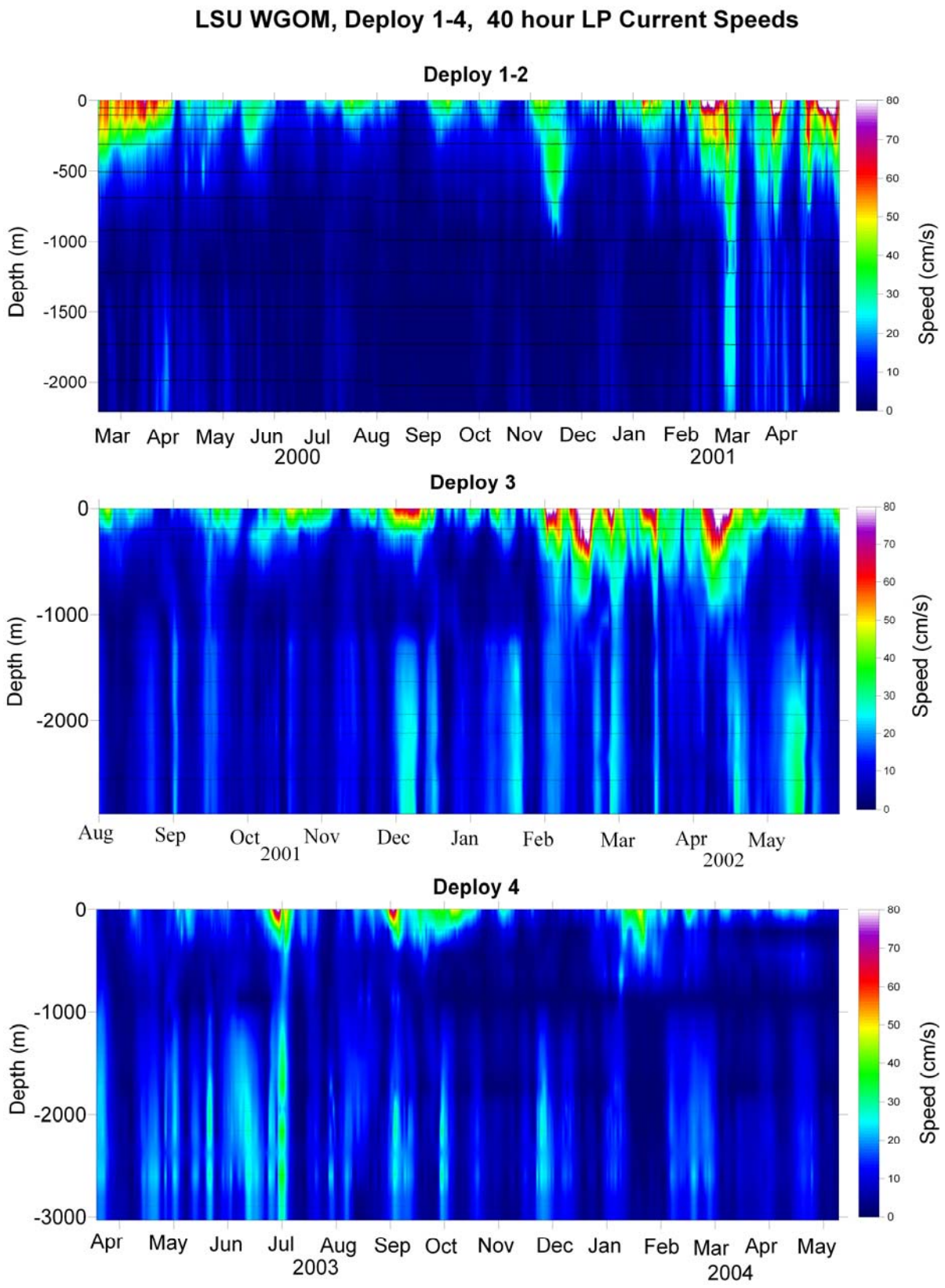

Figure 76. Full water column current speeds for all four deployments.

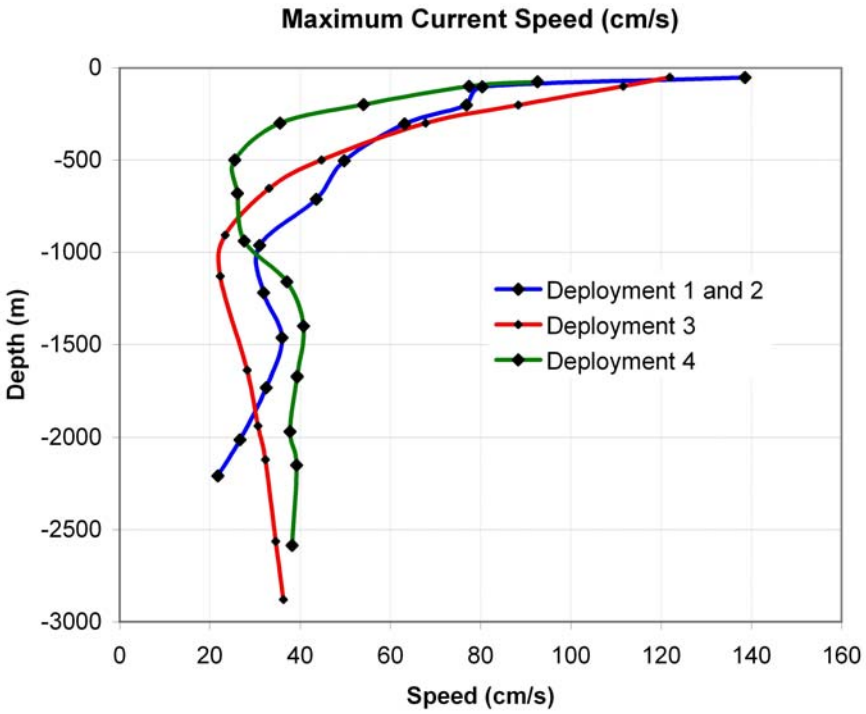

Figure 77. Maximum current speeds at LSU deep water moorings.

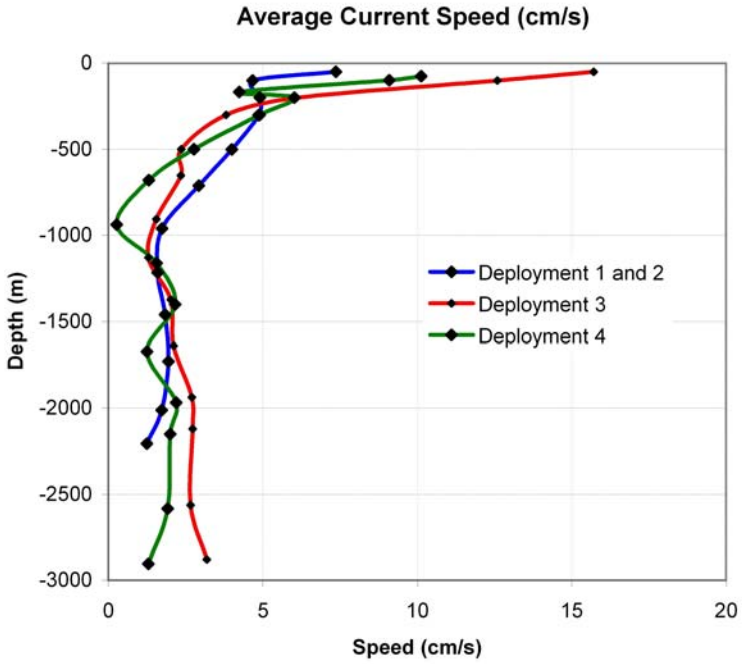

Figure 78. Average current speeds at LSU deep water moorings.

Topographic Rossby waves (TRW's) are thought to play a major role in the movement of water at the base of the Sigsbee escarpment (Hamilton 1990). TRW's are characterized by the coherent movement of a water column over 1000 m tall, with wavelengths from 100-300 km (Oey and Lee 2002). These massive columns of water oscillate with periods from 10-100 days using bottom topography as a restoring force. Others have used single moorings to detect topographic Rossby waves (Thompson 1975), but our data was inconclusive in determining if TRW's were affecting the moorings. One piece of strong evidence for TRW's was seen in the stick or vector plots. These plots showed water moving in a northeasterly direction for 5-10 days, switching to the southwest for another 5-10 days. The vector plots also revealed strong coherence throughout the bottom 1500 m of the water column. These two factors are strong indicators of TRW's. Spectral analysis also revealed strong signals in the 10-100 day period, another indicator of TRW's. The importance of characterizing TRW's is the possibility of prediction. Knowing TRW's are following the escarpment, and knowing the forcing of the TRW's would allow the prediction of these massive columns of water and strong currents that they cause. It is evident from earlier work that these types of waves are triggered by surface events (Oey and Lee 2002). It has become evident based on results of this project that the zone of strong shear between the LC and a growing LCFE is affecting the whole water column. A further study of this effect, especially near the Yucatan Channel where LCFE's are first formed or observed by satellite data could give further insight into the prediction of TRW's. To follow the motion of TRW's, complex EOF analysis could be used on an array of short bottom moorings over a large area from the Yucatan Channel to and along the base of the escarpment.

Multiple methods of spectral analysis were used to look for periodic signals in the current meter time series. This was a great opportunity to look for periodic signals in relatively long time series of currents in not only deep water, but throughout 2200-3000 m of water. With the turn around of Deployments 1 and 2 being only a few hours, the combination of these two moorings allowed for a time series over a year long (Figure 2). The Deployment 3 time series was close to a year long and Deployment 4 was over a year long (Figure 2). Coherent periodic signals in the bottom 1500 m from 10-100 days were investigated in all time series. Also analyzed was the increase in energy with depth of the spectral signals. The periods and increase in energy are indicative of TRW's. Cross-spectral analysis was used to look for possible surface to depth connections. Another goal of this project was to find possible forcing for the movement of deep water, which is thought to be mainly TRW's. With most TRW's being forced non-locally, and traditional spectral methods not able to isolate signals in time, surface forcing of deep water TRW's was not found.

As shown above in the wavelet Hovmöller diagrams, there is a connection between the surface and depth. Three major surface to depth events were analyzed using wavelet analysis and bandpassed wavelet Hovmöller diagrams (Figure 25). Both these methods showed significant 15-25 day signals occurring throughout the water column when the mooring was directly affected by a developing LCFE, along the margin of the LC. A fourth LSU deployment near the core of the LC (not this project) also revealed a similar signal. Our analyses indicate that these events may not involve eddy coupling between the upper and lower layer, but look to be full water column events. In particular wavelet rotary spectral analysis does not show a dominant clockwise or counter-clockwise signal at the surface or at depth, which would be expected if coupling was occurring. A more in-depth study of LCFE's as trigger mechanism for full water column events is warranted based on our results.

7.0 REFERENCES

Berger, T.J., P. Hamilton, J.J. Singer, and R.R. Leben. 1996. Louisiana/Texas physical oceanography program: Eddy circulation study, final synthesis report. U.S. Dept. of the Interior, Minerals Management Service, Gulf of Mexico OCS region, New Orleans, LA. OCS Study MMS 96-0051. 258 pp.

Bower, A.S. and N.G. Hogg. 1991. Evidence for barotropic wave radiation from the Gulf Stream. J. Phys. Oceanogr. 22:42-61.

Chatfield, C. 1996. The analysis of time series, 5th ed. Boca Raton, FL: Chapman & Hall/CRC. 283 pp.

Cooper, C., G.Z. Forristall, and T.M. Joyce. 1990. Velocity and hydrographic structure of two Gulf of Mexico warm-core rings. J. Geophys. Res. 95:1663-1679.

Donohue, K., P. Hamilton, K. Leaman, R. Leben, M. Prater, D.R. Watts, and E. Waddell. 2006. Exploratory study of deepwater currents in the Gulf of Mexico. U.S. Dept. of the Interior, Minerals Management Service, Gulf of Mexico OCS Region, New Orleans, LA. OCS Study MMS 2006-074. 399 pp.

Emery, W.J. and R.E. Thomson. 1997. Data analysis methods in physical oceanography. New York: Pergamon. 634 pp.

Grinstead, A., J.C. Moore, and S. Jevrejeva. 2004. Application of cross wavelet transform and wavelet coherence to geophysical time series. Nonlinear Processes in Geophysics. 11:561-566.

Hamilton, P. 1990. Deep currents in the Gulf of Mexico. J. Phys. Oceanogr. 20:1087-1104.

Hamilton, P. and A. Lugo-Fernandez. 2001. Observations of high speed deep currents in the northern Gulf of Mexico, Geophys. Res. Lett. 28:2867-2870.

Hogg, N.G. 1981. Topographic waves along 70° W on the continental rise. J. Mar. Res. 40:119-142.

Hoffmann, E.E. and S.J. Worley. 1986. An investigation of the circulation of the Gulf of Mexico. J Geophys. Res. 91:14221-14236.

Huh, O.K. and K.J. Schaudt. 1990. Satellite imagery tracks currents in Gulf of Mexico. Oil and Gas Journal. 88:70-76.

Huh, O.K., W.J. Wiseman, Jr., and L.J. Rouse, Jr.1981. Intrusion of Loop Current waters onto the west Florida shelf. J. Geophys. Res. 86:4186-4192.

Inoue, M., S.E. Welsh, L.J. Rouse, Jr., and E. Weeks. In preparation. Deepwater Currents in the Eastern Gulf of Mexico: Observations at 25.5ºand 87º W. U.S. Dept. of the Interior, Minerals Management Service, Gulf of Mexico OCS Region, New Orleans, LA.

Johns, W.E. and D.R. Watts. 1986. Time scales and structure of topographic Rossby waves and meanders in the deep Gulf Stream. J Mar. Res. 44:267-290.

Kantha, L. 2005. Barotropic tides in the Gulf of Mexico. In: Sturges, W. and A. Lugo-Fernandez, eds. Circulation in the Gulf of Mexico: Observations and Models. American Geophysical Union, Washington, DC. Pp. 159-163.

Leben, R., G. Born, and B.R. Engebreth. 2002. Operational altimeter data processing for mesoscale monitoring, Mar. Geodesy 25:3-18.

Leben, R.R. 2005. Altimeter-derived current metrics. In: Sturges, W. and A. Lugo-Fernandez, eds. Circulation in the Gulf of Mexico: Observations and Models. American Geophysical Union, Washington, DC. . Pp. 181-201.

Legeckis, R., C.W. Brown, and P.S. Chen. 2002. Geostationary satellites reveal motions of ocean surface fronts. J. Mar. Sys. 37:3-15.

Liu, P.C. and G.S. Miller. 1996. Wavelet transforms and ocean current data analysis. J Atmos. and Oceanic Tech. 13:1090-1099.

Louis, J.P., B.D. Petrie, and P.C. Smith. 1982. Observations of topographic Rossby waves on the continental margin off Nova Scotia. J Phys. Oceanogr. 17:47-55.

Maul, G.A, F. Williams, M. Roffer, and F.M. Sousa. 1984. Remotely sensed oceanographic patterns and variability of bluefin tuna catch in the Gulf of Mexico. Ocean. Acta. 7:469-479.

May, D.A., J.D. Hawkins, and R.L. Pickett. 1993. Detecting Gulf of Mexico oceanographic features in summer using AVHRR channel 3. J. of Atmosph. and Ocean. Tech. 10:64-75.

McKone, K.P. 2003. Multiple methods of spectral analysis with applications to the Florida Current. Ph.D. Thesis, Dept. of Marine Science, University of Southern Mississippi, Hattiesburg, MS. 120 pp.

Menzel, P.W. and J.F.W. Purdom. 1994. Introducing GOES-I: The first of a new generation of GOEStationary operational environmental satellites. Bull. Amer. Meteor. Soc. 75:757-781.

Mizuta, G. and N.G. Hogg. 2004. Structure of the circulation induced by a shoaling topographic wave. J. Phys. Oceanogr. 34:1793-1810.

Muller-Karger, F.E., J.J. Walsh, R.H. Evans, and M.B. Meyers. 1991. On the seasonal phytoplankton concentration and sea surface temperature cycles of the Gulf of Mexico as determined by satellites. J. Geophys. Res. 96:12645-12665.

Oey L.Y. and H.C. Lee. 2002. Deep eddy and topographic Rossby waves in the Gulf of Mexico. J. Phys. Oceanogr. 32:3499-3527.

Offshore Engineering. 2004. Current affairs. www.offshore-engineer.com. February. Pp. 20-22.

O'Reilly, J.E., S. Maritorena, B.G. Mitchell, D. Siegel, K. Carder, S. Garver. M. Kahru, and C. McClain. 1998. Ocean color chlorophyll algorithms for SeaWiFS. J. Geophys. Res. 103:24,937-24,953.

Paluszkiewicz, T., L.P. Atkinson, E.S. Posmentier, and C.R. McClain. 1983. Observations of a Loop Current frontal eddy intrusion onto the west Florida Shelf. J. Geophys. Res. 88:9639-9651.

Pedlosky, J. 1987. Geophysical fluid dynamics, 2nd ed. New York: Springer-Verlag. 710 pp.

Percival, D. and A.T. Walden. 1993. Spectral analysis for physical applications. New York: Cambridge. 583 pp.

Pickart, R.S. 1995. Gulf Stream generated topographic Rossby waves. J. Phys. Oceanogr. 25:574-584.

Rhines, P.B. 1970. Edge-, bottom-, and Rossby waves in a rotating stratified fluid. Geophys. Fluid Dyn. 1:273-302.

Smith, W.H.F. and D.T. Sandwell. 1997. Global sea floor topography from satellite altimetry and ship depth soundings. Science 277:1956-1962.

Sturges, W. 2005. Deep-water exchange between the Atlantic, Caribbean and Gulf of Mexico. In: Sturges, W. and A. Lugo-Fernandez, eds. Circulation in the Gulf of Mexico: Observations and Models. American Geophysical Union, Washington, DC.. Pp. 263-278.

Thompson, R.O.R.Y. 1977. Observations of Rossby waves near site D. Prog. Oceanogr. 7:135-162.

Thompson, R.O.R.Y. and J.R. Luyten. 1976. Evidence for bottom-trapped topographic Rossby waves from single moorings. Deep-Sea Res. 23:629-635.

Torrence, C. and G.P. Campo. 1998. A practical guide to wavelet analysis. Bull. Amer. Met. Soc. 79:61-78.

Torrence, C. and P.J. Webster. 1999. Interdecadal changes in the ENSO-Monsoon system. J. Clim. 12:2679-2690.

Vukovich, F.M., B.W. Crissman, M. Bushnell, and W. King. 1979. Some aspects of the oceanography of the Gulf of Mexico using satellite and in situ data. J. Geophys. Res. 84:7749-7768.

Vukovich, F.M and G.A. Maul. 1985. Cyclonic eddies in the eastern Gulf of Mexico. J. Phys. Ocean. 15:105-117.

Walker, N., S. Balasubramanian, R. Leben, S. Anderson, P. Coholan, and J. Feeney. 2007. Remote sensing of Loop Current frontal eddy cyclones. Proceedings, MMS Information Transfer Meeting, New Orleans, January 2007. 7 pp.

Walker, N.D., O.K. Huh, L.J. Rouse, and S.P. Murray. 1996. Evolution and structure of a coastal squirt off the Mississippi River delta: Northern Gulf of Mexico. J. Geophys. Res. 101:20,643-20,655.

Walker, N.D., Myint, A. Babin, and A. Haag. 2003. Advances in satellite radiometry for the surveillance of surface temperatures, ocean eddies and upwelling processes in the Gulf of Mexico using GOES-8 measurements during summer. Geophys. Res. Lett. 30. 1854, doi:10.1029/2003GL017555.

Walker, N.D., R.R. Leben, S Balasubramanian. 2005. Hurricane-forced upwelling and chlorophyll a enhancement within cold-core cyclones in the Gulf of Mexico, Geophysical Research Letters, vol. 32, L18610,doi:10.1029/2005GL023716.

Wiseman, W.J. and W. Sturges. 1999. Physical oceanography of the Gulf of Mexico: Processes that regulate its biology. In: Kump, H., K. Steidinger, and K. Sherman eds. The Gulf of Mexico Large Marine Ecosystem. Pp. 77-92.

The Department of the Interior Mission

As the Nation's principal conservation agency, the Department of the Interior has responsibility for most of our nationally owned public lands and natural resources. This includes fostering sound use of our land and water resources; protecting our fish, wildlife, and biological diversity; preserving the environmental and cultural values of our national parks and historical places; and providing for the enjoyment of life through outdoor recreation. The Department assesses our energy and mineral resources and works to ensure that their development is in the best interests of all our people by encouraging stewardship and citizen participation in their care. The Department also has a major responsibility for American Indian reservation communities and for people who live in island territories under U.S. administration.

The Minerals Management Service Mission

As a bureau of the Department of the Interior, the Minerals Management Service's (MMS) primary responsibilities are to manage the mineral resources located on the Nation's Outer Continental Shelf (OCS), collect revenue from the Federal OCS and onshore Federal and Indian lands, and distribute those revenues.

Moreover, in working to meet its responsibilities, the **Offshore Minerals Management Program** administers the OCS competitive leasing program and oversees the safe and environmentally sound exploration and production of our Nation's offshore natural gas, oil and other mineral resources. The MMS **Minerals Revenue Management** meets its responsibilities by ensuring the efficient, timely and accurate collection and disbursement of revenue from mineral leasing and production due to Indian tribes and allottees, States and the U.S. Treasury.

The MMS strives to fulfill its responsibilities through the general guiding principles of: (1) being responsive to the public's concerns and interests by maintaining a dialogue with all potentially affected parties and (2) carrying out its programs with an emphasis on working to enhance the quality of life for all Americans by lending MMS assistance and expertise to economic development and environmental protection.